# Quasilinear Control Theory for Systems with Asymmetric Actuators and Sensors

by

Hamid-Reza Ossareh

A dissertation submitted in partial fulfillment
of the requirements for the degree of
Doctor of Philosophy
(Electrical Engineering: Systems)
in the University of Michigan
2013

Doctoral Committee:

Professor Pierre Kabamba, Co-Chair,
Professor Semyon Meerkov, Co-Chair,
Professor Jessy Grizzle,
Professor Ilya Kolmanovsky,
Professor Demosthenis Teneketzis.

To my family.

# ACKNOWLEDGEMENTS

First and foremost, I would like to thank my advisors, Professors Pierre Kabamba and Semyon Meerkov, for all their efforts and guidance. They have been there with me throughout the course of my graduate studies and, for that, I am very grateful.

Next, I wish to thank Professors Jessy Grizzle, Ilya Kolmanovsky, and Demosthenis Teneketzis for their interest in my work and for serving as members of my dissertation committee.

I also want to thank Professor Domitilla Del Vecchio for her support and mentorship.

During my doctoral studies I collaborated with the following scholars, to whom I am grateful: Dr. Mads Almassalkhi, Professor Shinung Ching, Professor Yongsoon Eun, Dr. Eric Gross, Dr. Yi Guo, and Professor Choon Yik Tang.

Moreover, I want to thank my family and friends whose love and support made this achievement possible.

Finally, I acknowledge financial support from the National Science Foundation that made this work possible.

# TABLE OF CONTENTS

# LIST OF FIGURES

**Figure**

# LIST OF TABLES

**Table**

# LIST OF APPENDICES

**Appendix**

# ABSTRACT

Quasilinear Control Theory for Systems with Asymmetric Actuators and Sensors

by

Hamid-Reza Ossareh

Co-chairs: Professor Pierre Kabamba and Professor Semyon Meerkov

Quasilinear Control (QLC) theory provides a set of methods for analysis and design of systems with nonlinear actuators and sensors. In practice, actuators always saturate and sensors often have deadzone or quantization. One limitation of the current QLC theory is that it is applicable only to systems with symmetric nonlinearities. In many situations, however, nonlinearities are asymmetric. Examples of such systems abound: air-conditioning/heating systems, automotive torque and idle speed control, wind turbine control, etc. In this work, we provide an extension of the QLC theory to the asymmetric case. Similar to the symmetric case, the approach is based on the method of stochastic linearization, which replaces nonlinear systems by quasilinear ones. Unlike the symmetric case, however, stochastic linearization in the asymmetric case replaces each nonlinearity not only by an equivalent gain, but also by an equivalent bias. The latter leads to steady state errors incompatible with the usual error coefficients predicted by linear systems theory. For this reason, the extension to the asymmetric case is non-trivial. Specific problems addressed in this dissertation with regards to asymmetric systems are: (i) Introduction and investigation of the

notion of asymmetry. (ii) Development of a formalism of stochastic linearization for systems at hand. (iii) Analysis of tracking and disturbance rejection performance. (iv) Introduction and investigation of performance loci, i.e., root locus and tracking error locus. (v) Utilization of the performance loci for random reference and step reference tracking controller design. (vi) Recovery of linear performance in nonlinear systems. (vii) Disturbance rejection controller design using an LQR-type approach. (viii) Application of the methods developed to a wind farm controller design. In addition, a Matlab-based toolbox that implements most of the QLC methods has been developed and is available at www.QuasilinearControl.com.

# CHAPTER I

# Introduction

## 1.1 Motivation and Approach

### 1.1.1 Motivation

Consider the single-input single-output (SISO) linear system shown in Figure 1.1.1, where $P(s)$ and $C(s)$ are the plant and controller, respectively, and $r$ and $d$ are the reference signal and the disturbance. Over the past century, this system has been extensively studied, and a plethora of analysis and design techniques have been developed.

Control systems, however, always contain nonlinear instrumentation, i.e., actuators and sensors. Two ubiquitous nonlinearities are actuator saturation and sensor deadzone. This leads to the block diagram of Figure 1.1.2, where $f(\cdot)$ and $g(\cdot)$ are static nonlinearities representing the actuator and sensor, respectively. Here, the plant $P(s)$ is linear because the system is assumed to operate close to an operating point. However, while the plant is kept in the vicinity of an operating point, nonlinearities in the instrumentation might be activated in order to reject large disturbances or to track large references. For this reason, the system of Figure 1.1.2 is referred to as linear plant/nonlinear instrumentation (LPNI) system.

Stability of LPNI systems has been extensively studied in the literature (see the

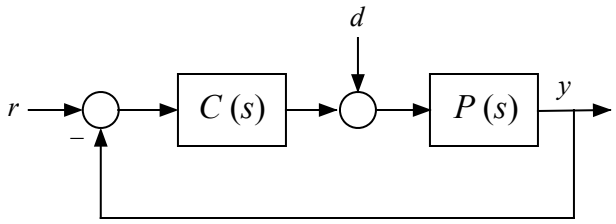


1.1.1: Linear control system.

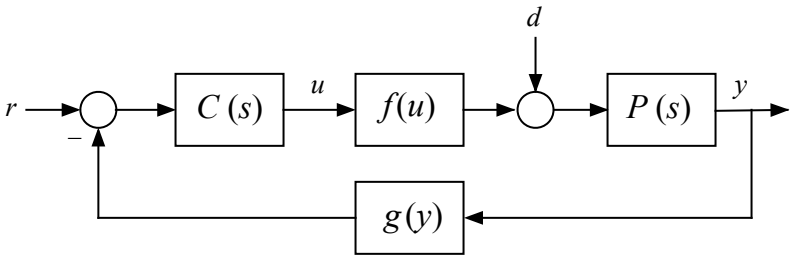


1.1.2: LPNI control system.

Figure 1.1: SISO linear system and LPNI system.

literature review in Subsection 1.5.1). Hence, we will not pursue the issue of stability of such systems in this work. The problems of performance analysis and controller design, however, have received far less attention. The earlier work [1] developed the theory of Quasilinear Control (QLC), which provides a set of methods for performance analysis and controller design of LPNI systems. One shortcoming of the existing QLC theory is that it is only applicable to systems with odd (i.e., *symmetric*) nonlinearities driven by zero-mean exogenous signals. In applications, however, these nonlinearities may be *asymmetric* or the exogenous signals may have non-zero mean. Roughly speaking, we refer to these systems as *asymmetric* LPNI (A-LPNI) systems (see Section 1.2 for a formal definition). Examples of A-LPNI systems abound:

- In the xerographic process, toner can be added to the process but cannot be removed [2]. Thus, the actuator can be modeled as a one-sided saturation, which can only actuate the plant in one direction.

- A simple model of a wind turbine consists of a first order system preceded by a saturation nonlinearity, which, for most operating conditions, is asymmetric.

The saturation appears in the model because the available wind power is always positive and finite [3] (see Chapter VIII for modeling and controller design of such a system).

- In aircraft, each elevator can typically be modeled by a saturation, which is asymmetric after trimming (i.e., has more authority in one direction than the other [4]).

- In simple heating (or cooling) systems, heat can be added to (or removed from) the process; however, the control action cannot remove (or add) heat. Thus, the actuator is a one-sided saturation, which can only actuate the plant in one direction [5].

Thus, motivated by applications, as well theoretical interests, the intention of this work is to develop methods for performance analysis and controller design of A-LPNI systems.

### 1.1.2 Technical approach

In the study of A-LPNI systems, rigorous analytical results are difficult to achieve because of the nature of such systems. However, these difficulties may be alleviated when the exogenous signals are random. In this situation, a powerful mathematical technique may be employed – stochastic linearization [6] – which replaces each static nonlinearity with an affine function, i.e., an equivalent gain and an equivalent bias (note that only an equivalent gain arises in the stochastic linearization of symmetric LPNI systems considered in [1]). For reasons that will become clear in Chapter II, the linearized system is referred to as quasilinear. As it turns out, if the plant has sufficiently slow dynamics, the quasilinear system provides faithful estimates of the first and second moments of the signals in the original A-LPNI system and can, thus, be used for performance analysis and controller design. Accordingly, in this

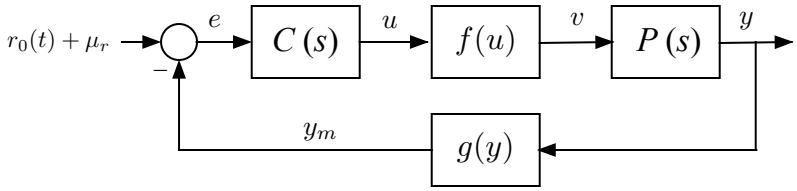


1.2.1: Original operating point.

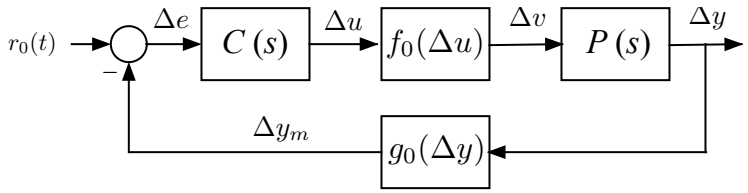


1.2.2: Translated operating point.

Figure 1.2: LPNI system with nonlinear actuator and sensor with the original and translated operating points.

work, we transfer methods of linear control theory to the quasilinear system. These methods include techniques for performance analysis, time domain design using root locus, step-tracking controller design, performance recovery, and an LQR approach for controller design.

Throughout, many examples are presented to illustrate the developed theory. All simulations and plots are created using the MATLAB and SIMULINK computational environments.

## 1.2 Definition of S- and A-LPNI Systems

Consider the LPNI system shown in Figure 1.2.1, where $P(s)$ and $C(s)$ are the plant and the controller, $f(u)$ and $g(y)$ are functions representing the actuator and sensor, $r_0$ is a wide-sense stationary zero-mean Gaussian process, and $\mu_r$ is a constant. Assume that the system is operating in the stationary regime so that all signals have average values that do not vary with time.

To define the notion of symmetry, we translate the operating point of this system such that, with respect to the new operating point, the reference signal has zero mean.

To accomplish this, introduce the new signals

$$\begin{aligned} \Delta e &= e - \frac{1}{1+C_0P_0}\mu_r, \quad \Delta u = u - \frac{C_0}{1+C_0P_0}\mu_r, \\ \Delta v &= v - \frac{C_0}{1+C_0P_0}\mu_r, \quad \Delta y = y - \frac{C_0P_0}{1+C_0P_0}\mu_r, \\ \Delta y_m &= y_m - \frac{C_0P_0}{1+C_0P_0}\mu_r, \end{aligned} \tag{1.1}$$

where $P_0$ and $C_0$ are the dc-gains of the plant and controller, and $e, u, v, y$, and $y_m$ are signals shown in Figure 1.2.1. Clearly, with respect to the translated operating point, the system is as illustrated in Figure 1.2.2, where

$$f_0(\Delta u) = f(\Delta u + \frac{C_0}{1+C_0P_0}\mu_r) - \frac{C_0}{1+C_0P_0}\mu_r, \tag{1.2}$$

$$g_0(\Delta y) = g(\Delta y + \frac{C_0P_0}{1+C_0P_0}\mu_r) - \frac{C_0P_0}{1+C_0P_0}\mu_r. \tag{1.3}$$

We refer to the system of Figure 1.2.2 as the canonical form of that of Figure 1.2.1. Based on the above, we define the notion of S- and A-LPNI systems.

**Definition I.1.** The system of Figure 1.2.1 is called symmetric (or S-LPNI) if $f_0$ and $g_0$ defined by (1.2), (1.3) are odd functions. Otherwise, it is called asymmetric (or A-LPNI).

As mentioned in Section 1.1, symmetric LPNI systems with $\mu_r = 0$ have been treated in [1] for analysis and design. In the current work, we focus on analysis and design of the general case.

**Example I.1.** Consider the LPNI system of Figure 1.2.1, where $f(u) = \text{sat}_\alpha^\beta(u)$ is the saturation function with limits $\alpha$ and $\beta$ (see Figure 1.3), and $g(\cdot)$ is a linear sensor. Then, $f_0$ in (1.2) is given by:

$$f_0(\Delta u) = \text{sat}_{\alpha_0}^{\beta_0}(\Delta u),$$

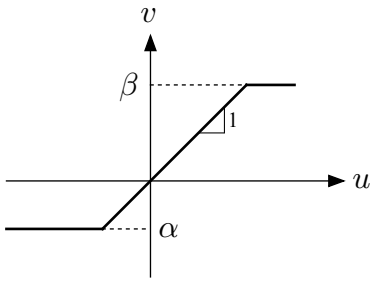


Figure 1.3: Saturation function $\text{sat}_{\alpha}^{\beta}(u)$.

where $\alpha_0 = \alpha - \frac{C_0}{1+C_0P_0}\mu_r$ and $\beta_0 = \beta - \frac{C_0}{1+C_0P_0}\mu_r$. Therefore, the LPNI system is symmetric iff $\alpha_0 = -\beta_0$, i.e.,

$$\frac{C_0}{1+C_0P_0}\mu_r = \frac{\alpha+\beta}{2}. \tag{1.4}$$

Otherwise, it is A-LPNI. □

**Remark I.1.** Taking the expected value of both sides of the first equation in (1.1) and rearranging the terms, we obtain

$$\mu_e = \frac{1}{1+P_0C_0}\mu_r + \mu_{\Delta e},$$

where $\mu_x$ denotes expected value of $x$. Note that the first term on the right hand side of the above expression is exactly the average value of the tracking error of the underlying linear system. Moreover, the second term is the tracking error of a LPNI system driven by zero-mean signals. Therefore, this expression provides a method for separating the average value of $e$ into two parts: the part which is caused by the underlying linear system, and the part that is induced because of the asymmetry in the nonlinearity. Similar reasoning applies to all other signals in (1.1). This idea is exploited later in this work.

## 1.3 Problems Considered

### 1.3.1 Problem 1: Formalism of stochastic linearization for A-LPNI systems

The first problem is to formulate stochastic linearization for closed loop A-LPNI systems. Unlike the symmetric case, each nonlinearity is replaced not only by a quasilinear gain, but also by a bias. The goals here are:

- present stochastic linearization of common nonlinearities in the open loop environment,
- develop the equations for the quasilinear gain and bias in the closed loop environment,
- study existence and uniqueness of the solutions of these equations,
- quantify the accuracy of stochastic linearization,
- define a measure of asymmetry, and, using this measure, investigate the effects of asymmetry on the quasilinear gain and bias.

### 1.3.2 Problem 2: Performance analysis of A-LPNI systems

To analyze tracking and disturbance rejection performance of A-LPNI systems, we assume that the references and disturbances are random processes. We, thus, stochastically linearize the A-LPNI system to obtain a quasilinear one. Block diagrams of the A-LPNI and quasilinear systems are shown in Figures 1.4.1 and 1.4.2, respectively. In these figures, $F_{\Omega_d}(s)$ and $F_{\Omega_r}(s)$ are low pass filters, $w_r$ and $w_d$ are independent standard Gaussian white noise processes, $f(\cdot)$ and $g(\cdot)$ are static nonlinearities representing actuator and sensor, and $N_a$, $N_s$, $m_a$, $m_s$ are quasilinear gains and biases of the actuator and sensor. The goals here are:

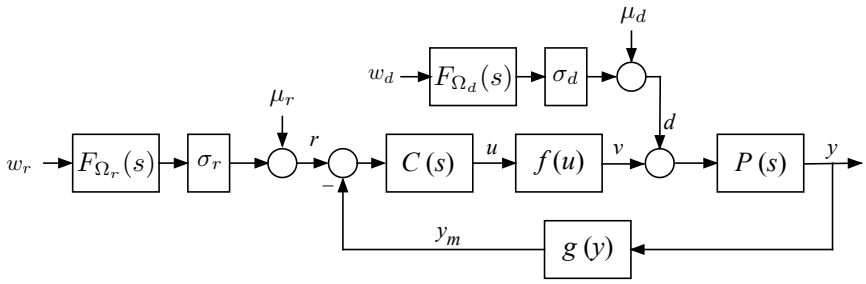


1.4.1: Closed loop A-LPNI system driven by random signals.

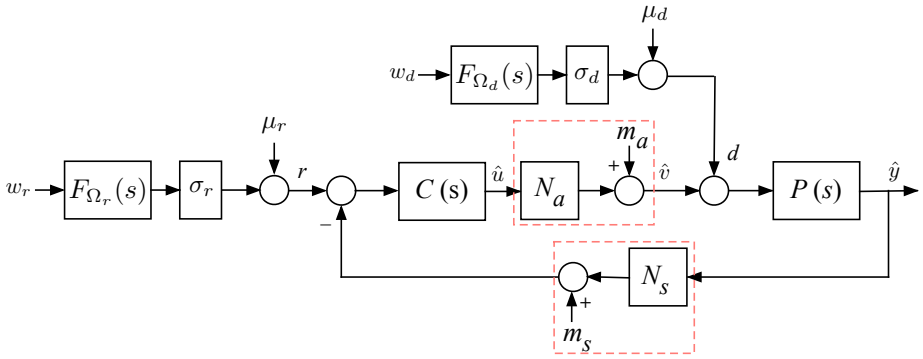


1.4.2: Stochastic linearization of the A-LPNI system

Figure 1.4: A-LPNI system and its stochastic linearization.

- investigate if the stochastically linearized system can indeed be used to study tracking and disturbance rejection performance of A-LPNI systems,
- develop a method for quantifying the quality of tracking and disturbance rejection in A-LPNI systems.

### 1.3.3 Problem 3: Time-domain design of A-LPNI systems

The third problem of interest is time domain design of A-LPNI systems. The focus is on systems with saturating actuator. Consider the system of Figure 1.5, where $f(u)$ is the saturation function. The goal is to choose $K > 0$ such that the closed loop system tracks the reference well, if at all possible. This problem has been solved for linear systems using the root locus method and for symmetric LPNI systems using the S-root locus method [1], where "S" stands for saturating. For A-LPNI systems, however, this problem has not been addressed.

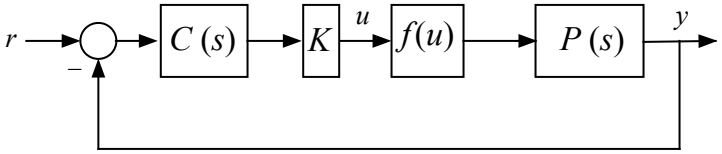


Figure 1.5: System considered for time domain design.

Since the tool used in our work is stochastic linearization, we model the reference $r(t)$ as a random process. We then stochastically linearize the system and consider the resulting quasilinear one. Since stochastic linearization of asymmetric systems results in not only a gain but also a bias, two loci must be investigated: the usual root locus modified appropriately to account for the quasilinear gain, and a tracking error locus to account for steady state errors. The goals here are:

- introduce a notion of closed loop poles for A-LPNI systems,
- develop the AS-root locus for A-LPNI systems, where "AS" stands for asymmetric saturating,
- develop the TE locus, where "TE" stands for tracking error,
- investigate the properties of these loci and rules for their sketching.

### 1.3.4 Problem 4: Design of step-tracking controllers for LPNI and A-LPNI systems

In classical control, the goal is often to design controllers that track step signals. To this end, specifications are typically based on overshoot, rise time, settling time, etc., of the step response. To design a controller that achieves the specifications, numerous techniques exist if the system is linear. If the system has nonlinear instrumentation, however, this problem has not been solved at any level of generality. The goals here are:

- investigate the possibility of "converting" step tracking specifications into random-signal tracking specifications,
- use the QLC theory to design controllers that track random signals with these specifications,
- explore whether the same controller tracks step signals and satisfies the original step-tracking specifications.

Note that this problem was not addressed in [1]. So the goal here is to address both symmetric and asymmetric cases.

### 1.3.5 Problem 5: Performance recovery in A-LPNI systems

Consider the system of Figure 1.6, where $d$ is a disturbance generated by passing standard Gaussian white noise $w_d$ through the low pass filter $F_{\Omega_d}(s)$. It is desired to design a controller $C(s)$ to achieve good disturbance rejection. A control designer typically ignores the nonlinearities in the actuator and sensor and designs $C(s)$ for the resulting linear system. The same controller implemented on the nonlinear system, however, typically exhibits a degradation in performance as compared with the linear system. Accordingly, the goals are:

- study whether it is possible to recover linear disturbance rejection performance by "boosting" the gain of the controller and introducing a bias at the input of the actuator nonlinearity,
- provide methods for computing the boosting gains and bias.

### 1.3.6 Problem 6: LQR approach for A-LPNI systems

Given a linear system, the LQR method provides an optimal way of selecting a controller that achieves good disturbance rejection. The approach is based on

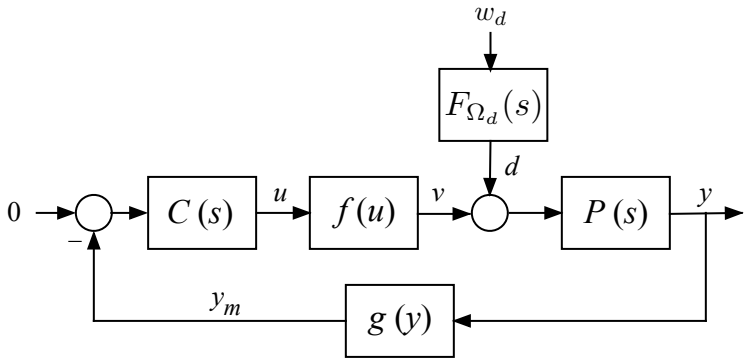


Figure 1.6: System considered for performance recovery.

designing a state feedback controller that minimizes a quadratic cost function. When there are nonlinearities in the instrumentation, however, the controller designed based on linear LQR theory is no longer optimal. In fact, attempting to use cheap control may activate significantly the nonlinearities and lead to poor performance. In [1], an LQR theory (called SLQR, where "S" stands for saturating) is developed for symmetric LPNI systems with saturating actuator. No such method exists for A-LPNI systems. Here, we focus on A-LPNI systems with saturating actuators, and

- develop stochastic linearization of state space models,
- formulate the relevant optimization problem, which accounts for the quasilinear gain and bias,
- provide methods for solving the optimization problem,
- evaluate the performance of the resulting controllers.

This LQR-type problem for asymmetric systems is referred to as A-SLQR, where "A" stands for asymmetric.

## 1.4 Original Contributions

The following contributions have been made by solving the problems addressed in Section 1.3:

### 1.4.1 Contributions to formalism of stochastic linearization in A-LPNI systems

- Stochastic linearization of common nonlinearities in the open loop environment has been developed.
- Equations for the gain and bias of the quasilinear closed loop system have been constructed.
- Conditions for existence of the solutions of these equations have been developed.
- The accuracy of stochastic linearization in the closed loop environment has been characterized.
- A measure of asymmetry has been introduced and the quasilinear gain and bias have been studied as a function of this measure.

### 1.4.2 Contributions to performance analysis in A-LPNI systems

- Stochastic linearization has been successfully employed to study tracking performance of A-LPNI systems. Specifically, it has been shown that the mean and variance of the tracking error in the quasilinear system can be used to study quality of tracking of the A-LPNI system. Moreover, since not all step sizes can be tracked in the presence of saturation, the notions of trackable domain and system types for A-LPNI systems have been developed. The saturating random sensitivity function and quality indicators have been introduced to quantify the quality of tracking. These developments parallel those in the symmetric case.
- Stochastic linearization has been shown to successfully predict disturbance rejection performance of A-LPNI systems. It has been shown that the mean and variance of the output of the quasilinear system can be used for this purpose.

- Stochastic linearization has been used to correctly quantify the phenomenon of noise-induced loss of tracking, which arises in systems with asymmetric saturating actuator, sensor noise, and anti-windup.

### 1.4.3 Contributions to time-domain controller design in A-LPNI systems

- The notion of closed loop poles for A-LPNI systems has been introduced. Similar to the symmetric case, these poles are are poles of the closed loop quasilinear system.

- The AS-root locus has been developed.

- It is shown that a new locus arises in asymmetric systems – the tracking error (TE) locus – which is the locus of the average value of the tracking error as a function of the controller gain.

- The properties of these loci have been investigated and methods for their sketching presented.

### 1.4.4 Contributions to step-tracking controller design in A-LPNI systems

- The step-tracking specifications have been converted to random-signal tracking specifications. The new specifications involve tracking a colored random process with bandwidth determined from the dynamic part of the step-tracking specifications. Using this random reference, the time domain design technique (AS-root locus and TE locus method) is employed to design a controller.

- It has been demonstrated that the same random reference tracking controller, implemented on the original system augmented with a precompensator, tracks step signals and satisfies the original step-tracking specifications.

### 1.4.5 Contributions to performance recovery

- The equations for boosting have been developed.
- It has been shown that if these equations have a solution, and if stochastic linearization is accurate, then the boosted controller performs better than the non-boosted one on the A-LPNI system.

### 1.4.6 Contributions to the A-SLQR technique

- Equations of stochastic linearization in state space form have been developed.
- The A-SLQR problem has been formulated and solved.
- Performance limitations of A-LPNI systems with saturating actuators have been quantified.

### 1.4.7 Application: Wind farms controller design

As mentioned in Section 1.1, a wind turbine can be modeled by an A-LPNI system with asymmetric saturation. In [3], the authors design two controllers for a wind farm consisting of $N$ wind turbines: a model predictive controller on the outer loop, which takes the saturation into account, and an adaptive controller in the inner loop, which ignores the saturation. It is desirable to include saturation in the design of the adaptive controller to obtain better performance of the A-LPNI system. Consequently, to address this issue, we developed:

- equations of stochastic linearization for the wind farm problem,
- formulation of an optimization problem for the adaptive controller,
- demonstration of the efficacy of the controllers obtained.

### 1.4.8 QLC toolbox

As part of this work, a Matlab-based QLC Toolbox has been developed. This toolbox, which is available for download at www.QuasilinearControl.com, could provide control engineers with a convenient means of using the QLC methods. While most of the functions in this toolbox are intended for the symmetric case, the important methods for the asymmetric case are also implemented.

A brief description of each of these functions, along with their syntax and example usage, are included in Appendix B.

## 1.5 Literature Review

In this section, we first briefly review the available literature on stability of A-LPNI systems. Then, the issues of design and performance analysis are reviewed. Finally, we discuss the appropriate literature on the mathematical method used in this work: stochastic linearization.

### 1.5.1 Stability

The issue of stability of both symmetric and asymmetric LPNI systems has been extensively studied in the literature. One of the most important works in this area is the theory of absolute stability ([7–12]), where stability of the closed loop system is established using, for example, sector conditions. A modern description of absolute stability can be found in [13]. Other works typically consider specific nonlinearities for actuators and sensors. In [14], the authors consider a system with saturating actuator in the framework of absolute stability. The works [15–18] study semi-global stability of LPNI systems with saturating actuators and linear feedback. The authors of [19] examine stability of pole-placement algorithms in systems with actuator saturation. In [20–22], the authors consider LMI methods to establish stability and region of

attraction. A thorough review of LPNI systems with saturating actuators is presented in the survey paper [23]. The issue of stability of A-LPNI systems with asymmetric actuator saturation is addressed in [24]. The authors of [25] consider stability of systems with deadzone in the actuator. In [26–30], the issue of stability of systems with sensor nonlinearities is addressed.

As reviewed above, stability analysis of LPNI systems has been studied extensively in the literature; however, the problems of performance analysis and controller design have received less attention [23, 31, 32]. For this reason, we do not pursue the issue of stability of these systems in this work. Instead, we focus on performance analysis and controller design. Indeed, while the controllers resulting from our methods ensure the desired dynamic and steady state performance of quasilinear systems, stability properties of A-LPNI systems with these controllers can be ascertained using the usual methods mentioned above.

### 1.5.2 Performance analysis and design in A-LPNI systems

Many works in the area of nonlinear control (see, e.g., [33, 13]) consider nonlinear differential equations of the form

$$\dot{x} = f(x) + g(x)u,$$

where $u$ enters the differential equation in an affine manner and $g(x)$ takes into account the effects of the actuator. Feedback linearization [34, 35, 13], for example, can be used to stabilize systems of this type. However, in A-LPNI systems considered in this work, $u$ does not enter in an affine manner and, therefore, LPNI systems cannot be studied in this framework.

For the issue of performance recovery and controller design, the main available methods can be classified into two approaches: anti-windup (see, e.g., [36–41]), and

model predictive/governor (see, e.g., [42–48]) approach. Within the former, a controller is designed without taking into account the saturation, and then the design is improved by using an anti-windup scheme. In the latter, the controller is designed on a receding horizon by solving an online optimization problem. In contrast to these methods, the approach here takes into account the actuator saturation at the initial stage of the design. Moreover, the controllers designed using our methods are all computed offline and have the same computational complexity as linear controllers.

Other approaches to control design of systems with actuator saturation are $\mathcal{L}_1$ analysis and synthesis techniques [49] and gain scheduling [50, 51]. In the former, actuator saturation is handled as a constraint in an optimization problem, while in the latter, the authority of the control is increased as the state of the system converges to the origin to improve system performance.

In the current work, performance analysis and design is performed by analyzing the system dynamics excited by random exogenous signals. For the problem of disturbance rejection, this can be done by means of the Fokker-Planck equation [52], which provides the stationary probability distribution of the signals in the loop. However, while solvable for low-order systems [53], Fokker-Planck equations are typically difficult to solve for high order systems. In the latter case, the method of stochastic linearization may be used to characterize the first and second moments of the relevant signals in the loop. A literature review of the method of stochastic linearization is provided in the next subsection.

### 1.5.3 Stochastic linearization

As mentioned in Section 1.1, the main tool used in this work is stochastic linearization, which replaces all nonlinearities with affine functions. In this sense, stochastic linearization is analogous to the well-known method of describing functions [54–56, 13]. However, the two methods are fundamentally different: the main focus of

describing functions is to study limit cycles in LPNI systems or periodic response of LPNI systems to periodic excitations, while the main focus of stochastic linearization is to study dynamics of LPNI systems driven by random signals.

Two of the earliest papers on stochastic linearization are [57] and [58] published in 1954. Since then, many authors have used stochastic linearization to study the behavior of nonlinear systems driven by random excitations (see, e.g., [59, 55, 6, 1]). Works [59, 55] include pioneering applications of stochastic linearization to feedback systems. A complete description of stochastic linearization appears in [6], in which stochastic linearization has been referred to as statistical linearization. In early work [1], stochastic linearization has been used for symmetric LPNI systems to study performance analysis and controller design.

Typically, the random excitations are assumed to be Gaussian since this assumption is both practical and simplifying. In the current work, we also assume that the signals are Gaussian. Some authors have examined other distributions as well (see, e.g., [60–62]).

The issue of open-loop accuracy of stochastic linearization has also been addressed in the literature (see, e.g., [63]). In our early work, [1], we addressed the issue of closed loop accuracy; however, the focus there is on symmetric systems, not asymmetric ones. In Chapter II of this work, we address the issue of accuracy of stochastic linearization in asymmetric systems.

## 1.6 Statement of Impact

The developed quasilinear control theory for A-LPNI systems has both theoretical significance and practical implications. Indeed, there are many applications in which A-LPNI systems arise. Examples in heating systems, xerography, wind farms, and aviation have already been provided in Section 1.1. The methods developed in this work can assist a control engineer to better predict the performance of such systems

and design controllers to satisfy given specifications. Furthermore, the QLC Toolbox could aid the engineer in applying the QLC methods to both S- and A-LPNI systems. It should be noted that all methods are systematic and proper extensions of linear control theory, which is a familiar subject to control engineers. Furthermore, the methods require only off-line computations, which greatly simplifies controller implementation.

## 1.7 Dissertation Outline

The outline of this dissertation is as follows. Chapter II presents the formalism of stochastic linearization for A-LPNI systems. In Chapter III, methods for analysis of reference tracking and disturbance rejection are developed and illustrated. Chapter IV introduces the performance loci for A-LPNI systems and utilizes them for controller design. Chapter V presents a method for designing step-tracking controllers. In Chapter VI, the problem of linear performance recovery by A-LPNI systems is discussed. Chapter VII solves the A-SLQR problem. In Chapter VIII, the developed theory is applied to controller design of a wind farm consisting of multiple wind turbines. The conclusions and future work are outlined in Chapter IX. All proofs are included in Appendix A. In Appendix B, the QLC Toolbox functions and their usage are summarized.

# CHAPTER II

# Stochastic Linearization for A-LPNI Systems

This chapter presents the main mathematical tool of this work, namely the method of stochastic linearization. First, the formalism of stochastic linearization in the open loop environment is presented. It is shown that, unlike the symmetric case, stochastic linearization in the asymmetric case results in not only an equivalent (or quasilinear) gain, but also a bias. Second, stochastic linearization in the closed loop environment is described and equations for computing the quasilinear gains and biases in the closed loop environment are provided. Third, the accuracy of stochastic linearization is discussed. It is shown that, even though accuracy in the asymmetric case is lower than the symmetric case, stochastic linearization still results in faithful prediction of first and second moments of the signals in the original LPNI system. Finally, the notion of asymmetry is formally introduced, and a measure for quantifying the degree of asymmetry is presented. The quasilinear gain and bias are studied with respect to this measure of asymmetry.

## 2.1 Open Loop Environment

### 2.1.1 General equations

Consider Figure 2.1, where $u_0(t)$ is a zero-mean wide-sense stationary (WSS) Gaussian process with standard deviation $\sigma_u$, $\mu_u$ a constant, and $f(u)$ a piece-wise

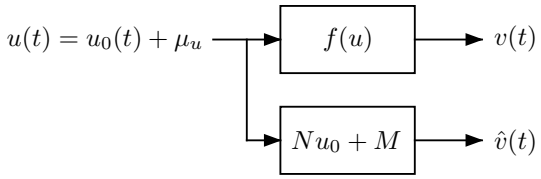


Figure 2.1: Stochastic linearization of an isolated nonlinearity.

differentiable function. Clearly, $u(t)$ is a WSS Gaussian process with mean $\mu_u$ and standard deviation $\sigma_u$. The problem of stochastic linearization is concerned with approximating $v(t) = f(u(t))$ by $\hat{v}(t) = Nu_0(t) + M$, where $N$ and $M$ are constants, such that the functional

$$\epsilon(N, M) := E\left[(v(t) - \hat{v}(t))^2\right] \tag{2.1}$$

is minimized. The solution of this problem is given by:

**Theorem II.1.** *If $f(u) : \mathbb{R} \to \mathbb{R}$ is piecewise differentiable, $u_0(t)$ is a zero-mean WSS Gaussian process, and $u(t) = u_0(t) + \mu_u$, functional* (2.1) *is minimized by*

$$N = E\left[f'(u)|_{u=u(t)}\right], \tag{2.2}$$

$$M = E\left[f(u)|_{u=u(t)}\right]. \tag{2.3}$$

*Proof.* See [6] Chapter 5. □

For the sake of convenience, we denote the right hand sides of (2.2) and (2.3) by $\mathcal{F}_N(\sigma_u, \mu_u)$ and $\mathcal{F}_M(\sigma_u, \mu_u)$, respectively, i.e.,

$$\mathcal{F}_N(\sigma_u, \mu_u) = \int_{-\infty}^{\infty} \frac{\frac{d}{dx}f(x)}{\sqrt{2\pi}\sigma_u} \exp\left(-\frac{(x-\mu_u)^2}{2\sigma_u^2}\right) dx, \tag{2.4}$$

$$\mathcal{F}_M(\sigma_u, \mu_u) = \int_{-\infty}^{\infty} \frac{f(x)}{\sqrt{2\pi}\sigma_u} \exp\left(-\frac{(x-\mu_u)^2}{2\sigma_u^2}\right) dx. \tag{2.5}$$

Note that the block diagram of Figure 2.1 can be equivalently represented as

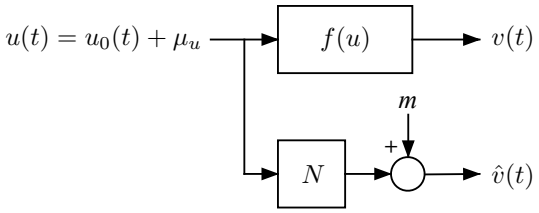


Figure 2.2: Alternative representation of Figure 2.1.

shown in Figure 2.2, where

$$m = M - N\mu_u. \tag{2.6}$$

This representation, which is used throughout this work, is more convenient in the closed loop environment because $N$ multiplies $u$, not $u_0$. The gain $N(\sigma_u, \mu_u)$ and bias $m(\sigma_u, \mu_u)$ are referred to as the *quasilinear gain* and *quasilinear bias*, respectively.

The following corollary is a direct consequence of Theorem 1.

**Corollary II.1.** *Let $f_1(u)$, $f_2(u)$, and $f_3(u)$ be piece-wise differentiable functions with stochastic linearization given by $N_{f_1}(\sigma_u, \mu_u), M_{f_1}(\sigma_u, \mu_u)$, $N_{f_2}(\sigma_u, \mu_u), M_{f_2}(\sigma_u, \mu_u)$, and $N_{f_3}(\sigma_u, \mu_u), M_{f_3}(\sigma_u, \mu_u)$, respectively, and let $a$ and $b$ be real constants. Then, the following holds:*

*(a) If $f_3(u) = f_1(u) + f_2(u)$, then $N_{f_3} = N_{f_1} + N_{f_2}$ and $M_{f_3} = M_{f_1} + M_{f_2}$.*

*(b) If $f_3(u) = af_1(u) + b$, then $N_{f_3} = aN_{f_1}$ and $M_{f_3} = aM_{f_1} + b$.*

*(c) If $f_3(u) = f_1(au + b)$, then $N_{f_3}(\sigma_u, \mu_u) = N_{f_1}(|a|\sigma_u,\, a\mu_u + b)$ and $M_{f_3}(\sigma_u, \mu_u) = M_{f_1}(|a|\sigma_u,\, a\mu_u + b)$.*

*(d) If $f_3(u) = au + b$, then $N_{f_3} = a$ and $M_{f_3} = a\mu_u + b$.*

*(e) If $f_3(u)$ is odd with respect to $\mu_u$, i.e., $f_3(\mu_u - u) = -f_3(\mu_u + u)$, then $M_{f_3} = \mu_u$.*

Note that, according to parts (b) and (c) of the above corollary, the quasilinear gain of $f(au)$ and $af(u)$ are not the same. For this reason, we call $N$ the quasilinear gain, rather than linear gain, of $f$. Similar arguments apply to the quasilinear bias.

### 2.1.2 Stochastic linearization of common nonlinearities

Using (2.2) and (2.3), we derive explicit expressions for $N$ and $M$ for common nonlinearities below.

- *Saturation:* The saturation function is depicted in Figure 2.3.1 and is given by

$$\text{sat}_\alpha^\beta(u) = \begin{cases} \beta, & u > \beta, \\ u, & \alpha \leq u \leq \beta, \\ \alpha, & u < \alpha, \end{cases} \tag{2.7}$$

where $\beta > \alpha$. If $\alpha = -\beta$, the saturation function is odd, otherwise it is not. Since

$$\frac{d}{du}\text{sat}_\alpha^\beta(u) = \begin{cases} 1, & \alpha < u < \beta, \\ 0, & u < \alpha \text{ or } u > \beta, \end{cases}$$

using (2.2) and (2.3), it follows that

$$N = \mathcal{F}_N(\sigma_u, \mu_u) = \frac{1}{2}\left[\text{erf}\left(\frac{\beta - \mu_u}{\sqrt{2}\sigma_u}\right) - \text{erf}\left(\frac{\alpha - \mu_u}{\sqrt{2}\sigma_u}\right)\right], \tag{2.8}$$

$$M = \mathcal{F}_M(\sigma_u, \mu_u) = \frac{\alpha + \beta}{2} + \frac{\mu_u - \beta}{2}\text{erf}\left(\frac{\beta - \mu_u}{\sqrt{2}\sigma_u}\right) - \frac{\mu_u - \alpha}{2}\text{erf}\left(\frac{\alpha - \mu_u}{\sqrt{2}\sigma_u}\right) - \frac{\sigma_u}{\sqrt{2\pi}}\left[\exp\left(-(\frac{\beta - \mu_u}{\sqrt{2}\sigma_u})^2\right) - \exp\left(-(\frac{\alpha - \mu_u}{\sqrt{2}\sigma_u})^2\right)\right], \tag{2.9}$$

where

$$\text{erf}(x) = \frac{2}{\sqrt{\pi}}\int_0^x e^{-t^2}dt \tag{2.10}$$

is the error function. Note that with $f(u) = \text{sat}_\alpha^\beta(u)$, (2.2) implies that $N = P\{\alpha \leq u \leq \beta\}$, i.e., $N$ is the probability that saturation does not take place. As a result, assuming that $\sigma_u \neq 0$, $N$ satisfies $0 < N < 1$. Furthermore, since $M = E[f(u)]$, it satisfies $\alpha < M < \beta$.

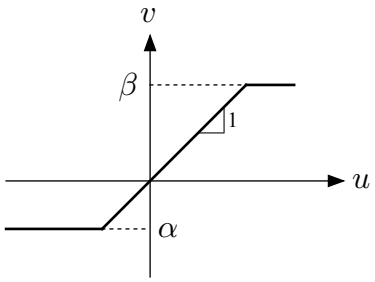


2.3.1: Saturation nonlinearity.

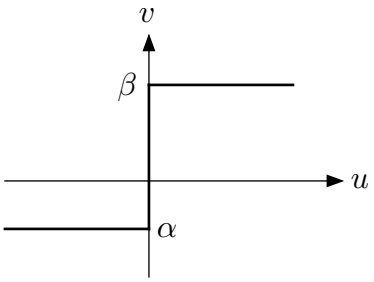


2.3.2: Relay nonlinearity.

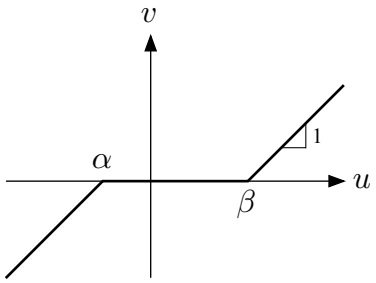


2.3.3: Deadzone nonlinearity.

Figure 2.3: Common piece-wise differentiable functions.

Since the saturation function is the main nonlinearity considered in this work, we provide below some additional properties.

**Proposition II.1.** *Consider* $v = \text{sat}_{\alpha}^{\beta}(u)$ *with stochastic linearization given by* $\hat{v} = Nu_0 + M$*, where* $u_0$ *is the zero-mean part of* $u$*, and let* $\mu_{(\cdot)}$ *and* $\sigma_{(\cdot)}$ *represent expected value and standard deviation, respectively. Then,*

1. *For a fixed* $\sigma_u$*,* $N$ *is maximized when* $\mu_u = \frac{\alpha+\beta}{2}$*;*
2. $N < \frac{\beta-\alpha}{\sqrt{2\pi}\sigma_u}$*;*
3. $\sigma_{\hat{v}} < \frac{\beta-\alpha}{2}$*;*
4. $\exists\ 0 < m^* < \infty$ *such that* $\forall\ \sigma_u \in \mathbb{R}^+$ *and* $\mu_u \in \mathbb{R}$*,* $m < m^*$*, where* $m$ *is given by* (2.6)*;*
5. $\mu_u = \frac{\alpha+\beta}{2} \iff \mu_v = \frac{\alpha+\beta}{2}$*;*

*6.* $\lim_{\sigma_u \to 0} N = \begin{cases} 1, & \alpha < \mu_u < \beta, \\ 0.5, & \mu_u = \alpha \text{ or } \mu_u = \beta, \\ 0, & \text{otherwise;} \end{cases}$

*7.* $\lim_{\sigma_u \to 0} M = \lim_{\sigma_u \to 0} \mu_v = \begin{cases} \mu_u, & \alpha \leq \mu_u \leq \beta, \\ \beta, & \mu_u > \beta, \\ \alpha, & \mu_u < \alpha; \end{cases}$

*Proof.* See Section A.1. □

- *Relay:* For the relay function (see Figure 2.3.2),

$$\text{rel}_{\alpha}^{\beta}(u) = \begin{cases} \beta, & u \geq 0, \\ \alpha, & u < 0, \end{cases} \tag{2.11}$$

the derivative is given by $(\beta - \alpha)\delta(u)$. Therefore, employing equations (2.2) and (2.3), we have:

$$N = \mathcal{F}_N(\sigma_u, \mu_u) = \frac{\beta - \alpha}{\sqrt{2\pi}\sigma_u} \exp\left(-(\frac{\mu_u}{\sqrt{2}\sigma_u})^2\right), \tag{2.12}$$

$$M = \mathcal{F}_M(\sigma_u, \mu_u) = \frac{\alpha + \beta}{2} + \frac{\beta - \alpha}{2} \text{erf}\left(\frac{\mu_u}{\sqrt{2}\sigma_u}\right). \tag{2.13}$$

From the above expressions, assuming that $\sigma_u \neq 0$, it follows that $N > 0$ and $\alpha < M < \beta$.

- *Deadzone:* Consider the deadzone nonlinearity (see Figure 2.3.3) given by

$$\text{dz}_{\alpha}^{\beta}(u) = \begin{cases} u - \beta, & u > \beta, \\ 0, & \alpha \leq u \leq \beta, \\ u - \alpha, & u < \alpha. \end{cases} \tag{2.14}$$

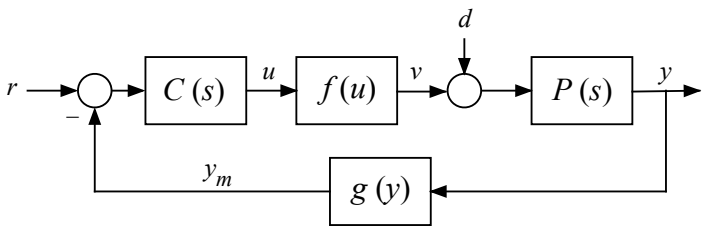


Figure 2.4: Closed loop LPNI system.

Using Corollary 1 and the fact that $\mathrm{dz}_\alpha^\beta(u) = u - \mathrm{sat}_\alpha^\beta(u)$, it follows that

$$N = 1 - N_{sat}, \tag{2.15}$$

$$M = \mu_u - M_{sat}, \tag{2.16}$$

where $N_{sat}$ and $M_{sat}$ are the quasilinear gain and bias for the saturation function as defined in (2.8) and (2.9). Note that $N = P\{u > \beta \text{ or } u < \alpha\}$, and as a result, $0 < N < 1$.

## 2.2 Closed Loop Environment

Consider the closed loop system of Figure 2.4, where $P(s)$ and $C(s)$ are the plant and the controller, respectively, $f(u)$ and $g(y)$ are piece-wise differentiable functions representing the actuator and sensor, respectively, $r$ and $d$ are the reference and the disturbance, respectively, and $u$, $v$, $y$, and $y_m$ are the controller output, actuator output, plant output, and measured output, respectively. The goal is to develop a method for performance analysis of this system using stochastic linearization. To accomplish this, we assume that $r(t)$ and $d(t)$ are random processes obtained by filtering the signals $w_r(t)$ and $w_d(t)$ (see Figure 2.5.1) through filters $F_{\Omega_r}(s)$ (with $\|F_{\Omega_r}(s)\|_2 = 1$) and $F_{\Omega_d}(s)$ (with $\|F_{\Omega_d}(s)\|_2 = 1$), respectively, where $w_r(t)$ and $w_d(t)$ are independent standard Gaussian white noise processes and $\|\cdot\|_2$ denotes the $H_2$ norm. The outputs of the filters are then scaled by $\sigma_r$ and $\sigma_d$ and shifted by $\mu_r$ and

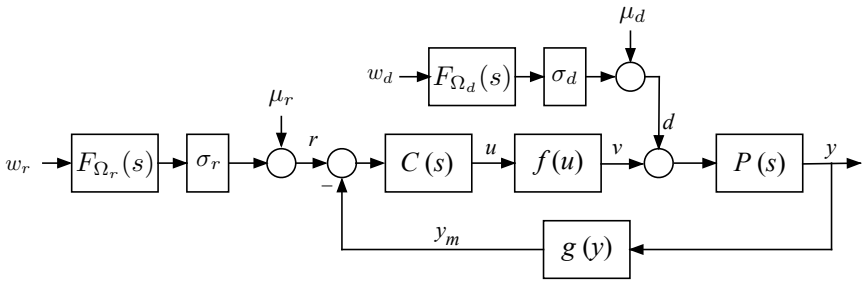


2.5.1: Closed loop LPNI system driven by white noise processes.

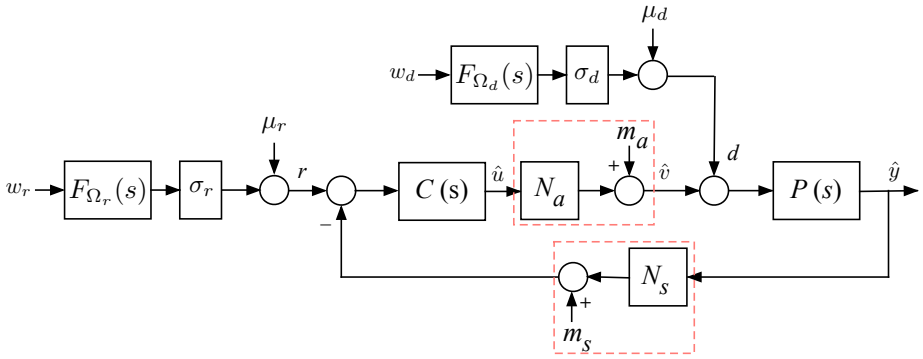


2.5.2: Stochastic linearization of the LPNI system

Figure 2.5: LPNI system and its stochastic linearization.

$\mu_d$ to generate $r(t)$ and $d(t)$. Clearly, $r(t)$ and $d(t)$ have standard deviations $\sigma_r$ and $\sigma_d$, expected values $\mu_r$ and $\mu_d$, and power spectral densities determined by $F_{\Omega_r}(s)$ and $F_{\Omega_d}(s)$, respectively. Applying stochastic linearization to the system of Figure 2.5.1 and using the representation of Figure 2.2, we obtain the *quasilinear* system of Figure 2.5.2, where

$$\begin{aligned} N_a &= E\left[f'(\hat{u})|_{\hat{u}=\hat{u}(t)}\right], \quad N_s = E\left[g'(\hat{y})|_{\hat{y}=\hat{y}(t)}\right], \\ M_a &= E\left[f(\hat{u})|_{\hat{u}=\hat{u}(t)}\right], \quad M_s = E\left[g(\hat{y})|_{\hat{y}=\hat{y}(t)}\right], \\ m_a &= M_a - N_a\mu_{\hat{u}}, \qquad m_s = M_s - N_s\mu_{\hat{y}}, \end{aligned} \tag{2.17}$$

and $\mu_{\hat{u}}$ and $\mu_{\hat{y}}$ are the expected values of $\hat{u}$ and $\hat{y}$, respectively. Note that stochastic linearization in the closed loop environment is different from that in the open loop environment in two respects. First, the signal at the input of the nonlinearity is not necessarily a Gaussian process. Second, signals $u$ and $\hat{u}$ are not the same. Therefore,

stochastic linearization of closed loop systems is sub-optimal. In Section 2.3, we address the accuracy of this approximation.

To evaluate (2.17), the standard deviations of $\hat{u}$ and $\hat{y}$ (denoted by $\sigma_{\hat{u}}$ and $\sigma_{\hat{y}}$), and the expected values $\mu_{\hat{u}}$ and $\mu_{\hat{y}}$ are required. To discuss how these quantities can be obtained, we first address the case of nonlinear actuators and sensors separately and then the case of nonlinearities in both actuators and sensors simultaneously.

### 2.2.1 Reference tracking with nonlinear actuator

Consider the closed loop system of Figure 2.5.1 with $d(t) = 0$ and $g(y) = y$, i.e., a linear sensor. Note that, since $g(y) = y$, Corollary 1 implies that $N_s = 1$ and $M_s = \mu_{\hat{y}}$, which results in $m_s = 0$.

Assuming that the system is operating in the stationary regime, the standard deviation $\sigma_{\hat{u}}$ can be evaluated as the $H_2$-norm of the transfer function from $w_r$ to $\hat{u}$:

$$\sigma_{\hat{u}} = \left\| \frac{F_{\Omega_r}(s)C(s)}{1 + P(s)N_aC(s)} \right\|_2 \sigma_r = \left( \sqrt{\frac{1}{2\pi} \int_{-\infty}^{\infty} \left| \frac{F_{\Omega_r}(jw)C(jw)}{1 + P(jw)N_aC(jw)} \right|^2 dw} \right) \sigma_r. \tag{2.18}$$

To derive an expression for the mean $\mu_{\hat{u}}$, note that stochastic linearization requires $E[v] = E[\hat{v}] = M_a$. As a result, $\mu_{\hat{u}}$ satisfies:

$$\mu_{\hat{u}} = C_0(\mu_r - P_0E[\hat{v}]) = C_0(\mu_r - P_0M_a), \tag{2.19}$$

where $C_0$ and $P_0$ are the DC gains of $C(s)$ and $P(s)$, respectively. As it turns out, to account for cases where either $P_0 = \infty$ or $C_0 = \infty$, it is more convenient to rewrite (2.19) as:

$$M_a = \frac{\mu_r}{P_0} - \frac{1}{C_0P_0}\mu_{\hat{u}}. \tag{2.20}$$

Substituting $M_a$ into (2.17) and using (2.18), we obtain the following system of equations for $\mu_{\hat{u}}$ and $N_a$:

$$N_a - \mathcal{F}_N(\left\| \frac{F_{\Omega_r}(s)C(s)}{1+P(s)N_aC(s)} \right\|_2 \sigma_r, \mu_{\hat{u}}) = 0, \tag{2.21}$$

$$\frac{\mu_r}{P_0} - \frac{\mu_{\hat{u}}}{C_0P_0} - \mathcal{F}_M(\left\| \frac{F_{\Omega_r}(s)C(s)}{1+P(s)N_aC(s)} \right\|_2 \sigma_r, \mu_{\hat{u}}) = 0, \tag{2.22}$$

where $\mathcal{F}_N$ and $\mathcal{F}_M$ are given in (2.4) and (2.5), respectively. Once (2.21) and (2.22) are solved, $M_a$ can be computed from (2.20) and $m_a$ can be found using (2.17):

$$m_a = \frac{\mu_r}{P_0} - (\frac{1}{C_0P_0} + N_a)\mu_{\hat{u}}.$$

These equations are used in this work for analysis and design of reference tracking systems.

The issue of the existence of solutions is considered next.

**Theorem II.2.** *Let $\mathscr{M}_a$ denote the range of $M_a$ and assume that either $C_0 = \infty$ or $P_0 = \infty$. Then, a necessary condition for* (2.21), (2.22) *to have a solution is:*

$$\frac{\mu_r}{P_0} \in \mathscr{M}_a. \tag{2.23}$$

*Proof.* See Section A.1. □

Clearly, for symmetric nonlinearities and $\mu_r = 0$, condition (2.23) is always met (because $0 \in \mathscr{M}_a$). For asymmetric nonlinearities, however, this is not always the case. For instance, if $P_0 = \infty$, (2.23) becomes $0 \in \mathscr{M}_a$, which, in turn, implies that for a "fully" asymmetric saturation, i.e., $\text{sat}_0^\beta(u)$, (2.23) does not hold. Similarly, if $P_0 < \infty$ but $C_0 = \infty$ and $\mu_r = 0$, for the fully saturating actuator, the condition again is not satisfied.

A sufficient condition for the existence of solutions of (2.21), (2.22) is given below.

**Theorem II.3.** *Let the range of $N_a$ be denoted by $\mathscr{N}_a$ and the range of $M_a$, as before, $\mathscr{M}_a$. Assume that the following holds:*

*1. $1 + \gamma P(s)C(s)$ has all zeros in the open left half plane for all $\gamma \in \mathscr{N}_a$;*

*2. The ranges $\mathscr{N}_a$ and $\mathscr{M}_a$ are bounded connected sets;*

*3. If $C_0 = \infty$ or $P_0 = \infty$, condition (2.23) holds.*

*Then, the system of equations (2.21), (2.22) has a solution.*

*Proof.* See Section A.1. □

Note that the first condition in Theorem II.3 implies that both $P(s)$ and $C(s)$ have all poles in the closed left half plane.

While Theorem II.3 guarantees existence of a solution, it does not guarantee its uniqueness. In fact, system (2.21), (2.22) may have multiple solutions. If (2.21), (2.22) has more than one solution, similar to the symmetric case, the system typically exhibits the undesirable "jumping phenomenon" [1]. In this situation, the controller must be modified to avoid this behavior.

Solutions of (2.21), (2.22) may be found using a plethora of numerical techniques, e.g., the 2-variable bisection algorithm. In the Matlab computational environment, the "fsolve" function provides a convenient method for solving this system.

### 2.2.2 Disturbance rejection with nonlinear actuator

Consider the closed loop system of Figure 2.5.1 with $r(t) = 0$ and $g(y) = y$, i.e., a linear sensor. Note that, similar to Subsection 2.2.1, $N_s = 1$, $M_s = \mu_{\hat{y}}$, and $m_s = 0$. In this subsection, we derive expressions for $\sigma_{\hat{u}}$ and $\mu_{\hat{u}}$ for this system. Assuming that the system is operating in the stationary regime, $\sigma_{\hat{u}}$ can be obtained from the $H_2$-norm of the transfer function from $w_d$ to $\hat{u}$:

$$\sigma_{\hat{u}} = \left\| \frac{F_{\Omega_d}(s)P(s)C(s)}{1 + P(s)N_aC(s)} \right\|_2 \sigma_d. \tag{2.24}$$

To compute $\mu_{\hat{u}}$, we follow a procedure similar to Subsection 2.2.1 and obtain $\mu_{\hat{u}} = -C_0P_0(M_a + \mu_d)$. Rewriting this in terms of $M_a$, we obtain:

$$M_a = -\mu_d - \frac{1}{C_0P_0}\mu_{\hat{u}}.$$

Using the above expressions for $M_a$ and $\sigma_{\hat{u}}$, we obtain the following system of equations:

$$\begin{aligned} &N_a - \mathcal{F}_N(\left\| \frac{F_{\Omega_d}(s)P(s)C(s)}{1+P(s)N_aC(s)} \right\|_2 \sigma_d, \mu_{\hat{u}}) = 0, \\ &-\mu_d - \frac{1}{C_0P_0}\mu_{\hat{u}} - \mathcal{F}_M(\left\| \frac{F_{\Omega_d}(s)P(s)C(s)}{1+P(s)N_aC(s)} \right\|_2 \sigma_d, \mu_{\hat{u}}) = 0, \end{aligned} \tag{2.25}$$

where $\mathcal{F}_N$ and $\mathcal{F}_M$ are as in (2.4) and (2.5), respectively, and the unknowns are $\mu_{\hat{u}}$ and $N_a$. These equations are used in Subsection 3.2 for the analysis of disturbance rejection of LPNI systems.

For this case, Theorems II.2 and II.3 also hold, except that the necessary condition (2.23) must be modified to $-\mu_d \in \mathscr{M}_a$.

### 2.2.3 Reference tracking with nonlinear sensor

Consider the closed loop system of Figure 2.5.1 with $d = 0$ and $f(u) = u$, i.e., a linear actuator. Note that, since $f(u) = u$, Corollary 1 implies that $N_a = 1$ and $M_a = \mu_{\hat{u}}$, which results in $m_a = 0$. By following a procedure similar to the case of nonlinear actuator, the following equations can be derived:

$$\begin{aligned} N_s - \mathcal{G}_N(\left\| \frac{F_{\Omega_r}(s)C(s)P(s)}{1+P(s)N_sC(s)} \right\|_2 \sigma_r, \mu_{\hat{y}}) = 0, \\ \mu_r - \frac{\mu_{\hat{y}}}{C_0P_0} - \mathcal{G}_M(\left\| \frac{F_{\Omega_r}(s)C(s)P(s)}{1+P(s)N_sC(s)} \right\|_2 \sigma_r, \mu_{\hat{y}}) = 0, \end{aligned}$$

where $\mathcal{G}_N$ and $\mathcal{G}_M$ are the same as $\mathcal{F}_N$ and $\mathcal{F}_M$ in (2.4) and (2.5), except that $f(\cdot)$ is replaced by $g(\cdot)$.

### 2.2.4 Disturbance rejection with nonlinear sensor

Consider the closed loop system of Figure 2.5.1 with $r = 0$ and $f(u) = u$, i.e., a linear actuator. Similar to Subsection 2.2.3, this implies that $N_a = 1$, $M_a = \mu_{\hat{u}}$, and $m_a = 0$. By following a procedure similar to the previous subsections, the following equations in $N_s$ and $\mu_{\hat{y}}$ can be derived:

$$\begin{aligned} N_s - \mathcal{G}_N(\left\| \frac{F_{\Omega_d}(s)P(s)}{1 + P(s)N_sC(s)} \right\|_2 \sigma_d, \mu_{\hat{y}}) &= 0, \\ \frac{\mu_d}{C_0} - \frac{\mu_{\hat{y}}}{C_0P_0} - \mathcal{G}_M(\left\| \frac{F_{\Omega_d}(s)P(s)}{1 + P(s)N_sC(s)} \right\|_2 \sigma_d, \mu_{\hat{y}}) &= 0, \end{aligned}$$

where $\mathcal{G}_N$ and $\mathcal{G}_M$ are the same as $\mathcal{F}_N$ and $\mathcal{F}_M$ in (2.4) and (2.5), except that $f(\cdot)$ is replaced by $g(\cdot)$.

### 2.2.5 Reference tracking with nonlinear actuator and nonlinear sensor

Consider the closed loop system of Figure 2.5.1 with $d = 0$ and both nonlinearities present. Similar to the previous cases, since $\mu_{\hat{u}} = C_0(\mu_r - M_s)$ and $\mu_{\hat{y}} = P_0M_a$, the following equations in the unknowns $N_a$, $N_s$, $\mu_{\hat{u}}$, and $\mu_{\hat{y}}$ can be derived:

$$\begin{aligned} N_a - \mathcal{F}_N(\left\| \frac{F_{\Omega_r}(s)C(s)}{1 + P(s)N_aN_sC(s)} \right\|_2 \sigma_r, \mu_{\hat{u}}) &= 0, \\ N_s - \mathcal{G}_N(\left\| \frac{F_{\Omega_r}(s)C(s)N_aP(s)}{1 + P(s)N_aN_sC(s)} \right\|_2 \sigma_r, \mu_{\hat{y}}) &= 0, \\ \frac{\mu_{\hat{y}}}{P_0} - \mathcal{F}_M(\left\| \frac{F_{\Omega_r}(s)C(s)}{1 + P(s)N_aN_sC(s)} \right\|_2 \sigma_r, \mu_{\hat{u}}) &= 0, \\ \mu_r - \frac{\mu_{\hat{u}}}{C_0} - \mathcal{G}_M(\left\| \frac{F_{\Omega_r}(s)C(s)N_aP(s)}{1 + P(s)N_aN_sC(s)} \right\|_2 \sigma_r, \mu_{\hat{y}}) &= 0, \end{aligned} \tag{2.26}$$

where $\mathcal{F}_N$ and $\mathcal{F}_M$ are as in (2.4) and (2.5), respectively, and $\mathcal{G}_N$ and $\mathcal{G}_M$ are the same as $\mathcal{F}_N$ and $\mathcal{F}_M$ in (2.4) and (2.5), except that $f(\cdot)$ is replaced by $g(\cdot)$. The modified version of Theorem II.3 for this case is given below:

**Theorem II.4.** *Let the ranges of $N_a$, $N_s$, and $N_aN_s$ be denoted by $\mathscr{N}_a$, $\mathscr{N}_s$ and $\mathscr{N}_{as}$,*

*respectively, and the ranges of $M_a$ and $M_s$ be denoted by $\mathscr{M}_a$ and $\mathscr{M}_s$, respectively. Then, system* (2.26) *has a solution if the following holds:*

1. *$1+\gamma P(s)C(s)$ has all zeros in the open left half plane for all $\gamma \in \mathscr{N}_{as}$.*

2. *The ranges $\mathscr{N}_a$, $\mathscr{N}_s$, $\mathscr{M}_a$, and $\mathscr{M}_s$ are all bounded and connected sets;*

3. *If $C_0 = \infty$ then $\mu_r \in \mathscr{M}_s$, and if $P_0 = \infty$ then $0 \in \mathscr{M}_a$.*

*Proof.* The proof is similar to the proof of Theorem II.3. □

### 2.2.6 Disturbance rejection with nonlinear actuator and nonlinear sensor

Consider the closed loop system of Figure 2.5.1 with $r = 0$ and both nonlinearities present. Similar to the previous case, the following equations can be derived:

$$\begin{aligned}
N_a - \mathcal{F}_N(\left\| \frac{F_{\Omega_d}(s)P(s)C(s)N_s}{1+P(s)N_aN_sC(s)} \right\|_2 \sigma_d, \mu_{\hat{u}}) &= 0,\\
N_s - \mathcal{G}_N(\left\| \frac{F_{\Omega_d}(s)P(s)}{1+P(s)N_aN_sC(s)} \right\|_2 \sigma_d, \mu_{\hat{y}}) &= 0,\\
-\mu_d + \frac{\mu_{\hat{y}}}{P_0} - \mathcal{F}_M(\left\| \frac{F_{\Omega_d}(s)P(s)C(s)N_s}{1+P(s)N_aN_sC(s)} \right\|_2 \sigma_d, \mu_{\hat{u}}) &= 0,\\
-\frac{\mu_{\hat{u}}}{C_0} - \mathcal{G}_M(\left\| \frac{F_{\Omega_d}(s)P(s)}{1+P(s)N_aN_sC(s)} \right\|_2 \sigma_d, \mu_{\hat{y}}) &= 0.
\end{aligned}$$

### 2.2.7 Simultaneous reference tracking and disturbance rejection with nonlinear actuator and nonlinear sensor

Consider the closed loop system of Figure 2.5.1, where both $r(t)$ and $d(t)$ are non-zero. In this subsection, we consider the general case of simultaneous nonlinear actuator and sensor and derive the equations for stochastic linearization of this system.

To obtain the standard deviations $\sigma_{\hat{u}}$ and $\sigma_{\hat{y}}$, assume that $\{A_p, b_p, c_p\}$, $\{A_c, b_c, c_c\}$, $\{A_r, b_r, c_r\}$, and $\{A_d, b_d, c_d\}$ are minimal realizations of $P(s)$, $C(s)$, $F_{\Omega_r}(s)$, and $F_{\Omega_d}(s)$, respectively. Moreover, let $x_p$, $x_c$, $x_r$, and $x_d$ denote the states of $P(s)$,

$C(s)$, $F_{\Omega_r}(s)$, and $F_{\Omega_d}(s)$, respectively, $x_G = [x_p^T\ x_c^T\ x_r^T\ x_d^T]^T$, $w = [w_r\ w_d]^T$, $m = [m_a\ -m_s]^T$, and $\mu = [\mu_d\ \mu_r]^T$. Then, the stochastically linearized closed loop system of Figure 2.5.2 can be represented as

$$\begin{aligned}
\dot{\hat{x}}_G &= A_G\hat{x}_G + B_G w + B_1(m+\mu),\\
\hat{u} &= c_1\hat{x}_G,\\
\hat{y} &= c_2\hat{x}_G,
\end{aligned}$$

where

$$A_G = \begin{bmatrix} A_p & b_pN_ac_c & 0 & \sigma_d b_p c_d \\ -b_cN_sc_p & A_c & \sigma_r b_c c_r & 0 \\ 0 & 0 & A_r & 0 \\ 0 & 0 & 0 & A_d \end{bmatrix}, B_G = \begin{bmatrix} 0 & 0 \\ 0 & 0 \\ b_r & 0 \\ 0 & b_d \end{bmatrix}, B_1 = \begin{bmatrix} b_p & 0 \\ 0 & b_c \\ 0 & 0 \\ 0 & 0 \end{bmatrix},$$
$$c_1 = [0\ c_c\ 0\ 0], c_2 = [c_p\ 0\ 0\ 0]. \tag{2.27}$$

It follows that the standard deviations $\sigma_{\hat{u}}$ and $\sigma_{\hat{y}}$ can be obtained from $\sqrt{c_1Pc_1^T}$ and $\sqrt{c_2Pc_2^T}$, respectively, where $P$ is the positive definite solution of the Lyapunov equation

$$A_GP + PA_G^T + B_GB_G^T = 0.$$

Therefore, the equations of stochastic linearization are:

$$\begin{aligned}
N_a - \mathcal{F}_N(\sqrt{c_1Pc_1^T}, \mu_{\hat{u}}) &= 0,\\
N_s - \mathcal{G}_N(\sqrt{c_2Pc_2^T}, \mu_{\hat{y}}) &= 0,\\
-\mu_d + \frac{\mu_{\hat{y}}}{P_0} - \mathcal{F}_M(\sqrt{c_1Pc_1^T}, \mu_{\hat{u}}) &= 0,\\
\mu_r - \frac{\mu_{\hat{u}}}{C_0} - \mathcal{G}_M(\sqrt{c_2Pc_2^T}, \mu_{\hat{y}}) &= 0,\\
A_GP + PA_G^T + B_GB_G^T &= 0,
\end{aligned}$$

where $A_G$, $B_G$, $c_1$, and $c_2$ are defined in (2.27), $\mathcal{F}_N$ and $\mathcal{F}_M$ are as in (2.4) and (2.5), respectively, and $\mathcal{G}_N$ and $\mathcal{G}_M$ are the same as $\mathcal{F}_N$ and $\mathcal{F}_M$ in (2.4) and (2.5), but with $f(\cdot)$ replaced by $g(\cdot)$.

## 2.3 Accuracy

In [1] it was shown that, for the case of symmetric nonlinearities, stochastic linearization in the closed loop environment results in accuracy well within 10%, as far as the difference between the standard deviations of the outputs, $\sigma_y$ and $\sigma_{\hat{y}}$, is concerned. Furthermore, it was noted that if the plant is sufficiently low-pass filtering, the accuracy is high because the plant "Gaussianizes" its input [64]. In this subsection, we focus on asymmetric saturating actuators and perform similar studies.

### 2.3.1 Statistical experiment

To characterize the accuracy of stochastic linearization for asymmetric nonlinearities and compare it with that of symmetric ones, we perform the following Monte Carlo experiment: We consider 2400 LPNI systems of Figure 2.5.1 with $r(t) = 0$. In 1200 of these systems, we assume that $P(s) = \frac{1}{Ts+1}$, and in the remaining 1200, we assume that $P(s) = \frac{w_n^2}{s^2+2\zeta w_n s+w_n^2}$. The parameters are randomly and equiprobably selected from the following intervals:

$$T \in [0.01, 10], w_n \in [0.01, 10], \zeta \in [0.05, 1].$$

Furthermore, we assume that, in all these systems, $\sigma_d = 1$, $\mu_d = 0$, and

$$C(s) = K, f(\cdot) = \text{sat}_\alpha^\beta(\cdot),$$

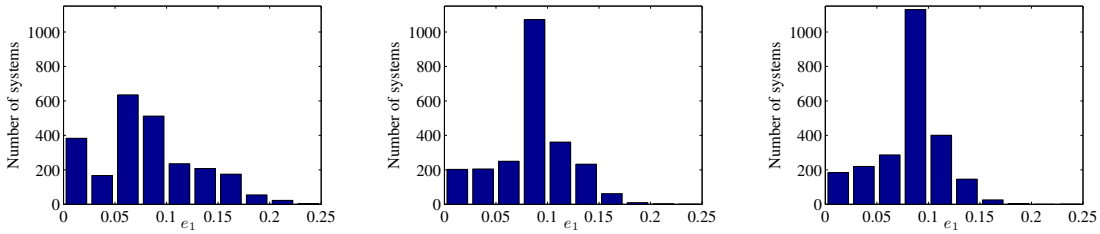


2.6.1: Symmetric case, $\beta/|\alpha| = 1$.

2.6.2: Asymmetric case, $\beta/|\alpha| = 5$.

2.6.3: Asymmetric case, $\beta/|\alpha| = 14$.

Figure 2.6: Histograms of $e_1$.

where $K$ is selected equiprobably from $[1, 20]$, $\beta + |\alpha| = 1.5$, and $F_{\Omega_d}(s)$ is the third order Butterworth filter with 3-dB bandwidth $\Omega_d = 1$ and dc-gain selected so that $\|F_{\Omega_d}(s)\|_2 = 1$, i.e.,

$$F_{\Omega_d}(s) = \frac{\sqrt{3}}{s^3 + 2s^2 + 2s + 1}.$$

For each of these systems, we consider three cases: one with the symmetric nonlinearity, i.e., $\beta/|\alpha| = 1$, and two with asymmetric ones, specifically, $\beta/|\alpha| = 5$ and $\beta/|\alpha| = 14$.

For each of the 2400 systems and each of the above three cases, we evaluate $\sigma_y$ by simulations and $\sigma_{\hat{y}}$ from (2.24), (2.25). The accuracy, as quantified by

$$e_1 = \frac{|\sigma_y - \sigma_{\hat{y}}|}{\sigma_y},$$

is illustrated by the histograms of Figure 2.6 and the data of Table 2.1. Clearly, the accuracy of stochastic linearization in predicting the standard deviation $\sigma_y$ is quite high, even for asymmetric nonlinearities. Furthermore, as the nonlinearity becomes asymmetric, the percentage of simulations resulting in high accuracy ($e_1 < 5\%$) decreases, while that resulting in lower accuracy ($e_1 < 20\%$) slightly improves; however, note that the improvement and degradation in accuracy are not significant.

Since $e_1$ does not seem to be sensitive enough, we consider another measure for

| | $\beta/\|\alpha\| = 1$ | $\beta/\|\alpha\| = 5$ | $\beta/\|\alpha\| = 14$ |
|---|---|---|---|
| percentage of systems that result in $e_1 < 5\%$ | 22.9 | 17.0 | 16.8 |
| percentage of systems that result in $e_1 < 10\%$ | 70.7 | 72.1 | 75.9 |
| percentage of systems that result in $e_1 < 20\%$ | 98.8 | 99.8 | 99.9 |
| average $e_1$ | 8.1% | 8.4% | 8.1% |

Table 2.1: Accuracy as quantified by $e_1$.

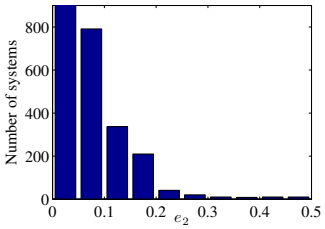


2.7.1: $\beta/|\alpha| = 1$.

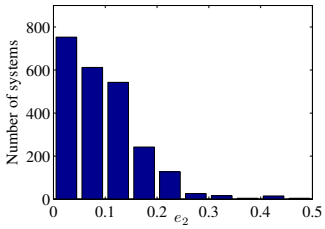


2.7.2: $\beta/|\alpha| = 5$.

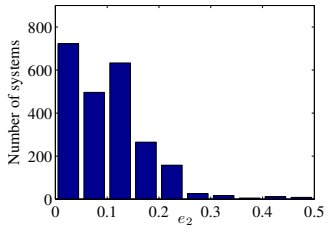


2.7.3: $\beta/|\alpha| = 14$.

Figure 2.7: Histograms of $e_2$.

accuracy given by

$$e_2 = \frac{\sqrt{E[(y - \hat{y})^2]}}{\sigma_r}.$$

Its histograms and numerical values are shown in Figure 2.7 and Table 2.2, respectively. These data clearly show that, although the accuracy in all cases remains relatively high, it monotonically degrades as a function of asymmetry.

| | $\beta/\|\alpha\| = 1$ | $\beta/\|\alpha\| = 5$ | $\beta/\|\alpha\| = 14$ |
|---|---|---|---|
| percentage of systems that result in $e_2 < 5\%$ | 38.0 | 31.4 | 30.1 |
| percentage of systems that result in $e_2 < 10\%$ | 70.9 | 56.9 | 50.7 |
| percentage of systems that result in $e_2 < 20\%$ | 92.5 | 88.4 | 86.8 |
| average $e_2$ | 10.8% | 12.9% | 13.4% |

Table 2.2: Accuracy as quantified by $e_2$.

### 2.3.2 Filtering hypothesis and accuracy of stochastic linearization for filtering plants

Consider the LPNI system of Figure 2.5.1 with

$$d(t) = 0,\ \sigma_r = 1,\ \mu_r = 0,$$

$$P(s) = \frac{1}{Ts+1},\ C(s) = 5,\ f(u) = \mathrm{sat}_\alpha^\beta(u),$$

and $F_{\Omega_r}(s)$ the third order Butterworth filter with bandwidth $\Omega_r = 1$. We assume that $\alpha = -0.1$ and $\beta = 0.3$ and consider two cases: $T = 1$ and $T = 10$. For each case, we simulate the system for a sufficiently long time. The histograms of $v$ and $y$ for both cases are shown in Figure 2.8. Clearly, the input to the plant $v$ is not Gaussian in either case. However, the output resembles the Gaussian distribution when the plant is more low-pass filtering (i.e., $T = 10$). This illustrates that the "Gaussianization" phenomenon takes place for asymmetric saturation as well.

The data of Subsection 2.3.1 characterizes the accuracy of stochastic linearization for both filtering and non-filtering plants (due to ranges of $T$, $\zeta$, and $w_n$). It is of interest to illustrate this accuracy for filtering plants that exhibit signal Gaussianization. We carry this out by considering the above system with $T = 10$ and $f(u) = \mathrm{sat}_\alpha^\beta(u)$, where $\beta + |\alpha| = 0.4$. Figure 2.9 illustrates the behavior of $e_2$, obtained via simulations, as a function of the midpoint of saturation $(\alpha + \beta)/2$. Clearly, for the filtering plant considered, $e_2$ is a monotonically increasing function of asymmetry; however, the accuracy deterioration is quite small.

## 2.4 Measure of Asymmetry

In this section, we introduce a measure to quantify the degree of asymmetry. The focus here is on the saturation function, which is the main nonlinearity examined in

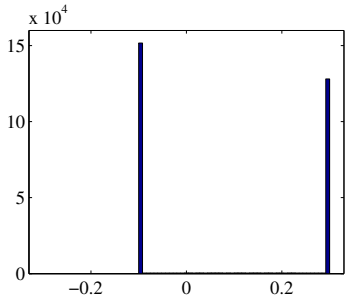


2.8.1: Histogram of $v$ for $T = 1$.

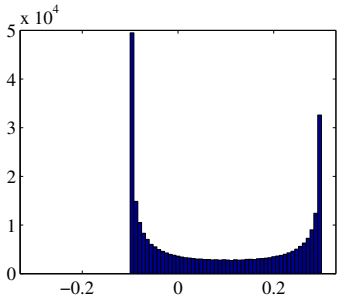


2.8.2: Histogram of $y$ for $T = 1$.

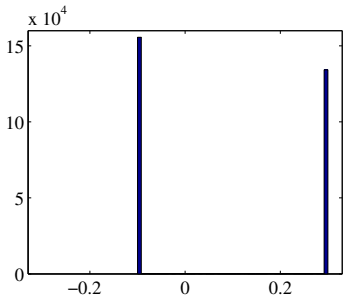


2.8.3: Histogram of $v$ for $T = 10$.

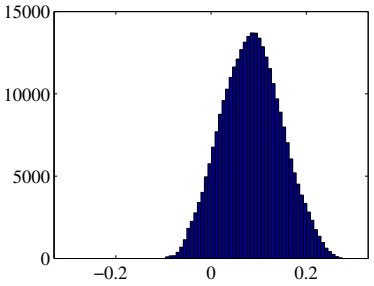


2.8.4: Histogram of $y$ for $T = 10$.

Figure 2.8: Histograms of $v$ and $y$.

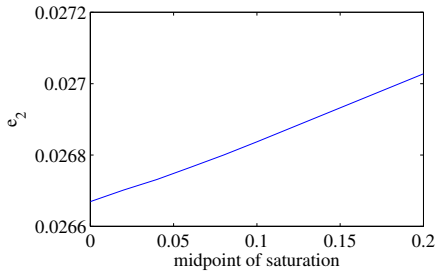


Figure 2.9: Accuracy as quantified by $e_2$ as a function of the midpoint of saturation, i.e., $(\alpha + \beta)/2$.

this work.

Consider the block diagram shown in Figure 2.1, where $f$ is the saturation function. To quantify asymmetry in this system, compute $P[u \leq \alpha]$ and $P[u \geq \beta]$, which determine the probability that the lower and upper saturation limits are activated. Accordingly, define the *degree of asymmetry*

$$A = P[u \geq \beta] - P[u \leq \alpha]. \tag{2.28}$$

If the saturation is activated equally from above and below, $A = 0$. If saturation is activated more on the upper limit, $A > 0$. Similarly, if saturation is activated more on the lower limit, $A < 0$. Note that, since $A$ is the difference of two probabilities, it satisfies the inequalities

$$-1 < A < 1.$$

The following theorem provides an explicit formula for $A$.

**Theorem II.5.** *An explicit formula for computing $A$ is given by*

$$A = -\frac{1}{2}\left(\operatorname{erf}(\frac{\beta - \mu_u}{\sqrt{2}\sigma_u}) + \operatorname{erf}(\frac{\alpha - \mu_u}{\sqrt{2}\sigma_u})\right). \tag{2.29}$$

*Proof.* See Section A.1. □

As it follows from equation (2.29), $A$ is small if one of the following holds:

- $\mu_u$ is close to the midpoint of the saturation, i.e., $\frac{\alpha+\beta}{2}$.
- $\sigma_u$ is small and $\mu_u$ is within the linear domain of saturation. In this case, $A$ is small because the nonlinearity is almost never activated – neither from above nor below. Thus, the input signal does not "sense" any asymmetry.
- $\sigma_u$ is much larger than the saturation authority. This is because large $\sigma_u$ implies that the saturation is significantly activated – almost equally from above and

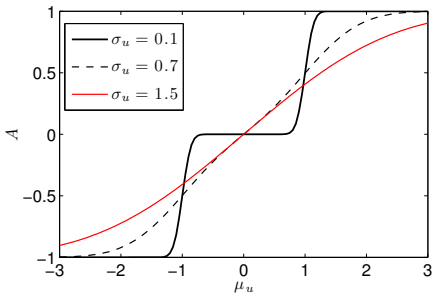


2.10.1: $A$ vs $\mu_u$.

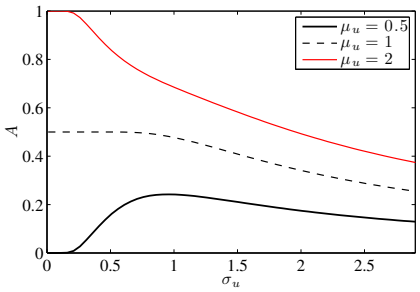


2.10.2: $A$ vs $\sigma_u$.

Figure 2.10: Degree of asymmetry $A$ as a function of $\mu_u$ and $\sigma_u$.

below. Therefore, again, the input signal does not sense any asymmetry.

To illustrate these findings, we let $\alpha = -1$ and $\beta = 1$, and compute $A$ using (2.29) for various $\sigma_u$'s and $\mu_u$'s. Figures 2.10.1 and 2.10.2 show $A$ as a function of $\mu_u$ and $\sigma_u$, respectively. As expected, asymmetry is an increasing function of $\mu_u$. Moreover, $A$ is small exactly when one of the above conditions is satisfied.

Notice the similarity between (2.29) and the equation for quasilinear gain (2.8). Indeed, the following relationship can be established:

**Corollary II.2.** *The degree of asymmetry $A$ given by* (2.29) *and the quasilinear gain $N$ for the saturation function given by* (2.8) *satisfy*

$$0 < N < 1 - |A|.$$

*Proof.* See Section A.1 □

According to this theorem, large asymmetry implies small quasilinear gain.

We now demonstrate the effect of asymmetry on the quasilinear gain and bias. To accomplish this, we let $\alpha = -1$ and $\beta = 1$, and compute the values of $N$, $m$, and $A$ for $\mu_u \in [-5, 5]$ and three $\sigma_u$'s: $\sigma_u = 0.1$, $\sigma_u = 0.7$, and $\sigma_u = 1.5$. Figure 2.11 shows $N$ and $m$ as a function of $A$. Clearly, the larger the asymmetry, the smaller the $N$ and the larger the $m$. In the framework of the closed loop environment, this

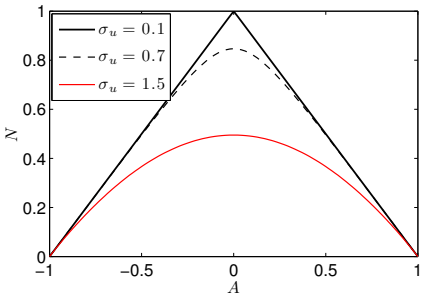


2.11.1: $N(A)$.

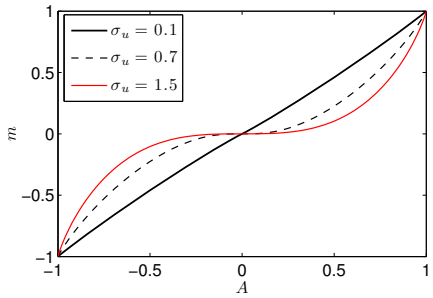


2.11.2: $m(A)$.

Figure 2.11: Quasilinear gain $N$ and quasilinear bias $m$ as a function of degree of asymmetry $A$.

implies that asymmetry could have two deteriorating effects: it could degrade dynamic performance of the system because the quasilinear gain is smaller as compared with the symmetric case, and it could degrade steady state performance because the bias, which acts as additional disturbance, is non-zero. These facts are investigated further in Chapter IV.

We now connect the measure of asymmetry $A$ with the notion of asymmetry defined by condition (1.4) in Section 1.2. Recall from Section 1.2 that, in the closed loop environment, an LPNI system is called symmetric if (1.4) is satisfied. Otherwise, it is called asymmetric. The following theorem connects the degree of asymmetry $A$ with condition (1.4).

**Theorem II.6.** *Assume that the closed loop LPNI system of Figure 1.2.1, with $f(\cdot)$ the saturation function and $g(\cdot)$ linear, is operating in the stationary regime. Then, condition* (1.4) *is satisfied iff $A = 0$, where $u$ in the definition of $A$ is the controller output shown in Figure 1.2.1.*

*Proof.* See Section A.1. □

The above theorem confirms that the notion of asymmetry defined by (1.4) is consistent with the notion of asymmetry defined in this subsection. Specifically, $A = 0$ when and only when the LPNI system is symmetric.

**Remark II.1.** In the closed loop environment, $\sigma_u$ and $\mu_u$ are difficult to compute analytically. We, therefore, consider the degree of asymmetry in the framework of the quasilinear system, i.e.,

$$A = -0.5 \left( \text{erf}(\frac{\beta - \mu_{\hat{u}}}{\sqrt{2}\sigma_{\hat{u}}}) + \text{erf}(\frac{\alpha - \mu_{\hat{u}}}{\sqrt{2}\sigma_{\hat{u}}}) \right). \tag{2.30}$$

This measure of asymmetry is used in the analysis of Chapter IV.

# CHAPTER III

# Performance Analysis in A-LPNI Systems

This chapter is devoted to the problem of performance analysis of A-LPNI systems. For linear systems, this problem has been extensively studied. For symmetric LPNI systems with zero-mean exogenous signals, this problem has been addressed in [1]. For asymmetric LPNI systems, however, this problem has not been solved at any level of generality. Consequently, in this chapter, we explore the problem of performance analysis of A-LPNI systems in the framework of stochastic linearization developed in Chapter II. Although the focus is on systems with saturating actuator and linear sensor, the obtained results can be easily extended to systems with other nonlinearities in actuators and sensors.

The outline of this chapter is as follows. First, the case of reference tracking is treated. Specifically, a motivating example is presented and the so-called trackable domain, system types, and quality indicators are introduced to quantify tracking quality. Second, the case of disturbance rejection is considered. Finally, the phenomenon of noise-induced loss of tracking in systems with sensor noise, anti-windup, and saturating actuator is quantified using stochastic linearization.

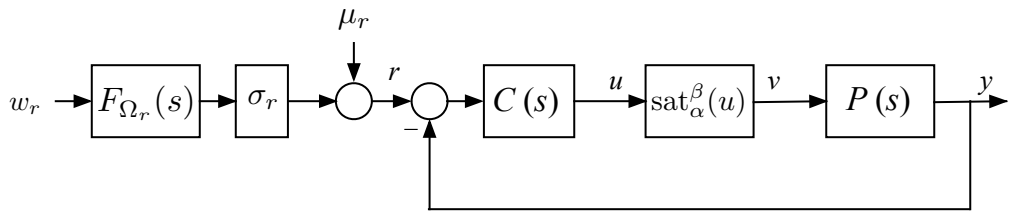


3.1.1: LPNI system.

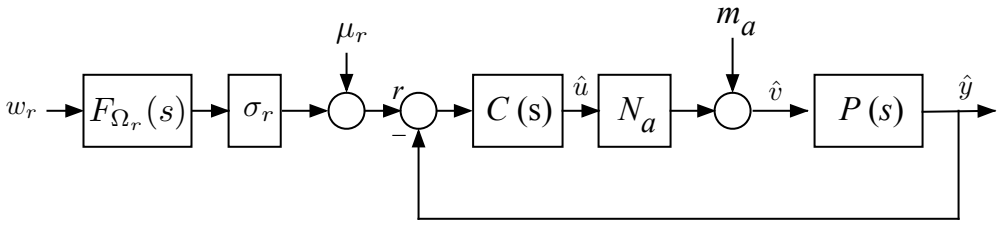


3.1.2: Quasilinear system.

Figure 3.1: LPNI and quasilinear systems for the tracking problem of Section 3.1.1.

## 3.1 Analysis of Tracking Performance

In this section, we apply stochastic linearization to analyze the tracking performance of A-LPNI systems.

First, we begin with a motivating example to demonstrate that stochastic linearization provides a good approach in studying tracking performance of LPNI systems. Second, we develop the notion of Trackable Domain for A-LPNI systems, which determines the set of step sizes that can be tracked in the presence of saturation. Finally, we introduce quality indicators, which quantify the tracking performance for A-LPNI systems. Some of the results are proper generalizations of the symmetric case while some are only pertinent to the asymmetric case.

### 3.1.1 Motivating example

Consider the closed loop system of Figure 3.1.1 with

$$P(s) = \frac{10}{s(s+10)}, \; C(s) = 5. \tag{3.1}$$

Assume that $w_r$ is the standard Gaussian white noise process, $\sigma_r = 1$, $\mu_r = 0$, and $F_{\Omega_r}(s)$ is the third order Butterworth filter with bandwidth $\Omega_r = 1$, i.e.,

$$F_{\Omega_r}(s) = \frac{\sqrt{3}}{s^3 + 2s^2 + 2s + 1}.$$

The quasilinear version of this LPNI system is shown in Figure 3.1.2. Since $P_0 = \infty$, stochastic linearization of this system can be calculated using (2.21), (2.22) as follows:

$$N_a - \mathcal{F}_N(\sigma_{\hat{u}}, \mu_{\hat{u}}) = 0, \tag{3.2}$$

$$\mathcal{F}_M(\sigma_{\hat{u}}, \mu_{\hat{u}}) = 0, \tag{3.3}$$

where $\mathcal{F}_N(\sigma_{\hat{u}}, \mu_{\hat{u}})$ and $\mathcal{F}_M(\sigma_{\hat{u}}, \mu_{\hat{u}})$ are as in (2.8), (2.9) and

$$\sigma_{\hat{u}} = \left\| \frac{5\sqrt{3}s(s+10)}{(s^3 + 2s^2 + 2s + 1)(s^2 + 10s + 50N_a)} \right\|_2.$$

We now consider three cases: $\alpha = -1, \beta = 1$; $\alpha = -0.5, \beta = 1.5$; and $\alpha = -0.2, \beta = 1.8$. Note that the total authority of saturation is the same in all three cases, specifically $\beta + |\alpha| = 2$. For each of the cases, we compute the unique solution $(N_a, \mu_{\hat{u}})$ of (3.2), (3.3) using Matlab's "fsolve" function, and, thus, obtain the quasilinear system. Then, using $N_a$ and $\mu_{\hat{u}}$, we compute the measure of asymmetry $A$ using (2.30). For case 1, $A = 0$, i.e., system is symmetric, while for cases 2 and 3, $A = -0.46$ and $A = -0.8$, i.e., system is asymmetric. Figure 3.2 shows traces of $r(t)$, $y(t)$, and $\hat{y}(t)$ obtained by simulations, for all three cases. Clearly, with larger asymmetry, the tracking performance of both $y(t)$ and $\hat{y}(t)$ deteriorates: with large asymmetry, $y(t)$ displays one-sided rate-saturation while $\hat{y}(t)$ approximates $y(t)$ as lagging in a linear manner.

Figure 3.3 shows the standard deviations, expected values, and square root of the second moment of the tracking errors $e$ and $\hat{e}$. Clearly, as $(\alpha + \beta)/2$ increases, the

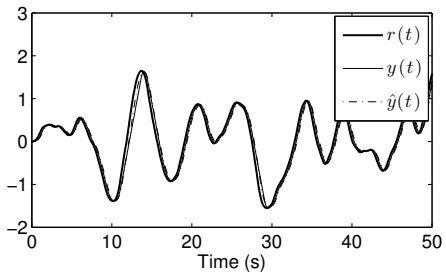


3.2.1: $\alpha = -1, \beta = 1$ (symmetric).

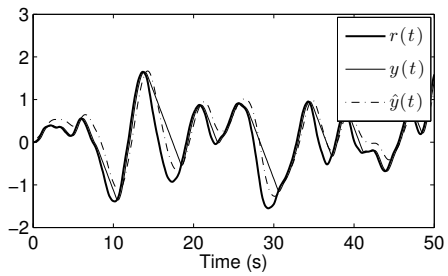


3.2.2: $\alpha = -0.5, \beta = 1.5$ (asymmetric).

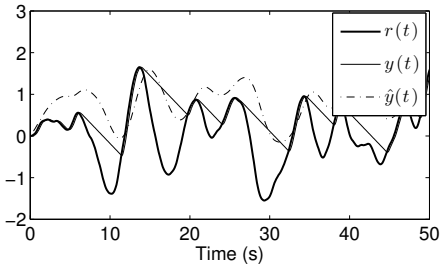


3.2.3: $\alpha = -0.2, \beta = 1.8$ (asymmetric).

Figure 3.2: Traces of $r(t)$, $y(t)$, and $\hat{y}(t)$ for the example of Subsection 3.1.1.

quality of tracking, as quantified by any of these quantities deteriorates monotonically. Furthermore, stochastic linearization provides a faithful estimate of all three quantities for the original nonlinear system. Consequently, the quasilinear system is a good approximation to the LPNI and A-LPNI systems, as far as prediction of loss of tracking is concerned.

This example demonstrates that stochastic linearization may be suitable to predict the quality of tracking in A-LPNI systems. Clearly, if $\sigma_{\hat{e}}$ is small, dynamic tracking is good and if $\mu_{\hat{e}}$ is small, steady state tracking of average values is good. It follows that for good tracking, both quantities must be small.

Obviously, if these quantities are large, the reason for poor tracking is not immediately clear. For this reason, below, we first develop the notions of step and ramp trackable domains, which determine the set of step sizes and ramp slopes that can be tracked in the presence of saturation. These domains are proper extensions of the ones in the symmetric case. We then introduce the quality indicators, which determine quality of tracking. Based on these indicators, we present a diagnostic chart,

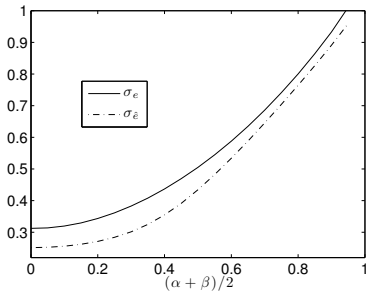


3.3.1: $\sigma_e$ and $\sigma_{\hat{e}}$.

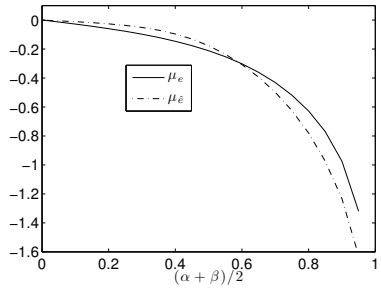


3.3.2: $\mu_e$ and $\mu_{\hat{e}}$.

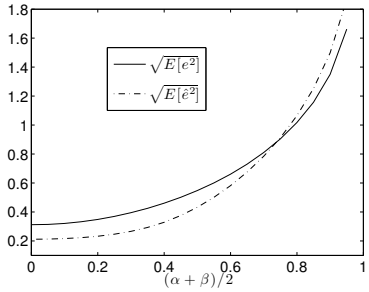


3.3.3: $\sqrt{E[e^2]}$ and $\sqrt{E[\hat{e}^2]}$.

Figure 3.3: The standard deviations $\sigma_e$ and $\sigma_{\hat{e}}$, average values $\mu_e$ and $\mu_{\hat{e}}$, and the square root of the second moments $\sqrt{E[e^2]}$ and $\sqrt{E[\hat{e}^2]}$ as a function of the midpoint of nonlinearity, for the tracking problem of Subsection 3.1.1.

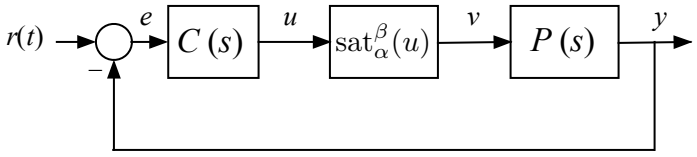


Figure 3.4: System for studying the trackable domain.

from which reasons for poor tracking can be determined.

### 3.1.2 Trackable domains for A-LPNI systems

Consider the system of Figure 3.4, where $r(t) = r_0\mathbf{1}(t)$. Here, $r_0 \in \mathbb{R}$ and $\mathbf{1}(t)$ is the unit step signal. Define the steady state error $e_{ss}$ as

$$e_{ss} = \lim_{t\to\infty} e(t).$$

The standing assumption in this section is that $e_{ss}$ exists and is unique. For linear systems, this error is given by

$$e_{ss} = \frac{1}{1 + P_0 C_0} r_0,$$

where $C_0$ and $P_0$ are the dc-gains of controller and plant, respectively. For A-LPNI systems this is not always the case, as established by the following theorem.

**Theorem III.1.** *Assume the system of Figure 3.4 has a unique $e_{ss}$. Then, the following hold:*

1. $e_{ss} = \frac{r_0}{1+P_0C_0}$ *if*

$$r_0 \operatorname{sign}(\frac{1}{C_0} + P_0) \in \left[ |\frac{1}{C_0} + P_0|\alpha, |\frac{1}{C_0} + P_0|\beta \right].$$

2. $e_{ss} = r_0 - P_0\alpha$ *if*

$$1 + P_0C_0 > 0, r_0 < |\tfrac{1}{C_0} + P_0|\alpha,$$
$$OR$$
$$1 + P_0C_0 < 0, r_0 < |\tfrac{1}{C_0} + P_0|(-\beta).$$

3. $e_{ss} = r_0 - P_0\beta$ *if*

$$1 + P_0C_0 > 0, r_0 > |\tfrac{1}{C_0} + P_0|\beta,$$
$$OR$$
$$1 + P_0C_0 < 0, r_0 > |\tfrac{1}{C_0} + P_0|(-\alpha).$$

*Proof.* See Section A.2. □

Using the above theorem, we introduce the following definition:

**Definition III.1.** The step Trackable Domain ($TD^{step}$) is the set of all step sizes

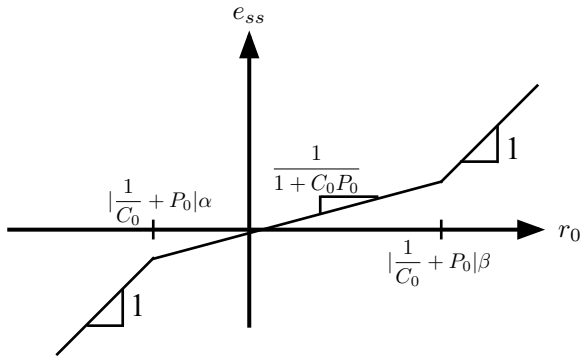


Figure 3.5: Illustration of $e_{ss}$ vs. $r_0$ when $\frac{1}{C_0}+P_0>0$ and $C_0>0$.

that can be tracked with the usual linear error, i.e.,

$$TD^{step}=\{r_0\in\mathbb{R}: r_0\,\mathrm{sign}(\frac{1}{C_0}+P_0)\in\left[|\frac{1}{C_0}+P_0|\alpha,|\frac{1}{C_0}+P_0|\beta\right]\}.$$

In typical systems, $C_0>0$ and $P_0>0$. The trackable domain for these systems is the closed interval

$$TD^{step}=\left[(\frac{1}{C_0}+P_0)\alpha,(\frac{1}{C_0}+P_0)\beta\right].$$

In the subsequent discussion, for simplicity, we assume that $C_0>0$ and $P_0>0$.

If $r_0\in TD^{step}$, the step signal can be tracked at steady state with the usual tracking error. However, if $r_0\notin TD^{step}$, tracking does not take place since $e_{ss}$ is given by $r_0$ shifted by a constant (either $P_0\alpha$ or $P_0\beta$). This can be illustrated by Figure 3.5.

Let us consider the step trackable domain for the special case where $P_0=\infty$. In this case, if $\alpha<0<\beta$, $TD^{step}=\mathbb{R}$, i.e., all step sizes can be tracked. If, however, $0\leq\alpha$ or $\beta\leq 0$, then the system cannot operate in the stationary regime, a case in which we are not interested.

If $P_0<\infty$ but $C_0=\infty$, we have that $TD^{step}=[P_0\alpha,P_0\beta]$. Clearly, not all step sizes can be tracked. Therefore, unlike linear systems, the poles at the origin of the

plant and controller play different roles as far as steady state tracking is concerned.

**Ramp inputs:** Consider system of Figure 3.4 with $r(t) = r_1 t\mathbf{1}(t)$, and let $e_{ss}$ be, as before, the steady state tracking error. Define $P_1$ by

$$P_1 = \lim_{s\to 0} sP(s).$$

In linear systems theory, the steady state error for ramp signals is given by

$$e_{ss} = \frac{r_1}{\lim_{s\to 0} sC(s)P(s)}.$$

However, this is not always the case in A-LPNI systems. The following theorem establishes this fact:

**Theorem III.2.** *Assume the system of Figure 3.4 with $r(t) = r_1 t\mathbf{1}(t)$ has a unique $e_{ss}$. Then, the following holds:*

$$e_{ss} = \frac{r_1}{C_0 P_1},$$

*if*

$$r_1 \text{sign}\,(P_1) \in [|P_1|\alpha, |P_1|\beta]\,.$$

*Proof.* See Section A.2. □

Using the above theorem, we introduce the following definition:

**Definition III.2.** The ramp Trackable Domain ($TD^{ramp}$) is defined as

$$TD^{ramp} = \{r_1 \in \mathbb{R} : r_1 \text{sign}\,(P_1) \in [|P_1|\alpha, |P_1|\beta]\}.$$

Note that if $P_1 = \infty$ and $\alpha < 0 < \beta$, then $TD^{ramp} = \mathbb{R}$. If $P_1 < \infty$, the ramp trackable domain is finite. Also note that the controller does not play any role in the ramp trackable domain. However, if $r_1 \in TD^{ramp}$, then the steady state tracking error

is inversely proportional to $C_0$. Clearly, similar to the case of step inputs considered above, the roles of the controller and plant poles at the origin are different.

The notions of step and ramp trackable domains can be extended to other signals (e.g., parabola) in a similar manner.

**System types:** In linear systems, the open loop (OL) transfer function specifies the system type. Specifically, system is of type $k$ if the OL transfer function has $k$ poles at the origin. Clearly, the plant and controller poles at the origin play equal roles as far as steady state tracking is concerned. According to Definitions III.1 and III.2, however, the integrators in the plant and controller play different roles in steady steady behavior of A-LPNI systems. Since the role of plant and controller integrators explained above is the same as those in the symmetric case described in [1], the notion of system types for A-LPNI systems remains the same as that in the S-LPNI case. Specifically, system is of type $k_S$ if the plant has $k$ poles at the origin. It is of type $k_s^+$ if, in addition, the controller has one or more integrators. For example, if system is of type $0_S$, then $TD^{step}$ is finite, and the tracking error is non-zero. If system is of type $0_S^+$, then $TD^{step}$ is finite, and the tracking error is zero. In both cases, the ramp trackable domain is empty. If system is of type $1_S$, then $TD^{step} = \mathbb{R}$, and the step tracking error is zero. Moreover, the ramp trackable domain is finite and the steady state tracking error for ramp signals is non-zero. If system is of type $1_S^+$, then the steady state tracking error for ramp signals is zero.

### 3.1.3 The quality indicators and the diagnostic flowchart

#### 3.1.3.1 Preliminaries

Consider the A-LPNI system shown in Figure 3.1.1, where, as before, reference $r(t)$ is a Gaussian colored process with standard deviation $\sigma_r$ and mean $\mu_r$. To study the quality of tracking for this system, we consider instead the quasilinear system of Figure 3.1.2, where $N_a$ and $m_a = \frac{\mu_r}{P_0} - (\frac{1}{C_0 P_0} + N_a)\mu_{\hat{u}}$ are, as before, given by the

solution of the transcendental equations

$$N_a - \mathcal{F}_N(\sigma_{\hat{u}}, \mu_{\hat{u}}) = 0, \tag{3.4}$$

$$\frac{\mu_r}{P_0} - \frac{\mu_{\hat{u}}}{P_0 C_0} - \mathcal{F}_M(\sigma_{\hat{u}}, \mu_{\hat{u}}) = 0. \tag{3.5}$$

Here, $\sigma_{\hat{u}}$ is given by

$$\sigma_{\hat{u}} = \left\| \frac{F_{\Omega_r}(s)C(s)}{1 + N_a P(s)C(s)} \right\|_2 \sigma_r,$$

where $\mathcal{F}_N$ and $\mathcal{F}_M$ are given in (2.8) and (2.9), respectively.

As explained in Subsection 3.1.1, to achieve good tracking, both $\sigma_{\hat{e}}$ and $\mu_{\hat{e}}$ must be small, where $\hat{e}$ is the tracking error in the quasilinear system. These quantities are given by

$$\sigma_{\hat{e}} = \left\| \frac{F_{\Omega_r}(s)}{1 + N_a P(s)C(s)} \right\|_2 \sigma_r, \tag{3.6}$$

$$\mu_{\hat{e}} = \frac{\mu_{\hat{u}}}{C_0}, \tag{3.7}$$

where $N$ and $\mu_{\hat{u}}$ are the solutions of (3.4) and (3.5).

Below, we first address the dynamic tracking quality. We accomplish this by employing the so-called Saturating Random Sensitivity (SRS) function. Based on the SRS, quality indicators $I_1$, $I_2$, and $I_3$ are introduced. Then, the phenomena of amplitude truncation and rate saturation are described. To quantify them, the quality indicators $I_0$ and $I_{0,rate}$ are introduced, respectively. Finally, to quantify the steady state tracking of average values, the quality indicator $I_{1,mean}$ is introduced. Based on these indicators, a diagnostic chart is presented that aids in determining causes of poor tracking. The results are illustrated using several examples.

As it is shown, the definition of SRS remains the same as that in the symmetric case defined in [1]. However, the indicators $I_0$, $I_1$, $I_2$, and $I_3$ are modified appropriately to account for asymmetry. Moreover, rate saturation, which has not been treated in [1], and steady state tracking, which does not arise in the symmetric case, lead to

new, novel indicators.

#### 3.1.3.2 Quantification of dynamic tracking quality

To address the dynamic tracking properties, we define the saturating random sensitivity function:

**Definition III.3.** The Saturating Random Sensitivity (SRS) function of the A-LPNI system of Figure 3.1.1 is the standard deviation of the error signal in the quasilinear system of Figure 3.1.2 normalized by $\sigma_r$, i.e.,

$$SRS(\Omega_r, \sigma_r, \mu_r) = \Big\| \frac{F_{\Omega_r}(s)}{1 + N_a P(s) C(s)} \Big\|_2, \tag{3.8}$$

where $N_a$ is the solution of (3.4) and (3.5).

The above definition of SRS is the same as that in the symmetric case. Note, however, that asymmetry is accounted for by the quasilinear gain $N_a$. Indeed, as seen in Chapter II, $N_a$ is smaller in the asymmetric case as compared with the symmetric case.

It can be shown that SRS satisfies the following properties:

**Theorem III.3.** *SRS satisfies the following:*

1. $\forall \Omega > 0$, $\lim_{\sigma_r \to 0} SRS(\Omega_r, \sigma_r, \mu_r) = \begin{cases} \Big\| \frac{F_{\Omega_r}(s)}{1+P(s)C(s)} \Big\|_2, & \mu_r \in TD^{step}, \\ 1, & \text{otherwise.} \end{cases}$

2. $\forall \sigma_r > 0, \forall \mu_r, \lim_{\Omega \to \infty} SRS(\Omega_r, \sigma_r, \mu_r) = 1.$

3. $\forall \sigma_r > 0, \forall \mu_r, \lim_{\Omega \to 0} SRS(\Omega_r, \sigma_r, \mu_r) = |\frac{1}{1+N_0 P_0 C_0}|$, *where* $N_0$ *is the solution of*

$$N_0 - \mathcal{F}_N\Big(\Big|\frac{F_{\Omega_r}(0) C_0}{1 + N_0 P_0 C_0}\Big| \sigma_r, \mu_{\hat{u}}\Big) = 0,$$
$$\frac{\mu_r}{P_0} - \frac{\mu_{\hat{u}}}{P_0 C_0} - \mathcal{F}_M\Big(\Big|\frac{F_{\Omega_r}(0) C_0}{1 + N_0 P_0 C_0}\Big| \sigma_r, \mu_{\hat{u}}\Big) = 0.$$

*4.* $\forall \sigma_r > 0, \forall \Omega > 0, \lim_{\mu_r \to \pm\infty} SRS(\Omega_r, \sigma_r, \mu_r) = \begin{cases} 1, & |P_0 C_0| \neq \infty, \\ \left\| \frac{F_{\Omega_r}(s)}{1+N_a P(s)C(s)} \right\|_2, & |P_0| = \infty, \\ undefined, & \text{otherwise}, \end{cases}$

*where* $N_a$ *is the solution of*

$$N_a - \mathcal{F}_N(\left\| \frac{F_{\Omega_r}(s)C(s)}{1+N_a P(s)C(s)} \right\|_2 \sigma_r, \mu_{\hat{u}}) = 0,$$
$$\mathcal{F}_M(\left\| \frac{F_{\Omega_r}(s)C(s)}{1+N_a P(s)C(s)} \right\|_2 \sigma_r, \mu_{\hat{u}}) = 0.$$

*Proof.* See Section A.2. □

To characterize the shape of the SRS function, we assume that $\mu_r \in TD^{step}$ (if not, tracking is poor due to significant amplitude truncation). Then, similar to the symmetric case, we introduce the following:

- Saturated random dc-gain: $SR_{dc}(\mu_r) = \lim_{\Omega_r \to 0, \sigma_r \to 0} SRS(\Omega_r, \sigma_r, \mu_r)$. This quantity represents the sensitivity of the error signal to the amplitude of a constant reference signal.

- Saturated random bandwidth: $SR\Omega_{BW}(\sigma_r, \mu_r) = \min_{\Omega>0}\{SRS(\Omega_r, \sigma_r, \mu_r) = \frac{1}{\sqrt{2}}\}$. This quantity represents the bandwidth of the SRS as a function of $\sigma_r$ and $\mu_r$.

- Saturated random resonance frequency: $SR\Omega_r(\sigma_r, \mu_r) = \arg\sup_{\Omega>0} SRS(\Omega_r, \sigma_r, \mu_r)$. This quantity denotes the frequency at which the peak of SRS takes place, as a function of $\sigma_r$ and $\mu_r$.

- Saturated random resonance peak: $SRM_r(\sigma_r, \mu_r) = \sup_{\Omega>0} SRS(\Omega_r, \sigma_r, \mu_r)$. This quantity designates the magnitude of the peak of SRS, as a function of $\sigma_r$ and $\mu_r$.

Using the above, following the same approach as the symmetric case, we introduce the following indicators:

$$I_1 = SR_{dc}(\mu_r),$$

$$I_2 = \frac{\Omega}{SR\Omega_{BW}(\sigma_r, \mu_r)},$$

$$I_3 = \min\{SRM_r(\sigma_r, \mu_r) - 1, \frac{\Omega}{SR\Omega_r(\sigma_r, \mu_r)}\},$$

where the quantities on the right hand side are evaluated at the mean and standard deviation of the reference signal. The indicator $I_1$ indicates static unresponsiveness, $I_2$ determines dynamic characteristics such as lagging or oscillations, and $I_3$ distinguishes between these two. In Subsection 3.1.3.6, we explain how these indicators can be employed in determining the quality of tracking.

#### 3.1.3.3 Quantification of amplitude truncation

In A-LPNI systems with saturating actuators, amplitude truncation may occur when the trackable domain is finite and the input signal is large enough that the saturation is occasionally activated.

To quantify amplitude truncation, we introduce an indicator, $I_0$, which is a proper generalization of the symmetric $I_0$ defined in [1]. When $\mu_r \in TD$, we define $I_0$ as

$$I_0 = \max\{\frac{\sigma_r}{|\frac{1}{C_0} + P_0|\beta - \mu_r}, -\frac{\sigma_r}{|\frac{1}{C_0} + P_0|\alpha - \mu_r}\}.$$

When $\mu_r \notin TD$, we define $I_0 = \infty$. If $I_0$ is small, amplitude truncation does not take place.

#### 3.1.3.4 Quantification of rate saturation

As discussed in Subsection 3.1.2, if the plant has a pole at the origin and $\alpha < 0 < \beta$, the trackable domain is infinite and $I_0 = 0$. However, in this case, a new phenomenon may occur: rate saturation. This occurs when the ramp trackable domain is small and the rate of change of the input signal is such that the nonlinearity is often activated. As an example, consider the example of Subsection 3.1.1. When $\alpha = -0.2$ and $\beta = 1.8$, significant rate saturation occurs at the falling slopes of the reference (see Figure 3.2.3).

To quantify rate saturation, we first assume that filter $F_{\Omega_r}(s)$ is the usual third order Butterworth filter with bandwidth $\Omega_r$. The standard deviation of the slope of $r(t)$ can be computed to be

$$\|sF_{\Omega_r}(s)\|_2\sigma_r = \frac{\sigma_r\Omega}{\sqrt{2}}.$$

Using the ramp trackable domain and above standard deviation, we introduce the following indicator:

$$I_{0,rate} = \max\{\frac{\sigma_r\Omega}{|P_1|\beta}, -\frac{\sigma_r\Omega}{|P_1|\alpha}\}.$$

If this indicator is large, rate saturation of the output occurs. If it is small, no rate saturation occurs. For the example of Subsection 3.1.1, we compute $I_{0,rate}$ for all three cases considered in the example:

- $\alpha = -1$, $\beta = 1$: $I_{0,rate} = 1$.
- $\alpha = -0.5$, $\beta = 1.5$: $I_{0,rate} = 2$.
- $\alpha = -0.2$, $\beta = 1.8$: $I_{0,rate} = 5$.

Clearly, in the first case, minimal rate saturation takes place, while in the third case significant rate saturation occurs.

#### 3.1.3.5 Steady state tracking

To characterize the tracking quality of average values, we introduce a new unitless quality indicator

$$I_{1,mean} = \frac{|\mu_{\hat{e}}|}{\sigma_r} = \frac{|\mu_{\hat{u}}|}{|C_0|\sigma_r}.$$

Clearly, if $C_0 = \infty$, $I_{1,mean} = 0$. The following proposition establishes bounds on $I_{1,mean}$.

**Proposition III.1.** *Assume $P_0 < \infty$. Then, $I_{1,mean}$ satisfies the following bound:*

$$I_{1,mean} < \max(\frac{|\mu_r - P_0\beta|}{\sigma_r}, \frac{|\mu_r - P_0\alpha|}{\sigma_r}).$$

*Proof.* See Section A.2. □

**Remark III.1.** In Section 1.2, it is shown that the mean of the error $\mu_e$ (or equivalently $\mu_{\hat{e}}$) can be decomposed in two parts: one due to the underlying linear system, and one due to asymmetry in the system. Therefore, two causes can contribute to large $I_{1,mean}$:

- The underlying linear system. This case arises when either $\mu_r$ is large or when the system is statically unresponsiveness, i.e., has small loop gain $P_0C_0$.
- The asymmetry in the system. This case arises when asymmetry is large (for a measure of asymmetry, see Section 2.4). In terms of the quasilinear system, large asymmetry implies large quasilinear bias $m_a$, which leads to large $\mu_{\hat{e}}$. However, note that asymmetry also affects the quasilinear gain $N_a$: $N_a$ is lower in the asymmetric case as compared with the symmetric case. Therefore, dynamic tracking, as quantified by SRS, may be poor as well. Finally, note that if $|P_0| = \infty$, then, according to Section 1.2, large $\mu_{\hat{e}}$ is *only* due to the asymmetry in the system.

#### 3.1.3.6 Quality of tracking and the diagnostic flowchart

As mentioned above, the indicators $I_0, I_{0,rate}, I_1, I_{1,mean}, I_2$, and $I_3$ indicate, respectively, the amount of amplitude truncation, rate saturation, static unresponsiveness, steady state tracking error, lagging or oscillatory behavior, and the distinction of the latter two. In our experience these quantities are small when: $I_0 < 0.4$, $I_{0,rate} < 0.8$, $I_1 < 0.1$, $I_{1,mean} < 0.1$, $I_2 < 0.3$, $I_3 < 0.3$. The diagnostic flowchart in Figure 3.6 provides a method for determining the quality of tracking using the quality indicators.

**Remark III.2.** Thus far, the focus of this section has been on A-LPNI systems with saturating actuator. However, the analysis of this section can be extended to systems with other nonlinearities. Specifically, the notion of saturating random sensitivity function can be generalized to the nonlinear random sensitivity (NRS) function:

$$NRS(\Omega_r, \sigma_r, \mu_r) = \frac{\sigma_{\hat{e}}}{\sigma_r}.$$

The quality indicators can be extended accordingly.

**Example III.1.** Consider the LPNI system of Figure 3.1.1, where $F_{\Omega_r}(s)$ is the usual 3rd order Butterworth filter with bandwidth $\Omega_r = 1$, and $\sigma_r = 1$. We consider five systems:

- System 1: $P(s) = \frac{4}{s}, C(s) = 0.005\frac{s+30}{s}, \alpha = -1, \beta = 2, \mu_r = 0, \Omega_r = 0.5$.
- System 2: $P(s) = \frac{0.5}{s+0.5}, C(s) = 100, \alpha = -2.5, \beta = 2.5, \mu_r = 1, \Omega_r = 1$.
- System 3: $P(s) = \frac{0.4}{s+0.2}, C(s) = 8, \alpha = 0, \beta = 7, \mu_r = 10, \Omega_r = 1$.
- System 4: System in the example of Subsection 3.1.1, with $\alpha = -1, \beta = 1$.
- System 5: System in the example of Subsection 3.1.1, with $\alpha = -0.2, \beta = 1.8$.

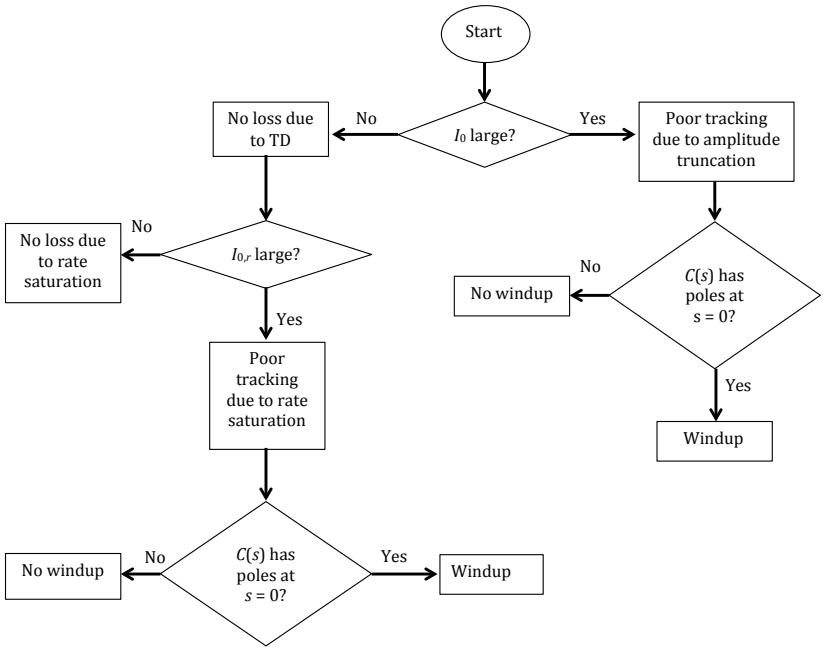


3.6.1: Diagnostic chart for $I_0$ and $I_{0,rate}$.

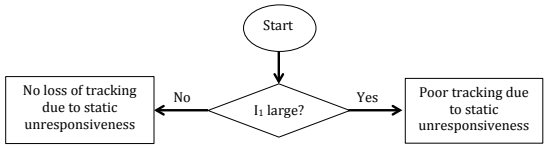


3.6.2: Diagnostic chart for $I_1$.

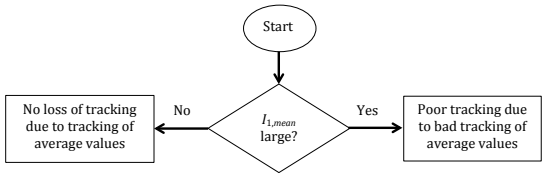


3.6.3: Diagnostic chart for $I_{1,mean}$.

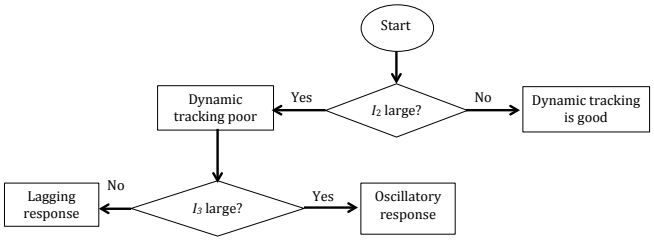


3.6.4: Diagnostic chart for $I_2$ and $I_3$.

Figure 3.6: Diagnostic chart for tracking performance.

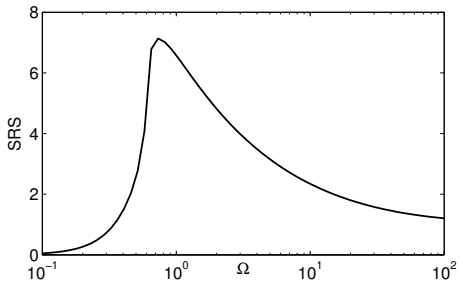


3.7.1: System 1.

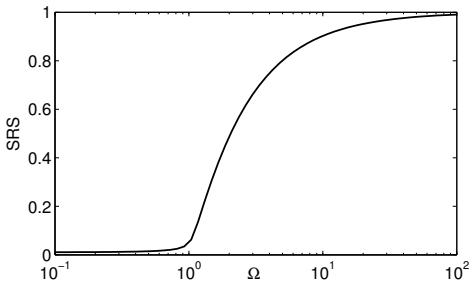


3.7.2: System 2.

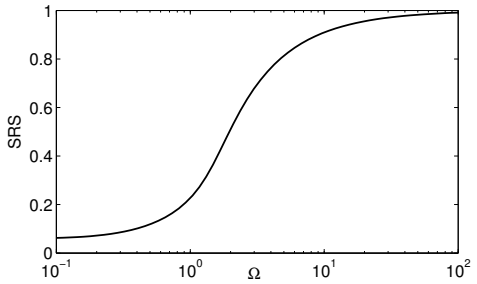


3.7.3: System 3.

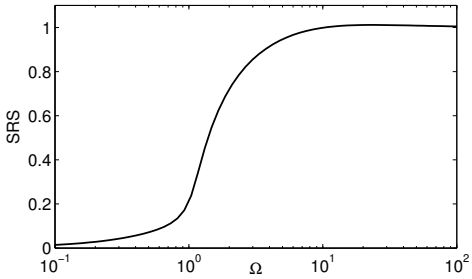


3.7.4: System 4.

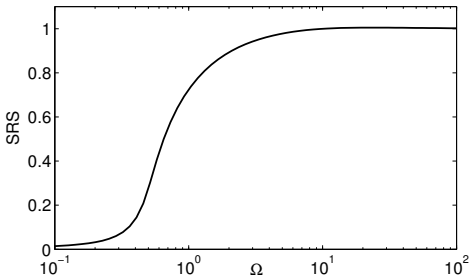


3.7.5: System 5.

Figure 3.7: SRS of systems in Example III.1

The SRS for each of the above systems are shown in Figure 3.7. The indicators for each system as well as the prediction for the quality of tracking is shown in Table 3.1.

Figure 3.8 shows time traces of the outputs of systems 1, 2, and 3. Time traces of systems 4 and 5 are plotted in Figures 3.2.1 and 3.2.3. Clearly, the predictions shown in Table 3.1 match the tracking performance of all systems considered.

| System | $I_0$ | $I_{0,rate}$ | $I_1$ | $I_{1,mean}$ | $I_2$ | $I_3$ | Quality of tracking |
|---|---|---|---|---|---|---|---|
| 1 | 0 | 0.125 | 0 | 0 | 1.67 | 0.68 | Poor due to oscillations and lag. |
| 2 | 0.65 | 0 | 0.01 | 0.03 | 0.28 | 0 | Poor due to amplitude truncation. |
| 3 | 0.21 | 0 | 0.06 | 0.60 | 0.30 | 0 | Poor due to bad tracking of average values. |
| 4 | 0 | 1 | 0 | 0 | 0.44 | 0.01 | Tracking good, minor lag and minor rate saturation in the output. |
| 5 | 0 | 5 | 0 | 0.79 | 1 | 0.04 | Poor due to lag, bad tracking of average values, and large rate saturation. |

Table 3.1: Indicators for the systems of Example III.1.

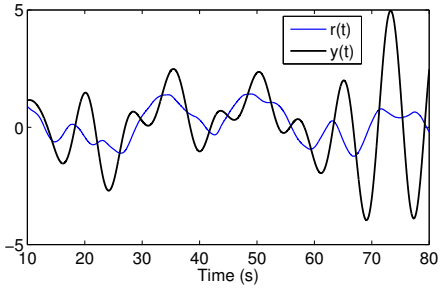


3.8.1: System 1.

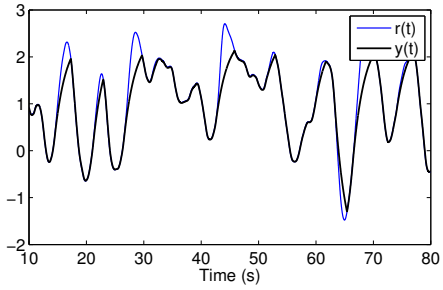


3.8.2: System 2.

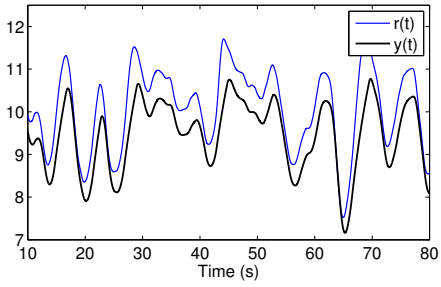


3.8.3: System 3.

Figure 3.8: Time traces of the output for systems in Example III.1.

## 3.2 Analysis of Disturbance Rejection Performance

Consider the closed loop LPNI system of Figure 2.5.1 with the same parameters as in (3.1) but assume that $r(t) = 0$, $w_d$ is the standard Gaussian white noise process, $\sigma_d = 1$, $\mu_d = 0$, and $F_{\Omega_d}$ the third order Butterworth filter with 3-dB bandwidth $\Omega_d = 2$. For this system, the equations of stochastic linearization are:

$$N_a - \mathcal{F}_N(\sigma_{\hat{u}}, \mu_{\hat{u}}) = 0, \tag{3.9}$$

$$\mathcal{F}_M(\sigma_{\hat{u}}, \mu_{\hat{u}}) = 0, \tag{3.10}$$

where $\mathcal{F}_N(\sigma_{\hat{u}}, \mu_{\hat{u}})$ and $\mathcal{F}_M(\sigma_{\hat{u}}, \mu_{\hat{u}})$ are as in (2.8), (2.9), and

$$\sigma_{\hat{u}} = \left\| \frac{400\sqrt{3/2}}{(s^3 + 4s^2 + 8s + 8)(s^2 + 10s + 50N_a)} \right\|_2.$$

We now consider the following three cases: $\alpha = -2, \beta = 2$; $\alpha = -1, \beta = 3$; $\alpha = -0.5, \beta = 3.5$. For each of the cases, we find the unique solution $(N_a, \mu_{\hat{u}})$ of (3.9), (3.10) and, thus, obtain the quasilinear system. Then, using $N_a$ and $\mu_{\hat{u}}$, we compute the measure of asymmetry $A$. For case 1, $A = 0$, i.e., system is symmetric, while for cases 2 and 3, $A = -0.3$ and $A = -0.73$, i.e., systems is asymmetric. Traces of $d(t)$, $y(t)$ and $\hat{y}(t)$ obtained by simulations are shown in Figure 3.9. Clearly, with more asymmetry, quality of disturbance rejection deteriorates in both LPNI and quasilinear systems. Figure 3.10 shows the standard deviations, means, and the square root of the second moment of $y$ and $\hat{y}$ as a function of $(\alpha + \beta)/2$. Clearly, as quantified by any of these quantities, disturbance rejection deteriorates with an increasing actuator asymmetry, and stochastic linearization is accurate as far as prediction of loss of performance is concerned.

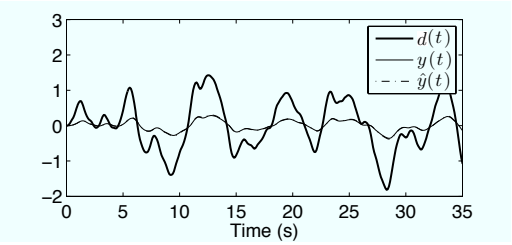


3.9.1: $\alpha = -2, \beta = 2$ (symmetric).

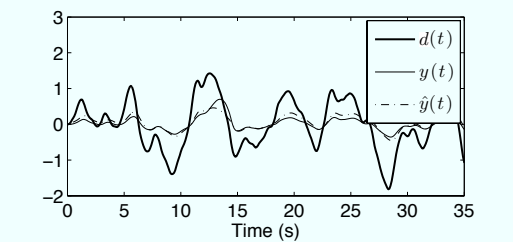


3.9.2: $\alpha = -1, \beta = 3$ (asymmetric).

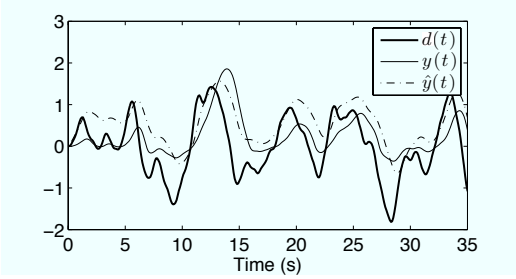


3.9.3: $\alpha = -0.5, \beta = 3.5$ (asymmetric).

Figure 3.9: Example of Section 3.2.

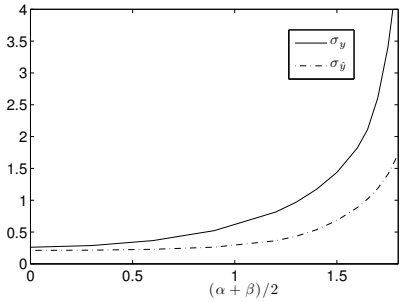


3.10.1: $\sigma_y$ and $\sigma_{\hat{y}}$.

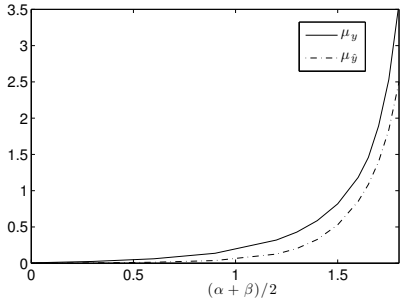


3.10.2: $\mu_y$ and $\mu_{\hat{y}}$.

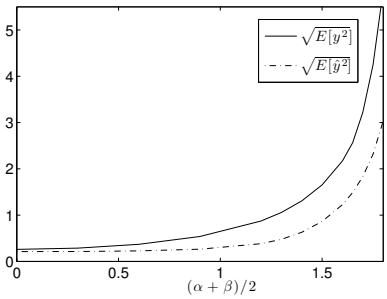


3.10.3: $\sqrt{E[y^2]}$ and $\sqrt{E[\hat{y}^2]}$.

Figure 3.10: The standard deviations, means, and square root of second moments of $y$ and $\hat{y}$ for the disturbance rejection problem of Section 3.2.

## 3.3 Analysis of Noise-Induced Loss of Tracking in Systems with PI Control and Anti-Windup

Consider the closed loop A-LPNI system of Figure 3.11.1, where $f(u) = \text{sat}_{\alpha}^{\beta}(u)$, $n$ is a zero-mean Gaussian white noise process, $r$ and $d$ are constants, $K_I$ is the integral gain, $K_P$ is the proportional gain, and $K_{AW}$ is the anti-windup gain. This system represents, for example, the Toner Concentration control in a Xerographic process (see [2]). In [2], the authors discovered that, in the presence of an asymmetric saturating actuator $f(u)$ and sensor noise, the mean of the output process $y_m(t)$ at steady-state exhibits a significant tracking error, inconsistent with the usual prediction by error coefficient, in the step response. They termed this error the *noise-induced tracking error* and quantified it using the method of *stochastic averaging theory.* In this section, we apply the method of stochastic linearization to the LPNI system of Figure 3.11.1 to obtain the stochastic linearization shown in Figure 3.11.2, and demonstrate that the latter system correctly predicts the noise-induced tracking error.

Clearly, in the quasilinear system of Figure 3.11.2, the saturation function $f(u)$ is replaced by the quasilinear gain $N_a$ and the bias $m_a = M - N\mu_{\hat{u}}$. Similar to the analysis of Subsection 2.2.1, to compute these values, we require $\sigma_{\hat{u}}$ and $\mu_{\hat{u}}$. The standard deviation $\sigma_{\hat{u}}$ can be computed using the $H_2$-norm of the transfer function from $n$ to $\hat{u}$:

$$\sigma_{\hat{u}} = \left\| \frac{(K_P s + K_I) F_\Omega(s)}{s(1 + N(K_P P(s) - K_{AW})) + K_{AW} + N P(s) K_I} \right\|_2 \sigma_n, \tag{3.11}$$

where $\sigma_n$ denotes the intensity of the noise process $n$. To obtain $\mu_{\hat{u}}$, note that the signal $h$ in Figure 3.11.2 is the input to an integrator and, as a result, must have zero mean (i.e., $\mu_h = 0$) in order for the system to be in the stationary regime. With

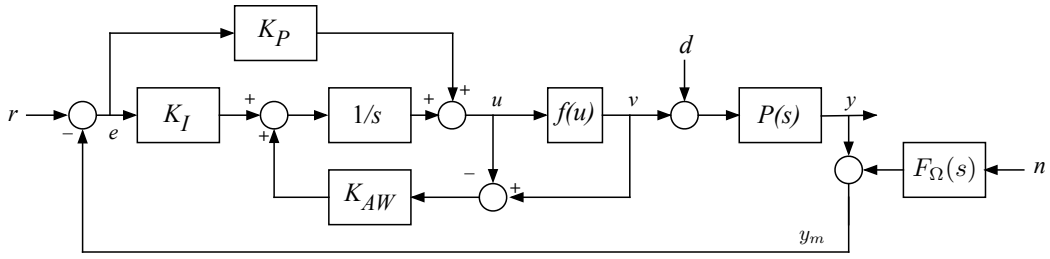


3.11.1: Closed loop A-LPNI system with sensor noise, saturating actuator, and anti-windup.

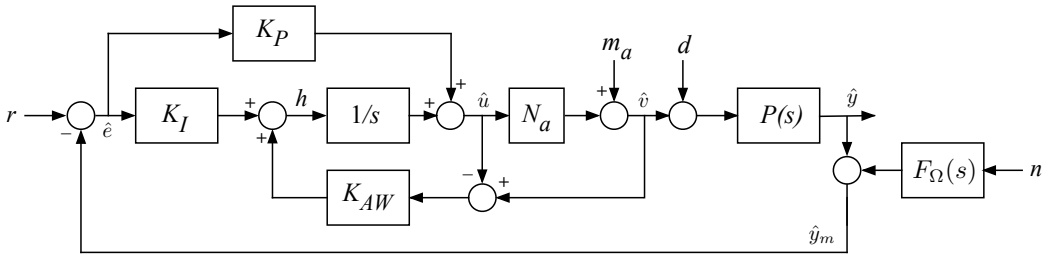


3.11.2: Stochastic linearization of the A-LPNI system.

Figure 3.11: System with noise-induced tracking error.

$\mu_h = 0$, we follow a procedure similar to the one in Subsection 2.2.1 and obtain

$$M_a = \frac{\mu_{\hat{u}} - \frac{K_I}{K_{AW}}(r - P_0 d)}{1 - \frac{K_I}{K_{AW}} P_0},$$

where $P_0$ is the dc-gain of the plant. Therefore, the equations of stochastic linearization for this system are:

$$N_a - \mathcal{F}_N(\sigma_{\hat{u}}, \mu_{\hat{u}}) = 0, \tag{3.12}$$

$$\frac{\mu_{\hat{u}} - \frac{K_I}{K_{AW}}(r - P_0 d)}{1 - \frac{K_I}{K_{AW}} P_0} - \mathcal{F}_M(\sigma_{\hat{u}}, \mu_{\hat{u}}) = 0, \tag{3.13}$$

where $\sigma_{\hat{u}}$ is defined in (3.11) and $\mathcal{F}_N(\sigma_{\hat{u}}, \mu_{\hat{u}})$ and $\mathcal{F}_M(\sigma_{\hat{u}}, \mu_{\hat{u}})$ are as in (2.8), (2.9).

We use the following parameters, also used in [2], for simulations:

$$P(s) = \frac{0.0322}{s},\ K_I = 0.0065,\ K_P = 0.82,\ r = 5,$$

$$d = -0.011,\ \sigma_n = 0.06.$$

We assume that $F_\Omega(s)$ is the third order Butterworth filter with bandwidth $\Omega = 100$ and consider three cases:

1. $K_{AW} = 0.25, \alpha = -0.33, \beta = 0.33$, i.e., symmetric saturation;

2. $K_{AW} = 0.25, \alpha = 0, \beta = 0.66$, i.e., asymmetric saturation (these parameters are used in [2]);

3. $K_{AW} = 0, \alpha = 0, \beta = 0.66$, i.e., asymmetric saturation with anti-windup inactive.

The traces of $y_m(t)$ and $\hat{y}_m(t)$ for all three cases are plotted in Figure 3.12. As can be seen, only the second case results in the noise-induced tracking error. The steady-state mean of the signals $y_m(t)$ and $\hat{y}_m(t)$ for all three cases are given in Table 3.2, along with the error $\frac{|\mu_{y_m} - \mu_{\hat{y}_m}|}{\mu_{y_m}}$. Clearly,

- The noise induced tracking error is present only when the anti-windup is active and the saturation is asymmetric. Therefore, the tracking error is a direct consequence of asymmetry.

- Stochastic linearization is accurate in predicting the noise-induced tracking error.

**Remark III.3.** Observe that the linearized system does not approximate the *transient* behavior of the LPNI system well (unlike [2], where both transient and steady-state behaviors are accurate). This is expected because the method of stochastic linearization assumes steady-state, stationary regime of the system.

To study the effects of the sensor noise intensity $\sigma_n$ on the noise-induced tracking error, Figure 3.13.1 plots $\mu_{\hat{y}}$ as a function of $\sigma_n$ for $K_{AW} = 0, 0.25, 0.5$. Clearly,

- the noise-induced tracking error is zero when $K_{AW} = 0$,

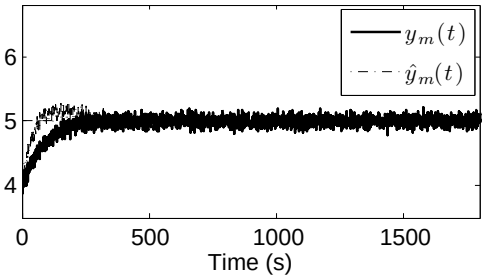


3.12.1: $K_{AW} = 0.25, \alpha = -0.33, \beta = 0.33$.

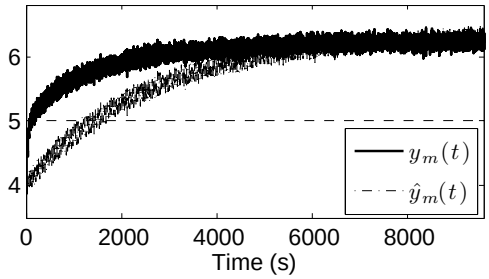


3.12.2: $K_{AW} = 0.25, \alpha = 0, \beta = 0.66$

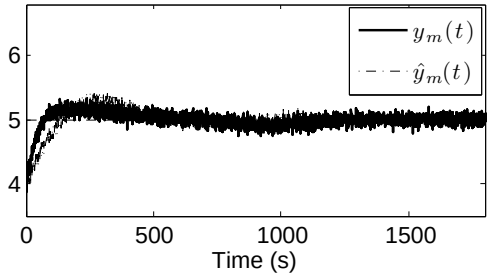


3.12.3: $K_{AW} = 0, \alpha = 0, \beta = 0.66$.

Figure 3.12: Simulation results for the noise-induced tracking error.

| | Case 1 | Case 2 | Case 3 |
|---|---|---|---|
| $\mu_{y_m}$ | 5.00 | 6.12 | 5.00 |
| $\mu_{\hat{y}_m}$ | 5.00 | 6.35 | 5.00 |
| $\frac{\lvert\mu_{y_m} - \mu_{\hat{y}_m}\rvert}{\mu_{y_m}}$ | 0% | 3.7 % | 0 % |

Table 3.2: The steady-state mean of signals $y_m$ and $\hat{y}_m$, and the accuracy of stochastic linearization.

- for non-zero $K_{AW}$, the error increases with $K_{AW}$,
- the error increases monotonically with $\sigma_n$ and is practically linear for large values of $\sigma_n$.

To study the effects of the anti-windup gain $K_{AW}$ on the noise-induced tracking error, Figure 3.13.2 plots $\mu_{\hat{y}}$ as a function of $K_{AW}$ for $\sigma_n = 0.06$. Clearly, the tracking error increases monotonically with $K_{AW}$ and is practically linear for all $K_{AW}$.

In sum, in this subsection, we have demonstrated that the method of stochastic linearization for asymmetric systems can be used to provide faithful prediction of the

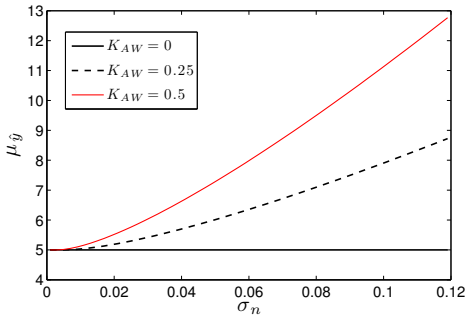


3.13.1: The steady state mean of the output as a function of $\sigma_n$ for three values of $K_{AW}$.

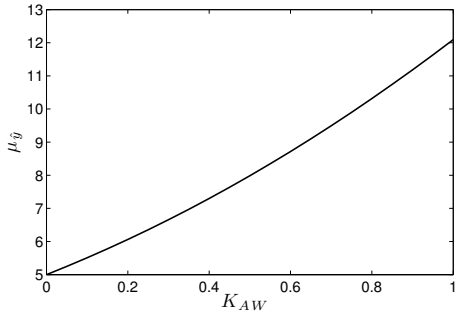


3.13.2: The steady state mean of the output as a function of $K_{AW}$ for $\sigma_n = 0.06$.

Figure 3.13: Demonstration of the noise induced tracking error as a function of $K_{AW}$ and $\sigma_n$.

phenomenon of noise-induced loss of tracking in systems with anti-windup, sensor noise, and asymmetric actuator. We have also demonstrated that this error increases monotonically with both sensor noise intensity and anti-windup gain.

# CHAPTER IV

# Time Domain Design of Tracking Controllers in A-LPNI Systems

In this chapter, a time domain method for design of A-LPNI tracking systems with saturating actuators is developed. This method is based on the so-called *performance loci*, which include the root locus for asymmetric saturating systems (*AS-root locus*) and tracking error locus (*TE locus*). Together, these loci are used for designing controllers that place closed loop poles and steady state tracking errors of quasilinear systems in appropriate admissible domains (defined by design specifications).

As it is shown, the AS-root locus is a proper generalization of the symmetric S-root locus developed in [1]. Similar to the symmetric case, the AS-root locus is a subset of the usual root locus and sometimes terminates prior to the open loop zeros. A method for computing these termination points is provided. In addition, similar to the symmetric case, the AS-root locus is equipped with truncation points to account for truncation of the output signal. However, in contrast to the symmetric case, a new phenomenon arises in the asymmetric case: the mean of the error signal may exhibit a tracking error, which depends on the controller gain. Therefore, we introduce the notion of the tracking error locus. Both loci must be placed within their respective admissible domains to ensure good tracking.

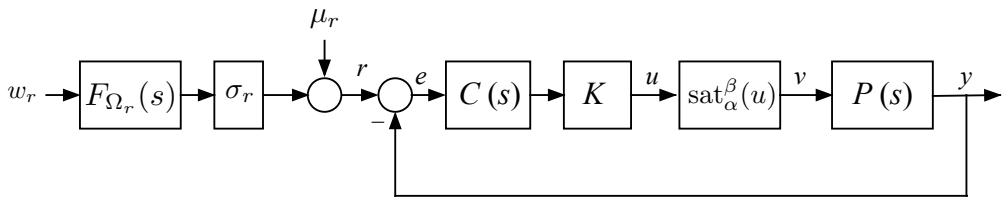


4.1.1: Closed loop A-LPNI system.

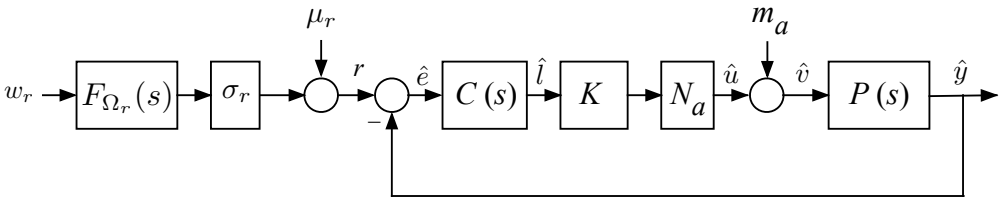


4.1.2: Closed loop quasilinear system.

Figure 4.1: A-LPNI system and equivalent quasilinear system.

## 4.1 Performance Loci

### 4.1.1 Preliminaries

Consider the SISO tracking system of Figure 4.1.1, where $P(s)$ is the plant, $KC(s)$ ($K > 0$) is the controller, and $F_{\Omega_r}(s)$ is the third order butterworth filter with dc-gain scaled so that $\|F_{\Omega_r}(s)\|_2 = 1$. The reference signal $r(t)$ is generated by passing standard Gaussian white noise $w_r$ through $F_{\Omega_r}(s)$, and scaling and shifting the output of the filter by $\sigma_r$ and $\mu_r$, respectively. Similar to the development in Chapter II, the stochastically linearized version of system of Figure 4.1.1 is the quasilinear system shown in Figure 4.1.2, where $m_a = \frac{\mu_r}{P_0} - (\frac{1}{KC_0P_0} + N_a)\mu_{\hat{u}}$, $N_a$ and $\mu_{\hat{u}}$ are solution of

$$N_a - \mathcal{F}_N(K\left\|\frac{F_{\Omega_r}(s)C(s)}{1+P(s)KN_aC(s)}\right\|_2\sigma_r, \mu_{\hat{u}}) = 0, \tag{4.1}$$

$$\frac{\mu_r}{P_0} - \frac{\mu_{\hat{u}}}{KC_0P_0} - \mathcal{F}_M(K\left\|\frac{F_{\Omega_r}(s)C(s)}{1+P(s)KN_aC(s)}\right\|_2\sigma_r, \mu_{\hat{u}}) = 0, \tag{4.2}$$

and $\mathcal{F}_N$ and $\mathcal{F}_M$ are given in (2.8) and (2.9), respectively.

The goal is to use the quasilinear system to design tracking controllers. To accomplish this, note from Figure 4.1.2 that the quasilinear gain $N_a$ and the quasilinear

bias $m_a$ enter the system as an additional gain and input disturbance, respectively. Also, as can be seen from (4.1) and (4.2), both of them are functions of the controller gain, $K$. Thus, to characterize the system behavior as $K$ changes from 0 to $\infty$, the behavior of "quasilinear" poles and quasilinear steady state errors as a function of $K$ must be investigated. As mentioned at the beginning of this chapter, this leads to two loci: the "usual" one – root locus, and a novel one – tracking error locus. Together, they are referred to as performance loci. These loci are characterized in Subsections 4.1.2 and 4.1.3.

To begin, we group together the controller gain $K$ and quasilinear gain $N_a$ in Figure 4.1.2 and denote the product by the *effective gain* $K_e$:

$$K_e(K) = KN_a(K).$$

Clearly, using (4.1), (4.2), for each $K > 0$, $K_e(K)$ and $\mu_{\hat{u}}$ can be obtained by solving

$$K_e - K\mathcal{F}_N(K\Big\|\frac{F_{\Omega_r}(s)C(s)}{1+P(s)K_eC(s)}\Big\|_2\sigma_r, \mu_{\hat{u}}) = 0, \tag{4.3}$$

$$\frac{\mu_r}{P_0} - \frac{\mu_{\hat{u}}}{KC_0P_0} - \mathcal{F}_M(K\Big\|\frac{F_{\Omega_r}(s)C(s)}{1+P(s)K_eC(s)}\Big\|_2\sigma_r, \mu_{\hat{u}}) = 0. \tag{4.4}$$

Throughout this paper, we assume that the solution of the above equations exists and is unique.

Denote by $\mu_{\hat{e}}$ the mean of the error signal $\hat{e}$ in the quasilinear system, which can be expressed as

$$\mu_{\hat{e}}(K) = \frac{\mu_{\hat{u}}(K)}{KC_0}. \tag{4.5}$$

Based on the above notations, we introduce the following definitions.

**Definition IV.1.** The saturated closed loop poles (AS-poles) of the system of Figure 4.1.1 are the poles of the system of Figure 4.1.2, i.e., the poles of the transfer function

from $r$ to $\hat{y}$:

$$T(s) = \frac{K_e(K)C(s)P(s)}{1 + K_e(K)C(s)P(s)}. \tag{4.6}$$

**Definition IV.2.** The AS-root locus is the path traced by the AS-poles when $K$ changes from 0 to $\infty$.

**Definition IV.3.** The TE locus is the plot of $\mu_{\hat{e}}(K)$ as $K$ changes from 0 to $\infty$.

As it turns out, the AS-root locus and the TE locus are continuous functions of $K$. To show this, the following lemma is required.

**Lemma IV.1.** *Assume that $K_e(K)$ and $\mu_{\hat{u}}(K)$ are unique for all $K > 0$. Then, $K_e(K)$ and $\mu_{\hat{u}}(K)$ are continuous for all $K > 0$.*

*Proof.* See section A.3. □

Continuity of the AS-root and TE loci is an immediate consequence of the above lemma.

Below, we develop the AS-root locus and the TE locus and investigate their properties.

### 4.1.2 The AS-root locus

In equation (4.6), $K_e(K)$ enters the transfer function as a usual gain. Furthermore, since $0 < N_a < 1$, we have that $0 \leq K_e(K) < K$. Therefore, the AS-root locus is a proper subset of the usual linear root locus. As in the linear root locus, we are interested in the points of origin and termination of the AS-root locus. Clearly, since $K_e(K) = 0$ when $K = 0$, the points of origin of the AS-root locus are the same as the linear root locus (i.e., at the poles of $P(s)C(s)$). The termination points, however, may not necessarily be at the open loop zeros. This is because $K_e(K)$ may not tend to infinity as $K$ tends to infinity. Therefore, we equip the AS-root locus with the so-called AS-termination points. In addition, saturation may lead to output truncation.

To account for this phenomenon, we equip the AS-root locus with the so-called AS-truncation points, beyond which the output does not follow the reference. Below, methods for computing both AS-termination and AS-truncation points are provided.

#### 4.1.2.1 Calculating AS-termination points

Denote by $K_e^*$ the limiting effective gain, i.e.,

$$K_e^* = \lim_{K\to\infty} K_e(K).$$

Clearly, if $K_e^* = \infty$, the termination points are the open loop zeros and the AS-root locus coincides with the usual root locus. However, if $K_e^* < \infty$, the root locus terminates prematurely.

As it turns out, to compute $K_e^*$, the following two equations in the unknowns $\phi^*$ and $\eta^*$ must first be solved:

$$\phi^* - \left\| \frac{F_{\Omega_r}(s)C(s)}{1 + \frac{\beta-\alpha}{\sqrt{2\pi}\phi^*} e^{-\frac{\eta^{*2}}{2}} P(s)C(s)} \right\|_2 \sigma_r = 0, \tag{4.7}$$

$$\frac{\mu_r}{P_0} - \frac{\phi^*\eta^*}{C_0 P_0} = \frac{\alpha+\beta}{2} + \frac{\beta-\alpha}{2}\mathrm{erf}(\frac{\eta^*}{\sqrt{2}}). \tag{4.8}$$

Before determining $K_e^*$, we establish some of the properties of the above equations in the following lemma.

**Lemma IV.2.** *The solutions of system* (4.7), (4.8) *have the following properties:*

1. $\phi^* \geq 0$.
2. *If* $\phi^* = 0$, *then* $\eta^* = \sqrt{2}\mathrm{erf}^{-1}(\frac{\frac{\mu_r}{P_0} - \frac{\alpha+\beta}{2}}{\frac{\beta-\alpha}{2}})$.
3. *The point*

$$(\phi^*, \eta^*) = \left(0, \sqrt{2}\mathrm{erf}^{-1}\left(\frac{\frac{\mu_r}{P_0} - \frac{\alpha+\beta}{2}}{\frac{\beta-\alpha}{2}}\right)\right) \tag{4.9}$$

*always satisfies system of equations* (4.7), (4.8).

*Proof.* See Section A.3. □

Note that (4.7) always has a solution $\phi^* = 0$. There may be positive solutions as well, which lead to the following theorem.

**Theorem IV.1.** *Assume that $K_e(K)$ and $\mu_{\hat{u}}(K)$ exist and are unique for all $K$. Then,*

1. *if $\phi^* = 0$ is the only solution of (4.7), (4.8), $K_e^* = \infty$.*

2. *if there exists another solution, $\phi^* > 0$, then*

$$K_e^* = \frac{\beta - \alpha}{\sqrt{2\pi}\phi^*} e^{-(\frac{\eta^{*2}}{2})}. \tag{4.10}$$

*Proof.* See section A.3. □

**Definition IV.4.** If $K_e^* < \infty$, the AS-termination points are the poles of the transfer function

$$T_{ter}(s) = \frac{K_e^* C(s)P(s)}{1 + K_e^* C(s)P(s)}. \tag{4.11}$$

Equations (4.10) and (4.11) are used to calculate the AS-termination points, which are marked by white squares on the AS-root locus.

As it turns out, unlike the linear root locus, the AS-root locus can never enter the right half plane. This is establishes by the following theorem.

**Theorem IV.2.** *Assume that $K_e(K)$ and $\mu_{\hat{u}}(K)$ are unique for all $K$, and let $\Gamma$, $0 < \Gamma < \infty$, be such that the closed loop transfer function*

$$T_\gamma(s) = \frac{C(s)P(s)}{1 + \gamma C(s)P(s)}$$

*is asymptotically stable only for $\gamma \in [0, \Gamma)$ and unstable for $\gamma = \Gamma$. Then,*

$$K_e^* < \Gamma.$$

*Proof.* See Section A.3. □

It is noteworthy to discuss the solutions $\phi^*$ and $\eta^*$ of (4.7), (4.8). As discussed in the proof of Theorem IV.1, $\phi^*$ and $\eta^*$ are, respectively, the limiting standard deviation and the inverse of the coefficient of variation of the signal at the input of gain $K$ in Figure 4.1.2, i.e.,

$$\phi^* = \lim_{K\to\infty} \sigma_{\hat{l}},$$

$$\eta^* = \lim_{K\to\infty} \frac{\mu_{\hat{l}}}{\sigma_{\hat{l}}}.$$

As far as solving (4.7), (4.8) is concerned, the 2-variable bisection algorithm or Matlab's "fsolve" function may be used. Note, however, that (4.7), (4.8) can be simplified by eliminating one of the variables from (4.8):

- If $C_0P_0 = \infty$, (4.8) can be solved explicitly for $\eta^*$:

$$\eta^* = \sqrt{2}\mathrm{erf}^{-1}\left(\frac{\frac{\mu_r}{P_0} - \frac{\alpha+\beta}{2}}{\frac{\beta-\alpha}{2}}\right).$$

  In this case, $\eta^*$ is a constant independent of $\phi^*$.

- If $C_0P_0 \neq \infty$, (4.8) can be solved explicitly for $\phi^*$:

$$\phi^* = \frac{C_0P_0}{\eta^*}\left(\frac{\mu_r}{P_0} - \frac{\alpha+\beta}{2} - \frac{\beta-\alpha}{2}\mathrm{erf}\left(\frac{\eta^*}{\sqrt{2}}\right)\right).$$

  In this case, $\phi^*$ depends on $\eta^*$.

In both cases, substituting the eliminated variable into (4.7) yields one equation in one unknown. The one-variable bisection algorithm or Matlab's "fsolve" function can be used to solve the resulting equation.

#### 4.1.2.2 Calculating the AS-truncation points.

The AS-truncation points are introduced based on the notion of the trackable domain $TD$ and the quality indicator $I_0$ introduced in Chapter III. In the subsequent discussion, we assume, for simplicity, that $C_0 > 0$, $P_0 > 0$, and $\mu_r \in TD$ for all $K > 0$.

The indicator $I_0$ is defined in Chapter III as:

$$I_0 = \max\{\frac{\sigma_r}{(\frac{1}{KC_0} + P_0)\beta - \mu_r}, -\frac{\sigma_r}{(\frac{1}{KC_0} + P_0)\alpha - \mu_r}\}.$$

Clearly, $I_0$ depends on $K$. Therefore, we denote it by $I_0(K)$. As a rule of thumb, amplitude truncation is typically small when $I_0(K) < 0.4$ (see Chapter III). Based on this idea, the following definition for the AS-truncation points is introduced.

**Definition IV.5.** The AS-truncation points are the poles of

$$T_{tr} = \frac{K_e(K_{I_0})C(s)P(s)}{1 + K_e(K_{I_0})P(s)C(s)},$$

where

$$K_{I_0} = \min_{K>0}\{K : I_0(K) = 0.4\}.$$

Since the termination points occur when $K$ tends to infinity, the AS-truncation points, when they exist, must occur prior to the AS-termination points. We use black squares to denote the AS-truncation points on the AS-root locus.

**Example IV.1.** Consider the system of Figure 4.1.1 with

$$C(s) = 1, P(s) = \frac{s + 20}{(s + 15)(s + 0.5)}, \sigma_r = 1,$$

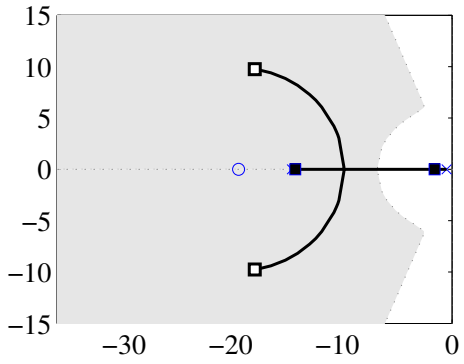


Figure 4.2: AS-root locus.

and $F_{\Omega_r}(s)$ as the third order butterworth filter with bandwidth $\Omega_r = 1$, i.e.,

$$F_{\Omega_r}(s) = \frac{\sqrt{3}}{s^3 + 2s^2 + 2s + 1}. \tag{4.12}$$

Initially, assume that $\alpha = -0.92$, $\beta = 0.92$, and $\mu_r = 0$. This system, which, according to Definition I.1, is symmetric for all $K$, has been studied in Example 5.3 of [1]. Specifically, it has been shown that $K_e^* = \infty$ (i.e., the termination points are at the open loop zeros). Now, assume that $\mu_r = 1$, i.e., the system is asymmetric. The limiting effective gain $K_e^*$, calculated using Theorem IV.1, becomes $K_e^* = 21.4$. The AS-termination points, therefore, are at $-18.5 \pm 9.8j$ instead of the open loop zeros. Furthermore, the gain $K_{I_0}$ calculated using Definition IV.5 is 0.88, and the AS-truncation points are at $-14.7$ and $-1.5$. The complete AS-root locus is shown in Figure 4.2, where, as before, the white squares denote AS-termination points, the black squares denote the AS-truncation points, the x's denote open loop poles and the circle denotes the open loop zero. The shaded area is referred to as the "admissible domain", which is discussed in Section 4.2. Note that, in this example, the truncation points are close to the open loop poles, which, as we show in Section 4.2, implies that amplitude truncation takes place even for small values of controller gain.

#### 4.1.2.3 Calibration of the AS-root locus

Let $\overline{s}$ be a point on the AS-root locus. Clearly, there exists a unique $0 < \overline{K_e}(K) < K_e^*$ such that, with this gain, one of the AS-poles is exactly at $\overline{s}$. But how can we find the gain $K$ that generates $\overline{K_e}(K)$? In this subsection, we explain how the AS-root locus can be calibrated, i.e., given an arbitrary point $\overline{s}$ on the AS-root locus, how can we find the gain $K$ such that

$$1 + \overline{K_e}(K)C(\overline{s})P(\overline{s}) = 0.$$

This can be accomplished using (4.3) and (4.4):

$$\overline{K_e} - K\mathcal{F}_N(K\left\|\frac{F_{\Omega_r}(s)C(s)}{1+P(s)\overline{K_e}C(s)}\right\|_2\sigma_r, \mu_{\hat{u}}) = 0, \tag{4.13}$$

$$\frac{\mu_r}{P_0} - \frac{\mu_{\hat{u}}}{KC_0P_0} - \mathcal{F}_M(K\left\|\frac{F_{\Omega_r}(s)C(s)}{1+P(s)\overline{K_e}C(s)}\right\|_2\sigma_r, \mu_{\hat{u}}) = 0, \tag{4.14}$$

where

$$\overline{K_e} = -\frac{1}{C(\overline{s})P(\overline{s})}.$$

The unknowns in the above two equations are $\mu_{\hat{u}}$ and $K$. The solution $K$ is the desired calibrated gain.

### 4.1.3 TE locus

The TE locus may be plotted for each $K$ using (4.3)-(4.5). As it turns out, it can be either increasing, or decreasing, or even non-monotonic function of $K$. As an example, consider the A-LPNI system of Figure 4.1.1, with

$$P(s) = \frac{1}{s+1}, C(s) = 1, \sigma_r = 1, \tag{4.15}$$

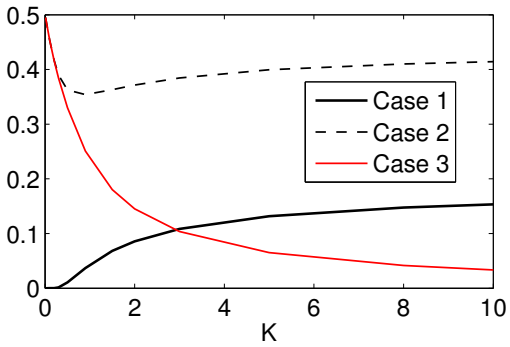


Figure 4.3: TE loci of system (4.15) for three cases.

and $F_{\Omega_r}$ given by (4.12) with $\Omega_r = 1$. Figure 4.3 shows the TE locus of this system for three different cases:

- Case 1: $\alpha = -1.5$, $\beta = 0.5$, $\mu_r = 0$;
- Case 2: $\alpha = -1.5$, $\beta = 0.5$, $\mu_r = 0.5$;
- Case 3: $\alpha = -0.5$, $\beta = 1.5$, $\mu_r = 0.5$;

Clearly, in case 1, the TE locus is increasing for all $K$, in case 2, it is non-monotonic, and in case 3, it is decreasing for all $K$. Furthermore, in cases 1 and 2, this locus does not tend to zero and as $K$ tends to infinity. This is in contrast with linear systems, in which large $K$ implies arbitrarily small steady state tracking error. Note that, using the measure

$$|\frac{\mu_{\hat{e}}}{\mu_r}|,$$

case 2 implies that the steady state tracking error for large gains is 82%, which is significant. The above measure cannot be used in case 1 because $\mu_r = 0$. However, it can be said that in absolute terms, the error is 16%. In case 3, the error tends to zero, similar to linear systems.

The TE loci of Figure 4.3 have been constructed by solving (4.3)-(4.5) for various $K$'s. The following theorem provides a way of sketching TE locus without solving

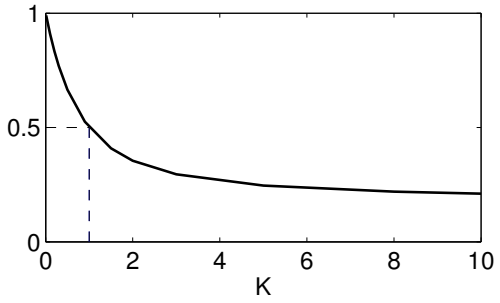


Figure 4.4: A sketch of the TE locus for system (4.15) with $\mu_r = 1$, $\alpha = -0.5$, $\beta = 1.5$.

these equations, but using the properties of the locus at $K = 0$ (origination), $K = \infty$ (termination), and an intermediate $K$ for which the system is symmetric.

**Theorem IV.3.** *Assume that* $\alpha \leq 0 \leq \beta$ *and that* (4.3), (4.4) *admit unique solutions for all* $K$. *Then,* $\mu_{\hat{e}}(K)$ *has the following properties:*

*a.* $\lim_{K\to 0^+} \mu_{\hat{e}}(K) = \begin{cases} \mu_r, & P_0C_0 \neq \infty, \\ 0, & P_0C_0 = \infty; \end{cases}$

*b.* $\lim_{K\to\infty} \mu_{\hat{e}}(K) = \frac{\phi^*\eta^*}{C_0}$, *where* $\phi^*$ *and* $\eta^*$ *are the solution of* (4.7) *and* (4.8)*;*

*c. If* $\frac{\mu_r}{P_0} > \frac{\alpha+\beta}{2}$, *then* $\mu_{\hat{e}}(K) = \frac{\mu_r}{1+KP_0C_0}$, *where* $K = \frac{1}{C_0(\frac{\mu_r}{\frac{\alpha+\beta}{2}} - P_0)}$

*Proof.* See Section A.3. □

For instance, applying this theorem to system (4.15) with $\mu_r = 1$, $\alpha = -0.5$, $\beta = 1.5$, we obtain:

$$\mu_{\hat{e}}(0) = 1, \mu_{\hat{e}}(\infty) = 0.18, \mu_{\hat{e}}(1) = 0.5. \tag{4.16}$$

Therefore, the TE locus can be sketched as shown in Figure 4.4.

Returning to Example IV.1, the TE locus of the system is plotted in Figure 4.5. This locus originates at $\mu_{\hat{e}}(0) = 1$ and terminates at $\mu_{\hat{e}}(\infty) = 0.016$.

The following theorem provides structural properties of the TE locus.

**Theorem IV.4.** *Assume that* (4.3), (4.4) *admit unique solutions for all* $K$. *Then,* $\mu_{\hat{e}}(K)$ *has the following properties:*

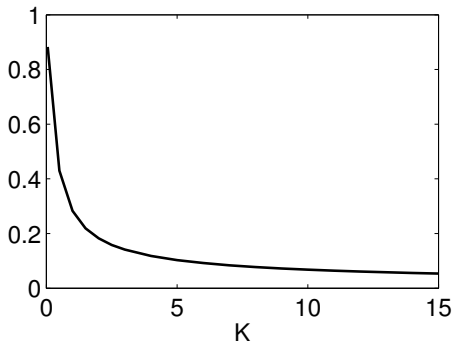


Figure 4.5: The TE locus for Example IV.1.

*a. If* $C_0 = \infty$*, then* $\mu_{\hat{e}}(K) = 0$ *for all* $K$*;*

*b.* $\lim_{K\to\infty} \mu_{\hat{e}}(K) = 0 \iff (K_e^* = \infty)$ *or* $(C_0 = \infty)$ *or* $(\frac{\mu_r}{P_0} = \frac{\alpha+\beta}{2})$*, where* $K_e^*$ *is given in Theorem IV.1.*

*c. If* $P_0 \neq \infty$*,* $\mu_r - P_0\beta < \mu_{\hat{e}} < \mu_r - P_0\alpha$*.*

*d. If* $\mu_{\hat{e}}(\infty) < \mu_{\hat{e}}(0)$*, then there exists a portion of the TE locus that is decreasing.*

*e. If* $\mu_{\hat{e}}(\infty) > \mu_{\hat{e}}(0)$*, then there exists a portion of the TE locus that is increasing.*

*Proof.* See Section A.3. □

Thus, when $C_0 = \infty$, the TE is identically zero. Moreover, the TE locus tends to zero (similar to linear systems) when $K_e^* = \infty$, i.e., when the AS-root locus coincides with the usual linear root locus, or when $\frac{\mu_r}{P_0} = \frac{\alpha+\beta}{2}$, i.e., the system becomes symmetric at $K = \infty$.

### 4.1.4 Effect of asymmetry on the performance loci

In this subsection, we first study, with an example, the effect of controller gain $K$ on the degree of asymmetry. We then explore the effects of asymmetry on the performance loci.

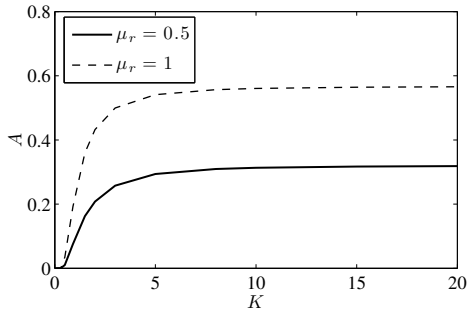


Figure 4.6: $A$ as a function of $K$.

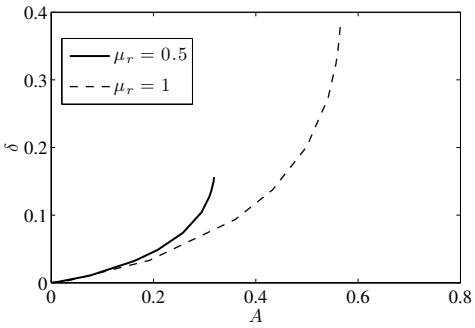


Figure 4.7: $\delta$ as a function of $A$.

Consider

$$P(s) = \frac{1}{s+1}, C(s) = 1, \sigma_r = 1, \alpha = -1, \beta = 1,$$

and two $\mu_r$'s: $\mu_r = 0.5$ and $\mu_r = 1$. For each $\mu_r$, Figure 4.6 plots $A$ defined in (2.30) as a function of $K$. Clearly, for both cases, as $K$ increases, asymmetry increases. Furthermore, asymmetry is larger for larger $\mu_r$.

The following theorem provides, similar to Theorem IV.3, a method for computing $A(K)$ when $K \to 0$ and $K \to \infty$.

**Theorem IV.5.** *Assume that* (4.3), (4.4) *admit unique solutions for all* $K$ *and* $\alpha < 0 < \beta$. *Then, the degree of asymmetry* $A$ *satisfies the following properties:*

*a.* $\lim_{K \to 0^+} A(K) = \begin{cases} 0, & (C_0 \neq \infty) \text{ or } (C_0 = \infty \text{ and } \frac{\mu_r}{P_0} \in [\alpha, \beta]), \\ 1, & \text{otherwise.} \end{cases}$

*b.* $\lim_{K\to\infty} A(K) = \begin{cases} 0, & \frac{\mu_r}{P_0} = \frac{\alpha+\beta}{2}, \\ \operatorname{erf}(\frac{\eta^*}{\sqrt{2}}), & otherwise, \end{cases}$

*where* $\eta^*$ *is given by* (4.7) *and* (4.8).

*Proof.* See Section A.3. □

We now explore the effect of asymmetry on the performance loci. To accomplish this, we consider again the above example. To illustrate the effect of asymmetry on the TE locus, note that, without saturation, the TE locus of the linear system behaves as $\frac{1}{1+KC_0P_0}\mu_r$. Thus, to study how detrimental the effect of asymmetry is, we introduce $\delta$, the deviation of the TE locus from $\frac{1}{1+KC_0P_0}\mu_r$:

$$\delta = \mu_{\hat{e}} - \frac{1}{1+KC_0P_0}\mu_r.$$

When $\delta = 0$, the TE locus of the A-LPNI system coincides with that of the linear system; otherwise, it does not. Figure 4.7 plots $\delta$ as a function of $A$ for both $\mu_r = 0.5$ and $\mu_r = 1$. Clearly, in both cases, $\delta$ increases with asymmetry.

We now study the effects of asymmetry on the TE and AS-root loci for fixed controller gains. To accomplish this, we consider three $K$'s: $K = 1$, $K = 5$, and $K = \infty$. For each $K$, we compute $A(K)$, $K_e(K)$, and $\mu_{\hat{e}}(K)$ for $\mu_r \in [-2, 2]$. Figures 4.8.1 and 4.8.2 illustrate, respectively, the effective gain $K_e$ and $\delta$ as a function of $A$. Clearly, for each $K$, as magnitude of asymmetry increases, the effective gain decreases. Specifically, the termination gain $K_e^*$ decreases, which implies that the termination points move closer to the open loop poles as asymmetry increases. Furthermore, as the magnitude of the asymmetry increases, $|\delta|$ increases. Therefore, the TE locus of the LPNI system deteriorates with asymmetry. This example suggests that with increasing asymmetry, both dynamic and steady state tracking of A-LPNI systems degrade.

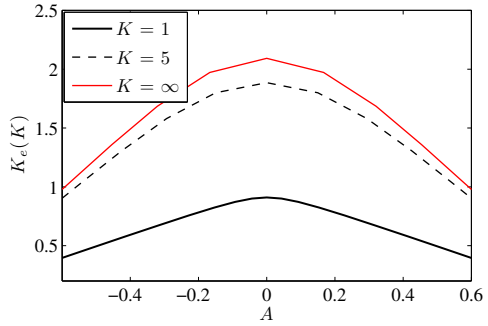


4.8.1: $K_e$.

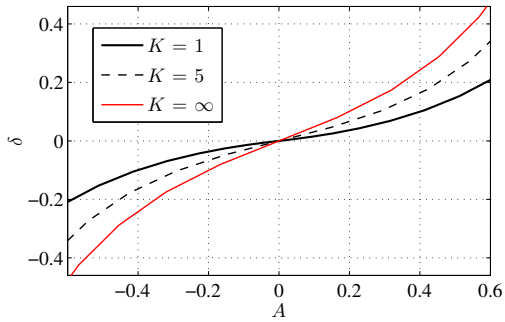


4.8.2: $\delta$.

Figure 4.8: $K_e$ and $\delta$ as a function of $A$.

## 4.2 Design using the performance loci

### 4.2.1 Design for required dynamic performance

#### 4.2.1.1 Review of the admissible domain for random reference tracking

In linear systems theory, the admissible domain for deterministic signals is derived based on overshoot, rise time, etc., of the step response. For random references, however, the admissible domain is based on the quality indicators $I_2$ and $I_3$, which were presented in [1] for linear systems:

$$I_2 = \frac{\Omega}{R\Omega_{BW}}, I_3 = \min\{RM_r - 1, \frac{\Omega}{R\Omega_r}\}.$$

Here, $\Omega$ is the bandwidth of the input coloring filter, $R\Omega_{BW}$ is the random bandwidth, i.e.,

$$R\Omega_{BW} = \min_{\Omega>0}\{RS(\Omega) = \frac{1}{\sqrt{2}}\},$$

and $RM_r$, $R\Omega_r$ are, respectively, the resonance peak and resonance frequency of the RS:

$$R\Omega_r = \arg\sup_{\Omega>0} RS(\Omega),$$

$$RM_r = \sup_{\Omega>0} RS(\Omega).$$

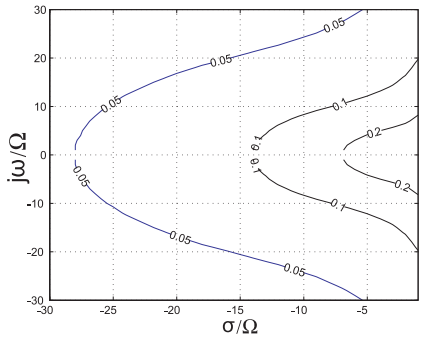


4.9.1: The level curves of $I_2$.

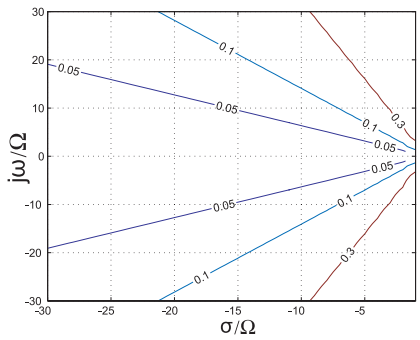


4.9.2: The level curves of $I_3$.

Figure 4.9: The level curves of $I_2$ and $I_3$ for the prototype second order system.

In the above definitions, the random sensitivity function is defined as $RS(\Omega) = \left\| \frac{F_\Omega(s)}{1+C(s)P(s)} \right\|_2$, where $F_\Omega$ is assumed to be the Butterworth filter with bandwidth $\Omega$: $F_\Omega(s) = \sqrt{\frac{3}{\Omega}} \frac{\Omega^3}{s^3+2\Omega s^2+2\Omega^2 s+\Omega^3}$.

To derive the admissible domain for random reference tracking, the authors in [1] assume that $C(s)P(s)$ is such that the closed loop transfer function is the prototypical second order system with natural frequency $w_n$ and damping ratio $\zeta$: $T(s) = \frac{w_n^2}{s^2+2\zeta w_n s+w_n^2}$. The authors then proceed to compute the level curves of $I_2$ and $I_3$, using the definitions above, for different values of $w_n$ and $\zeta$. These level curves are shown in Figure 4.9.1 and Figure 4.9.2, respectively. Note that the axes of these figures are scaled by the input bandwidth $\Omega$. The complete admissible domain is the superposition of the level curves for $I_2$ and $I_3$. For example, for $I_2 < 0.1$ and $I_3 < 0.3$, the admissible domain is the shaded area shown in Figure 4.10.

Lastly, it is shown in [1] that the notion of dominant poles in linear systems theory also holds for tracking random references. In other words, to design a good tracking controller, it suffices to place the dominant closed loop poles within the admissible domain.

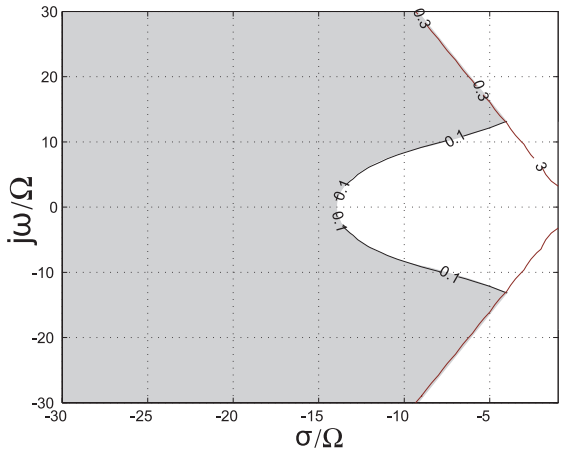


Figure 4.10: The admissible domain for $I_2 < 0.1$ and $I_3 < 0.3$.

#### 4.2.1.2 Design methodology

The design goal is to choose gain $K$ so that all AS-poles are within the admissible domain and positioned prior to the AS-truncation points. Note that there exists a fundamental trade-off in the size of $K$: it must be large enough to achieve static responsiveness, but small enough to avoid amplitude truncation.

Returning to the AS-root locus of the system in Example IV.1 (see Figure 4.2), the AS-truncation points are outside the admissible domain; therefore, the quality of tracking is bad due to amplitude truncation. To alleviate this problem, the authority of the actuator must be increased. With $\beta = 1.3$, the termination gain is $K_e^* = 10^4$ and the truncation gain $K_{I_0}$ is 39. The AS-root locus for this case is shown in Figure 4.11. Selecting $4 < K < 39$, the AS-poles are within the admissible domain and prior to the AS-truncation points. As far as static responsiveness is concerned, assume that the specifications call for $\frac{1}{1+KC_0P_0} < 0.05$. This implies that $K > 7.2$. Therefore, to achieve both good dynamic tracking and static responsiveness, $K$ must satisfy

$$7.2 < K < 39. \tag{4.17}$$

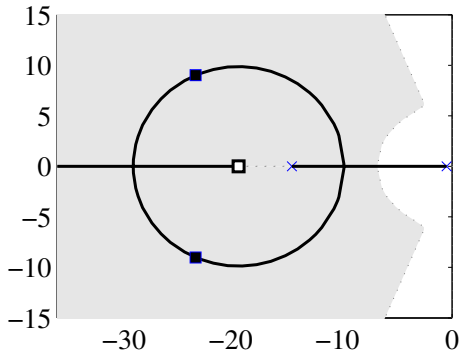


Figure 4.11: AS-root locus with $\beta = 1.3$.

### 4.2.2 Design for required steady state performance

Assume that the steady state specifications call for $|\mu_{\hat{e}}(K)| < \overline{\mu}_e$. Based on this specification, an admissible domain for TE can be introduced (see the shaded area in Figure 4.12). For design, gain $K$ must be selected such that the TE locus is in the admissible domain.

Returning to Example IV.1, assume that the specifications call for $|\mu_{\hat{e}}(K)| < 0.05$. The TE locus of the system, along with the admissible domain, is plotted in Figure 4.12. As it follows from Figure 4.12, the TE loci for $\beta = 0.92$ and $\beta = 1.3$ are in the admissible domain for $K > 17$ and $K > 7.6$, respectively.

Combining the above results, we conclude that, for the case of $\beta = 1.3$, for good static and dynamic tracking, $K$ must satisfy

$$7.6 < K < 39.$$

Selecting $K = 35$, we illustrate the quality of tracking for both $\beta = 0.92$ and $\beta = 1.3$ in Figure 4.13. Clearly, the quality of tracking is good for $\beta = 1.3$, but poor for $\beta = 0.92$ because of amplitude truncation.

There may be cases where the AS-poles and TE cannot be placed in their respective admissible domains simultaneously. An example of this situation is as follows.

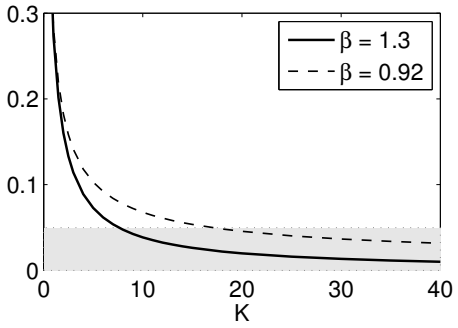


Figure 4.12: The TE locus for Example 1 with $\beta = 0.92$ and $\beta = 1.3$.

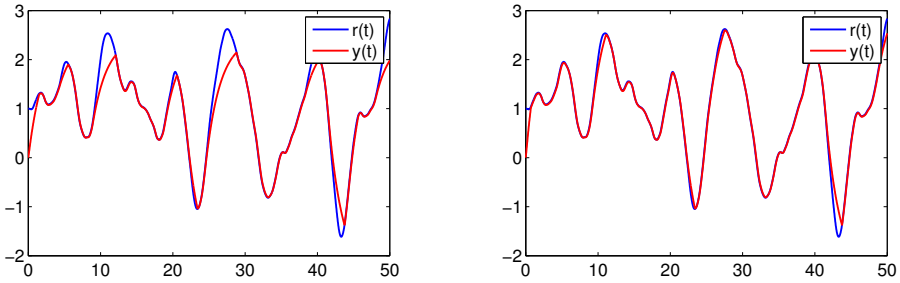


4.13.1: $\beta = 0.92$.

4.13.2: $\beta = 1.3$.

Figure 4.13: Responses of the system of Example IV.1.

**Example IV.2.** Consider the system of Figure 4.1.1 with

$$C(s) = 1, P(s) = \frac{3}{0.5s + 1}, \sigma_r = 1, \mu_r = 5, \alpha = 0, \beta = 2,$$

and $F_{\Omega_r}(s)$ as the third order butterworth filter with bandwidth $\Omega_r = 2$. Assume that the steady state specifications call for $TE < 0.1$. The AS-root locus and TE locus of this system are plotted in Figure 4.14. As it follows from the AS-root locus, to place the AS-poles within the admissible domain and prior to the truncation points, K must satisfy $1.24 < K < 1.33$. However, to place the TE within the admissible domain, $K$ must satisfy $K > 21.5$. Clearly, no $K$ satisfies both requirements. Figure 4.15 shows the response of the system with $K = 1.3$ and $K = 22$. Clearly, with $K = 1.3$, dynamic tracking is good but there exist significant error in tracking of average values. With $K = 22$, the steady state tracking is good but significant output truncation occurs.

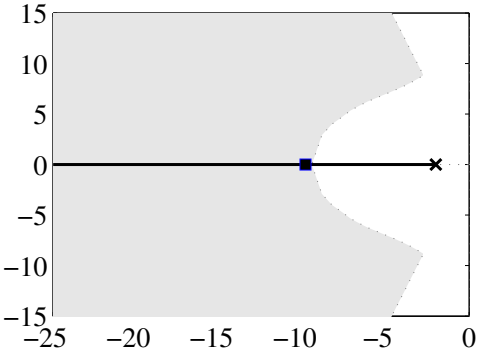


4.14.1: AS-root locus.

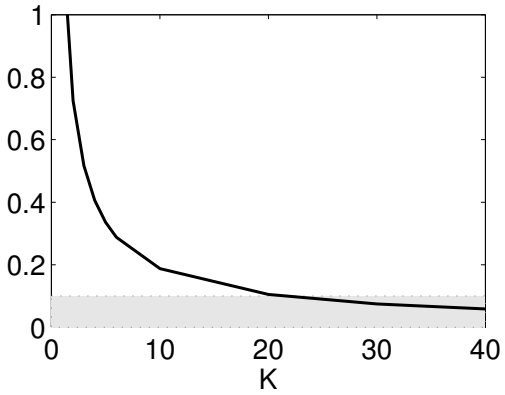


4.14.2: TE locus.

Figure 4.14: AS-root locus and TE locus of Example IV.2.

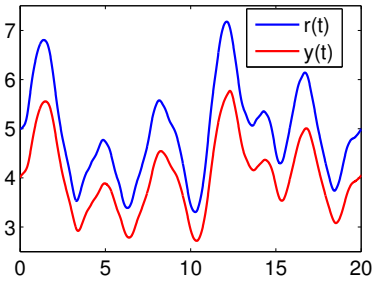


4.15.1: $K = 1.3$.

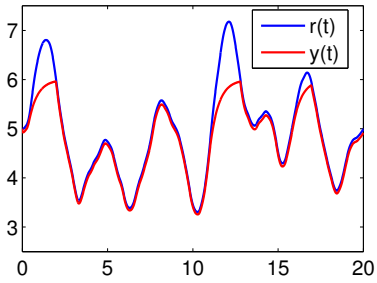


4.15.2: $K = 22$.

Figure 4.15: Response of the system of Example IV.2.

# CHAPTER V

# Design of Step-Tracking Controllers in LPNI Systems

This chapter presents a QLC-based method for step-tracking controller design of systems with saturating actuators. Since this problem has not been addressed for the symmetric case, we begin the development with S-LPNI systems and then extend the results to the A-LPNI case. Although the focus throughout this chapter is on the saturating actuator, the methods developed here can be applied to other nonlinearities as well. Based on the developed methodology, in the second part of this chapter, we address the problem of anti-windup design.

## 5.1 Design of Step-Tracking Controllers

### 5.1.1 Motivation

Consider the feedback system of Figure 5.1.1, where

$$P(s) = \frac{1}{s^2 + 0.4s + 1}, \tag{5.1}$$

and $\text{sat}_\alpha(u)$ is the symmetric saturation function shown in Figure 5.1.2. The problem is to design a controller, $C(s)$, so that the closed loop system tracks unit step reference

signal satisfying the following specifications:

$$\begin{aligned} &\text{Steady state error} \leq 1\%; \quad \text{Overshoot} \leq 5\%; \\ &\text{Settling time} \leq 1\,\text{sec}. \end{aligned} \tag{5.2}$$

Since there are no rigorous methods for designing step-tracking controllers for systems with saturating actuators, one usually designs a controller satisfying (5.2) assuming that the actuator is linear and then verifies the performance using simulations. For the system of Figure 5.1 a controller can be selected, for example, as

$$C(s) = \frac{22s + 200}{0.01s + 1}, \tag{5.3}$$

and the resulting performance meets the specifications if, say, $\alpha = 25$ (see Figure 5.2.1). However, if $\alpha = 10$, the step response does not meet the dynamic part of the specs (overshoot degrades – see Figure 5.2.2). If $\alpha = 5$, not only does overshoot degrade, but the settling time spec is also violated (see Figure 5.2.3). Finally, if $\alpha = 0.5$, not only is the dynamic part of the specs violated, but the steady state spec is also violated (see Figure 5.2.4).

So, given a specific $\alpha$, how can a step-tracking controller be designed so that the step response meets the specs, if at all possible? This is the question addressed in this section.

The development here is based on the time domain design method of Chapter IV.

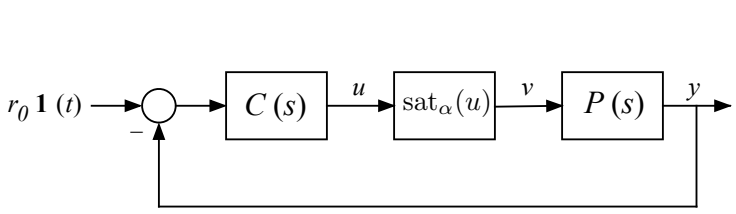


5.1.1: System with saturating actuator.

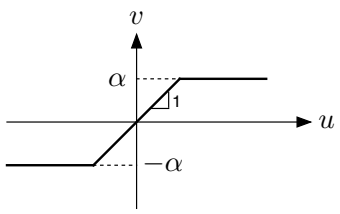


5.1.2: Saturation function $v = \text{sat}_\alpha(u)$.

Figure 5.1: Motivating example.

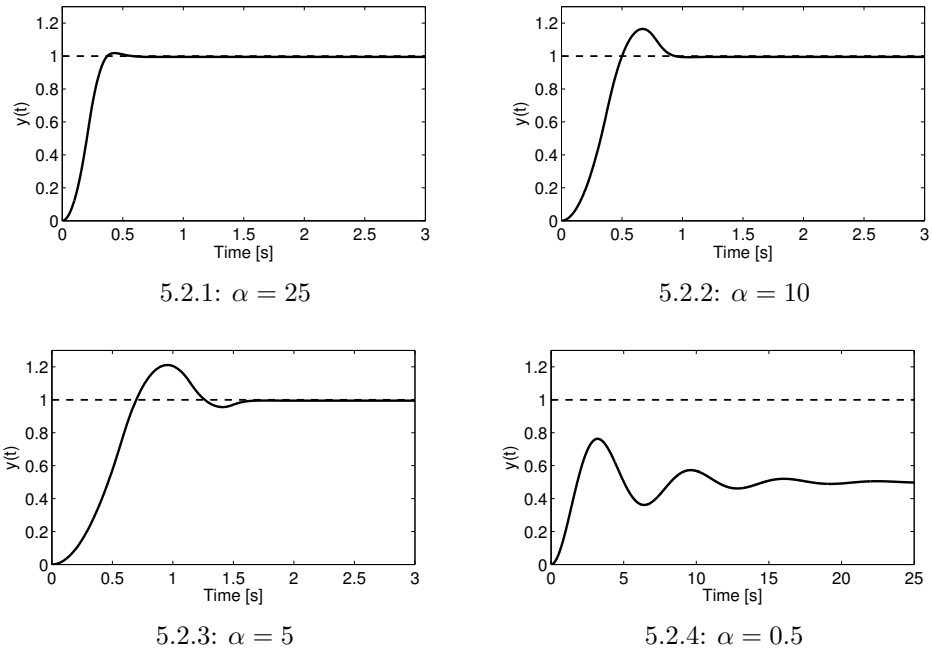


5.2.1: $\alpha = 25$ 5.2.2: $\alpha = 10$

5.2.3: $\alpha = 5$ 5.2.4: $\alpha = 0.5$

Figure 5.2: Step responses of the motivating example.

In Chapter IV, these controllers are designed to track random references. Here, we extend the results to track steps.

The QLC block-diagram relevant to this chapter is shown in Figure 5.3.1 (the case of asymmetric saturation function is treated in Subsection 5.1.6). Here, the reference signal $r(t)$ is generated by filtering a standard Gaussian white noise process scaled by $r_0$ through a 3rd order Butterworth filter with 3dB bandwidth $\Omega$:

$$F_\Omega(s) = \sqrt{\frac{3}{\Omega}} \left( \frac{\Omega^3}{s^3 + 2\Omega s^2 + 2\Omega^2 s + \Omega^3} \right). \tag{5.4}$$

In the current section, this block-diagram is modified as shown in Figure 5.3.2. Here, the reference signal is generated by processing a step signal of size $r_0$ by a nominal second order system,

$$F_d(s) = \frac{\omega_n^2}{s^2 + 2\zeta\omega_n s + \omega_n^2}, \tag{5.5}$$

where $\zeta$ and $\omega_n$ are selected so that the output of $F_d(s)$ (i.e., $r(t)$) satisfies specifications of type (5.2). The goal is to design a controller $C(s)$, if at all possible, such

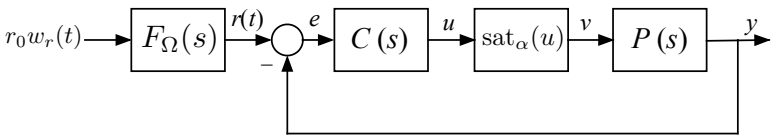


5.3.1: Random reference tracking system.

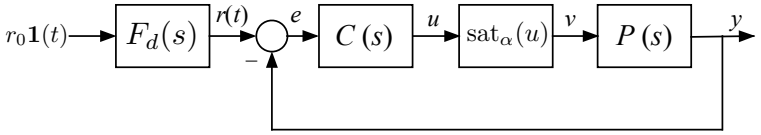


5.3.2: Step reference tracking system.

Figure 5.3: Systems for tracking random and step inputs.

that the output $y(t)$ tracks well $r(t)$ (instead of the step-signal itself) and, therefore, satisfies the specs. To this end, in this section we

1. Verify if a necessary condition for existence of a controller that meets the specs is satisfied.

2. Convert the dynamic part of the step tracking specifications to random-signal tracking specifications. This is carried out by determining $\Omega$ from the dynamic part of the specs such that if a controller for the system of Figure 5.3.1 tracks well the random reference $r(t)$ with this bandwidth, the same controller tracks well $r(t)$ in Figure 5.3.2; we refer to this $\Omega$ as the *adjoint bandwidth* and denote it by $\Omega_a$.

3. Design such a controller for the system of Figure 5.3.1 with $\Omega = \Omega_a$, using the S-root locus approach (note that S-root locus, developed in [1], is a special case of AS-root locus and is only applicable to symmetric systems).

4. Finally, use the same controller in the system of Figure 5.3.2. By doing so, we view the output of $F_d(s)$, i.e., $r(t)$, as the function to be tracked, rather than the step signal itself. In other words, $F_d(s)$ can be viewed as a pre-compensator in a 2 degree-of-freedom architecture [65].

The two key ideas that lead to this design method are:

1. "connecting" step tracking specs (5.2) with adjoint bandwidth $\Omega_a$;

2. viewing the output of $F_d(s)$, i.e., $r_2(t)$, as the function to be tracked (rather than the step signal itself). We refer to this $r(t)$ as the *modified step* signal.

The above approach may lead to a conservative design since the adjoint bandwidth may be too large. Nevertheless, as demonstrated in this section, the proposed method is practical and systematic.

Summarizing, the original contribution of this section is in employing Quasilinear Control Theory to provide a direct method for linear step tracking controller design in systems with saturating actuators.

Below, we first provide a necessary and sufficient condition for existence of a step-tracking controller satisfying steady state specs. We then present a method for calculating the adjoint bandwidth, $\Omega_a$. Next, we show several examples indicating that if a controller tracks well random references in Figure 5.3.1, it also tracks well $r(t)$ of Figure 5.3.2, thereby satisfying the specs. Lastly, we compare the QLC method with the anti-windup technique

### 5.1.2 Necessary and Sufficient Condition for Existence of Step Tracking Controllers Satisfying Steady State Specifications

Consider the system of Figure 5.3.2 and the following steady state specifications:

$$\begin{aligned} &r_0 \leq r_0^*, \\ &\text{Steady state error} = \frac{\lim_{t\to\infty} |e(t)|}{r_0} \leq e_{ss}^*, \end{aligned} \tag{5.6}$$

where $r_0^*$ is the maximum step size to be tracked, $e(t)$ is the tracking error, i.e., $e(t) = r(t) - y(t)$, and $e_{ss}^* < 1$. For simplicity, we assume that only positive steps are required to be tracked. Let $P_0$ and $C_0$ be the dc-gains of the plant and controller, respectively. The following proposition provides a necessary and sufficient condition

for existence of a controller that satisfies the above specifications.

**Proposition V.1.** *Assume $P_0 > 0$ and $C_0 > 0$. Then, a controller that satisfies* (5.6) *exists if and only if*

$$r_0^* \leq \frac{P_0 \alpha}{1 - e_{ss}^*}. \tag{5.7}$$

*Proof.* See Section A.4. □

Note that while (5.7) is a necessary and sufficient condition for existence of a controller satisfying the steady state part of the specs, it is also a necessary condition for existence of a controller satisfying all specs, steady state and dynamic.

Returning to the motivating example of Section 5.1.1, we observe that for $\alpha = 5$, the value of $\frac{P_0 \alpha}{1-e_{ss}^*}$ is 5.05, and therefore, the condition for existence of a unit step tracking controller is satisfied. On the other hand, for $\alpha = 0.5$, $\frac{P_0 \alpha}{1-e_{ss}^*} = 0.505$, and therefore, no controller satisfying the specs exists.

### 5.1.3 Calculating the Adjoint Bandwidth

Assume that the dynamic part of step-tracking specifications is as follows:

$$\begin{aligned} &\text{Overshoot} \leq OS^*\%; \\ &\text{Settling time} \leq t_s^* \text{ sec}; \\ &\text{Rise time} \leq t_r^* \text{ sec}. \end{aligned} \tag{5.8}$$

**Proposition V.2.** *Let $F_d(s)$ be the nominal second order transfer function* (5.5)*, whose step response satisfies specs* (5.8)*. Then, the adjoint bandwidth is given by*

$$\Omega_a = \sqrt{2}\omega_n \exp\left(-\frac{\sigma}{\omega_d} \tan^{-1}(\frac{\omega_d}{\sigma})\right), \tag{5.9}$$

*where $\sigma = \zeta\omega_n$ and $\omega_d = \omega_n\sqrt{1-\zeta^2}$.*

*Justification:* The adjoint bandwidth is defined by equating the maximum rate of change of $r(t)$ in Figure 5.3.2 with the standard deviation of the rate of change of $r(t)$ in Figure 5.3.1. It can be shown that the maximum rate of change of $r(t)$ in Figure 5.3.2 is given by

$$\max_{t\geq 0} \dot{r}(t) = \omega_n \exp(-\frac{\sigma}{\omega_d} \tan^{-1}(\frac{\omega_d}{\sigma}))r_0, \tag{5.10}$$

and the standard deviation of the rate of change of $r(t)$ in Figure 5.3.1 is the $H_2$-norm of $sF_\Omega(s)$, i.e.,

$$\left\| sF_\Omega(s) \right\|_2 = \frac{\Omega}{\sqrt{2}} r_0. \tag{5.11}$$

Therefore, $\Omega_a$ is defined by the equation

$$\omega_n \exp(-\frac{\sigma}{\omega_d} \tan^{-1}(\frac{\omega_d}{\sigma}))r_0 = \frac{\Omega_a}{\sqrt{2}} r_0,$$

which leads to (5.9). □

For the motivating example of Section 5.1.1, based on the dynamic part of the specs, we select

$$F_d(s) = \frac{34}{s^2 + 8s + 34}. \tag{5.12}$$

Using (5.9) and this $F_d(s)$, the adjoint bandwidth for the motivating example is $\Omega_a = 3.8$.

### 5.1.4 Examples of QLC-based controller design

In this section, we illustrate the method developed above for the motivating example and three types of step tracking specs: those with non-zero steady state error, those with zero steady state error, and those with zero overshoot.

#### 5.1.4.1 Design for the motivating example

In this subsection, we illustrate the method of this Chapter for the motivating example of Section 5.1.1.

Figure 5.4.1 shows the admissible domain (shaded area) and the S-root locus for the motivating example of Section 5.1.1 with $\alpha = 25$, adjoint bandwidth $\Omega_a = 3.8$, and the controller selected as:

$$C(s) = K\frac{22s + 200}{0.01s + 1}. \tag{5.13}$$

For this example, the termination and truncation points of the S-root locus coincide with the open loop zeros; therefore, the S-poles can be selected within the admissible domain. With $K = 1$, the resulting trajectories of the closed loop system of Figure 5.3.1 are shown in Figure 5.5.1. Clearly, the quality of random reference tracking is good.

Since the unit step is in the trackable domain when $\alpha = 25$, we use the same controller in Figure 5.3.2. The resulting response is shown in Figure 5.5.2. Clearly, the quality of tracking is good, and specs (5.2) are satisfied.

With $\alpha = 10$, using the same controller (5.13), the S-root locus of the motivating example is shown in Figure 5.4.2. Obviously, the S-root locus terminates before entering the admissible domain. Consequently, the quality of tracking is low for random references (see Figure 5.6.1). Figure 5.6.2 shows the tracking quality for the system of Figure 5.3.2. As can be seen, overshoot does not meet the specs and the quality of tracking is poor.

When $\alpha$ is even smaller, the termination points move closer to the open loop poles, and the quality of tracking degrades further.

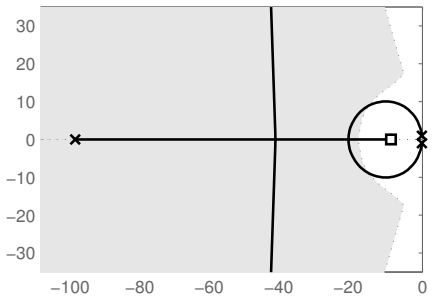


5.4.1: $\alpha = 25$.

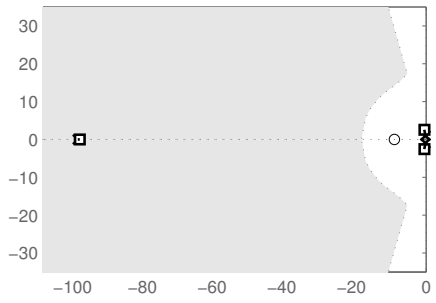


5.4.2: $\alpha = 10$.

Figure 5.4: S-root loci of the motivating example.

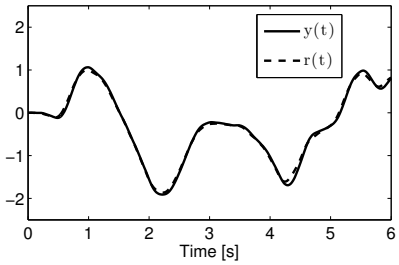


5.5.1: Random signal tracking.

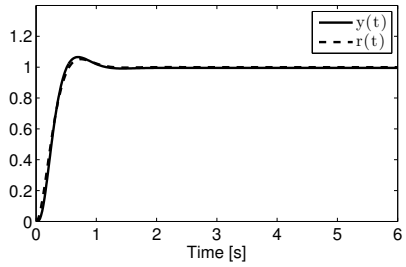


5.5.2: Step tracking.

Figure 5.5: Trajectories of the systems of Figure 5.3.1 and 5.3.2 for the motivating example of Section 5.1.1 with $\alpha = 25$ and $K = 1$.

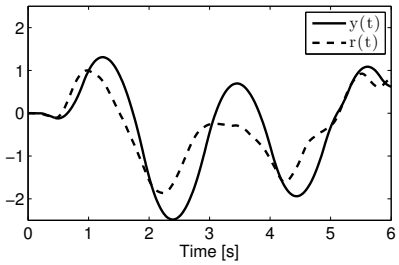


5.6.1: Random signal tracking.

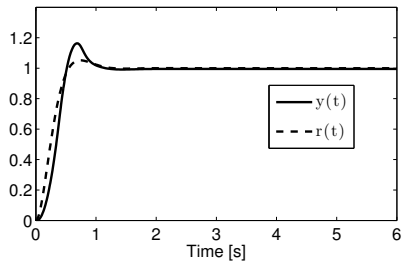


5.6.2: Step tracking.

Figure 5.6: Trajectories of the systems of Figure 5.3.1 and 5.3.2 for the motivating example of Section 5.1.1 with $\alpha = 10$ and $K = 1$.

#### 5.1.4.2 Specs with non-zero steady state tracking error

Consider the system of Figure 5.3.2 with

$$P(s) = \frac{116}{(s^2 + 20s + 116)(0.02s + 1)}$$

and $\alpha = 1.5$. The goal is to design a pre-compensator $F_d(s)$ and a controller $C(s)$ that achieve the following step-tracking specifications:

$$\begin{aligned} &r_0 \leq 1.5; \\ &\text{Steady state error} < 2.5\%; \\ &\text{Overshoot} \leq 5\%; \\ &\text{Settling time} \leq 1\,\text{sec}. \end{aligned} \tag{5.14}$$

First, we check condition (5.7). Since $r_0^* = 1.5 < \frac{P_0\alpha}{1-e_{ss}^*} = 1.54$, this condition is satisfied and the steady state spec can be met. As far as the dynamic part of the specs is concerned, since it is the same as (5.2), filter $F_d(s)$ is given by (5.12) and the adjoint bandwidth is $\Omega_a = 3.8$ as before.

The poles of the plant $P(s)$ are at $-10 \pm 4j, -50$. Clearly, the complex conjugate poles are dominant. In [1], it is shown that the idea of dominant poles works in systems with saturating actuators in the same manner as it does in the linear case. Accordingly, we design a controller such that these dominant poles enter the admissible domain, while still remaining dominant in the closed loop.

Given the above plant, we select the following controller:

$$C(s) = K\frac{s + 30}{0.01s + 1}.$$

The S-root locus of the resulting system is shown in Figure 5.7. With the controller gain $K = 1.5$, the S-poles are within the admissible domain and prior to the truncation

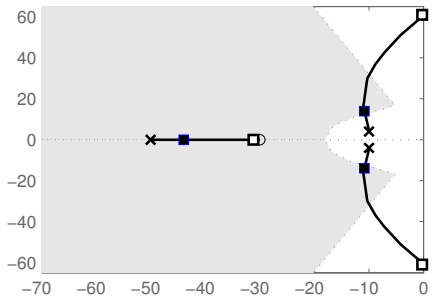


Figure 5.7: S-root locus for the example of Subsection 5.1.4.2.

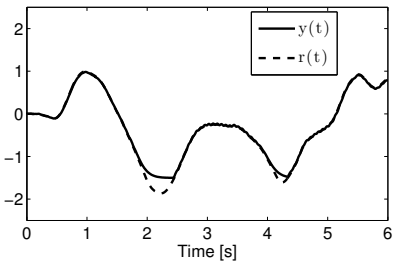


5.8.1: Random tracking.

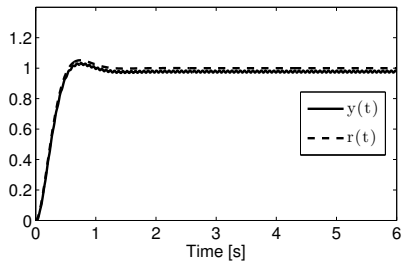


5.8.2: Step tracking.

Figure 5.8: Trajectories of the system in Subsection 5.1.4.2.

points (black squares on the S-root locus); thus, both steady state and dynamic specs are satisfied. The resulting performance of systems of Figures 5.3.1 and 5.3.2 is illustrated in Figures 5.8.1 and 5.8.2, respectively. Clearly, step tracking specifications are satisfied.

Note that in Figure 5.8.1, the quality of random reference tracking deteriorates at two time moments (around $t = 2$s and $t = 4$s). This is because with the selected $K$, the S-poles are close to the S-truncation points. However, since $r_0 = 1$ is inside the trackable domain, tracking of the unit step in Figure 5.8.2 is good.

#### 5.1.4.3 Specs with zero steady state tracking error

In this subsection, we consider two examples. In the first one, the plant has a pole at the origin, while in the second, it does not.

**Designing a controller for a plant with a pole at the origin:**

Consider the system of Figure 5.3.2 with

$$P(s) = \frac{10}{s(s+10)}$$

and $\alpha = 3$. The goal is to design pre-compensator $F_d(s)$ and controller $C(s)$ that achieve the following step tracking specifications:

$$\begin{aligned} &r_0 \leq 2; \\ &\text{Steady state error} = 0; \\ &\text{Overshoot} \leq 5\%; \\ &\text{Settling time} \leq 1\,\text{sec}. \end{aligned} \tag{5.15}$$

Clearly, since $P_0 = \infty$, from (5.7) we conclude that the steady state part of the specs are satisfied by any controller without a zero at the origin.

Based on the dynamic part of the specs, the filter $F_d(s)$ is still given by (5.12) (since the dynamic specs remain the same), for which the adjoint bandwidth is again $\Omega_a = 3.8$. Select the phase-lead controller

$$C(s) = K\frac{s+z}{s+p},\ p > z, \tag{5.16}$$

where $p$ and $z$ are design parameters. The S-root locus of this closed loop system with $z = 20$ and $p = 100$ is shown in Figure 5.9. Clearly, it does not enter the admissible domain. Moreover, calculations using different $p$'s and $z$'s show that for any finite $p$ and $z$ with $z < p$, the S-root locus still remains outside the admissible domain and, thus, a lead controller cannot satisfy the dynamic part of the specs if $\alpha = 3$.

However, if one uses an actuator with $\alpha = 4$, controller (5.16) with $z = 20$ and $p = 100$ leads to the S-root locus shown in Figure 5.10, which does enter the admissible domain. Selecting $K = 200$ results in responses of the systems of Figures 5.3.1 and

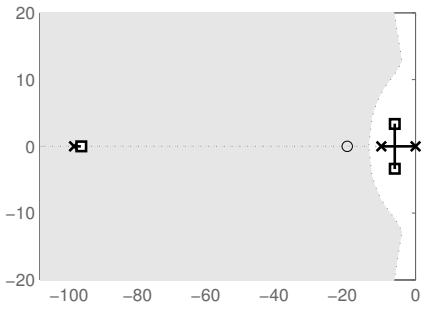


Figure 5.9: S-root locus of the example of Subsection 5.1.4.3 with $\alpha = 3$

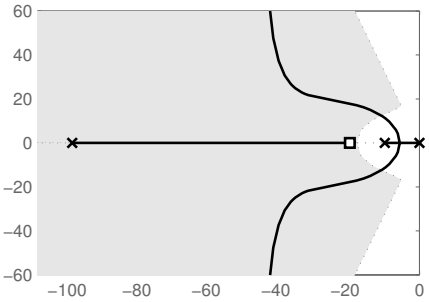


Figure 5.10: S-root locus of the example of Subsection 5.1.4.3 with $\alpha = 4$

5.3.2 shown in Figures 5.11.1 and 5.11.2, respectively. Clearly, the quality of tracking is good in both cases, and the step tracking specifications are satisfied. Note that in this example no windup occurs, since the controller has no pole at the origin.

**Designing a controller for a plant without a pole at the origin:**

Consider the system of Figure 5.3.2 with

$$P(s) = \frac{150}{s^2 + 28s + 232} \tag{5.17}$$

and $\alpha = 4$. The goal is to design a pre-compensator and controller such that the

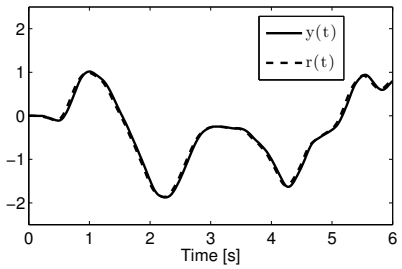


5.11.1: Random tracking.

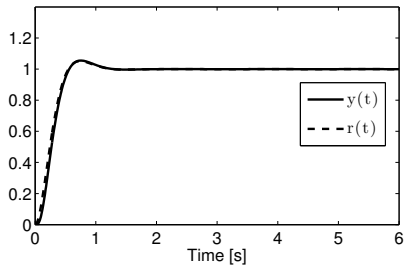


5.11.2: Step tracking.

Figure 5.11: Trajectories of the system in Subsection 5.1.4.3 with $\alpha = 4$.

closed loop system satisfies the following specifications:

$$\begin{aligned} &r_0 \leq 1; \\ &\text{Steady state error} = 0; \\ &\text{Overshoot} \leq 5\%; \\ &\text{Settling time} \leq 1\,\text{sec}. \end{aligned} \tag{5.18}$$

Since $r_0^* = 1 < \frac{P_0\alpha}{1-e_{ss}^*} = 2.58$, (5.7) is satisfied, and to meet the steady state specs, the controller must have a pole at the origin.

Similar to the previous subsection, $F_d(s)$ is given by (5.12) and the adjoint bandwidth is $\Omega_a = 3.8$. Select a PI controller as follows:

$$C(s) = K\left(3 + \frac{75}{s}\right).$$

The S-root locus is shown in Figure 5.12, which enters the admissible domain. With $K = 1$, the S-poles are within the admissible domain. For this $K$, the quality of tracking for the system of Figures 5.3.1 and 5.3.2 are shown in Figures 5.13.1 and 5.13.2, respectively. As can be seen, the quality of tracking is good in both cases, and the step tracking specs are satisfied. Also, we remark that with this PI controller, no integrator windup takes place (see Fig 5.14, where the trace of the output of saturation of the System in Figure 5.3.2 is illustrated).

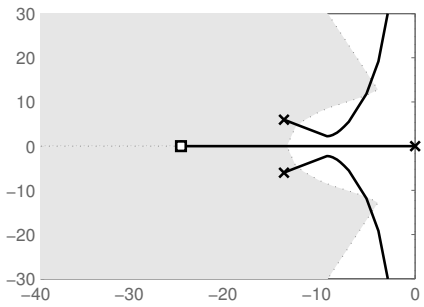


Figure 5.12: S-root locus of the example of Subsection 5.1.4.3.

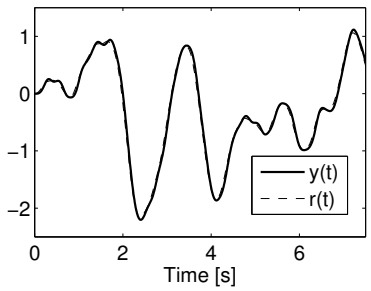


5.13.1: Random tracking.

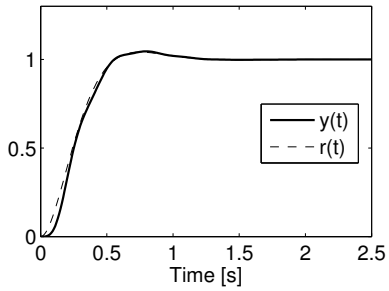


5.13.2: Step tracking.

Figure 5.13: Trajectories of the system in Subsection 5.1.4.3.

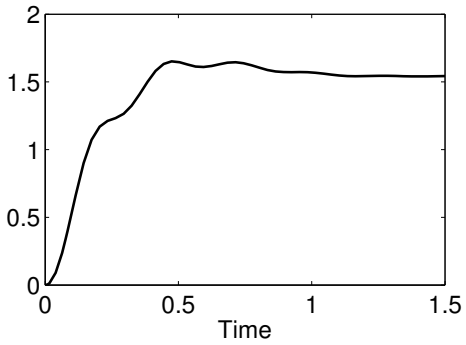


Figure 5.14: Output of saturation for the example of Subsection 5.1.4.3.

#### 5.1.4.4 Specs with zero overshoot

Consider the plant (5.1) of the motivating example in Section 5.1.1 and $\alpha = 10$. The goal is to design a controller such that the closed loop system tracks steps satisfying the following specifications:

$$\begin{aligned} &r_0 \leq 1.5; \\ &\text{Steady state error} \leq 1\%; \\ &\text{Overshoot} = 0\%; \\ &\text{Settling time} \leq 1\,\text{sec}. \end{aligned} \tag{5.19}$$

Since $r_0^* = 1.5 < \frac{P_0\alpha}{1-e_{ss}^*} = 10.1$, condition (5.7) is satisfied and the steady state specs can be met.

Next, we turn to the dynamic part of the specs. Since they call for zero overshoot, the underdamped pre-compensator $F_d(s)$ given in (5.5) with $0 < \zeta < 1$ cannot be used. Rather, the required pre-compensator must be either critically damped or overdamped. Selecting $\zeta = 1$, similar to Subsection 5.1.3, it is possible to show that the adjoint bandwidth is defined by

$$\Omega_a = \sqrt{2}\omega_n e^{-1}. \tag{5.20}$$

Thus, for the example at hand, the pre-compensator can be selected as

$$F_d(s) = \frac{28}{s^2 + 10s + 28},$$

which results in $\Omega_a = 2.77$. Further, selecting the phase-lead controller

$$C(s) = K\frac{s+5}{0.01s+1},$$

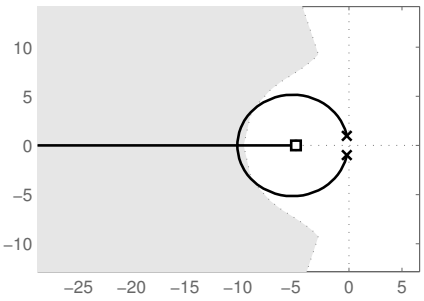


Figure 5.15: S-root locus of the example of Subsection 5.1.4.4.

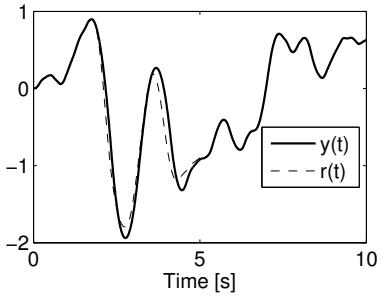


5.16.1: Random tracking.

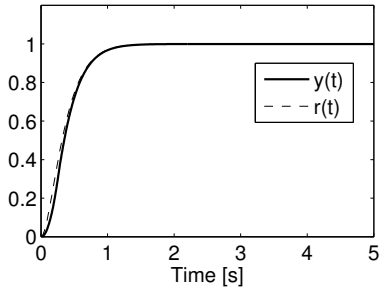


5.16.2: Step tracking.

Figure 5.16: Trajectories of the system in Subsection 5.1.4.4.

we obtain the S-root locus entering the admissible domain (see Figure 5.15). With $K = 20$, the response of systems of Figures 5.3.1 and 5.3.2 are shown in Figures 5.16.1 and 5.16.2, respectively. Clearly, the specs are satisfied. Note that the quality of random reference tracking slightly degrades around 4 seconds. This is because the S-poles are placed at the edge of the admissible domain, and the system exhibits a slight lagging behavior.

### 5.1.5 Comparison of QLC-based and anti-windup-based design methodologies

As shown above, QLC-based design takes into account the actuator saturation during the initial design stage. In contrast, the anti-windup (AW) approach first designs a linear controller satisfying step tracking specs ignoring the saturation, and

then adds an additional feedback loop to prevent controller windup.

There are numerous ways of designing the AW mechanism – linear and nonlinear (see [41], where 25 various AW techniques are described). Obviously, a comparison of QLC-based design with all possible AW implementations is impossible and, perhaps, unnecessary in this paper. Hence, we limit our considerations to issues of general nature.

#### 5.1.5.1 Areas of applicability

One of the main differences between QLC and AW design methods is that of applicability: QLC is applicable to any performance specs, while AW is applicable only to specs that call for a controller with an integrator. For instance, returning to the motivating example of Section 5.1.1 (with the plant and specs given by (5.1) and (5.2), respectively, and with the actuator saturation level $\alpha = 10$), a controller designed using the QLC approach is given by

$$C(s) = 100\frac{s+6}{0.001s+1}. \tag{5.21}$$

The resulting behavior, illustrated in Figure 5.17, satisfies the specs. As far as the AW approach is concerned, the current literature does not offer methods for AW design applicable to the problem at hand, because the controller has fast dynamics.

As an aside note, we would like to point out that both controllers (5.3) and (5.21) lead to saturation activation in the respective systems (Figure 5.1.1 for controller (5.3) and Figure 5.3.2 for controller (5.21)). These saturating trajectories are shown in Figure 5.18. However, controller (5.3) leads to detrimental saturation (specs are not met), while controller (5.21) does not (specs are satisfied). Additionally, we would like to note that even in the architecture of Figure 5.3.2, controller (5.3) still violates specifications (the behavior of $y(t)$ is almost identical to that of Figure 5.2.2 and

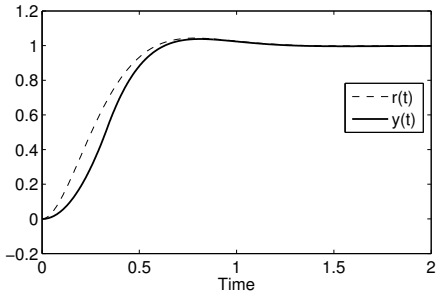


Figure 5.17: Trajectories of the system of Subsection 5.1.5.1.

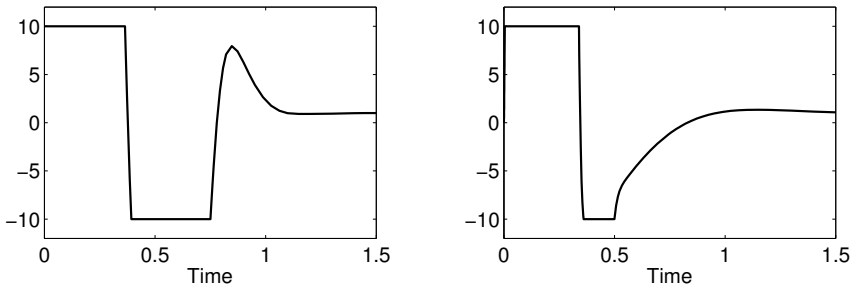


5.18.1: With controller (5.3). 5.18.2: With controller (5.21).

Figure 5.18: Output of saturation in the example of Subsection 5.1.5.1.

overshoot is still 16%).

#### 5.1.5.2 QLC-based design enlarges the set of possible linear controllers as compared to AW

Consider the plant

$$P(s) = \frac{325}{s^2 + 40s + 375}, \tag{5.22}$$

actuator saturation level $\alpha = 1.5$, and the specifications

$$\begin{aligned} &r_0 \leq 1.25; \\ &\text{Steady state error} = 0; \\ &\text{Overshoot} \leq 5\%; \\ &\text{Settling time} \leq 1\,\text{sec}. \end{aligned} \tag{5.23}$$

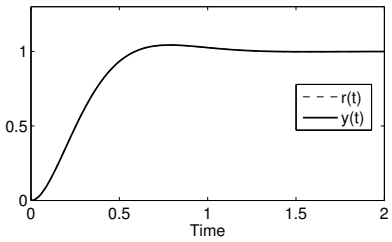


5.19.1: Performance under QLC-based approach.

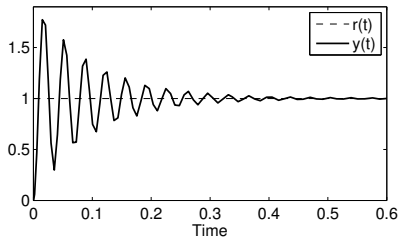


5.19.2: Performance at the initial stage of AW approach.

Figure 5.19: Trajectories of the tracking systems in Subsection 5.1.5.2.

The necessary condition (5.7) is met, $F_d(s)$ is selected as in (5.12), and to satisfy the specs, the following QLC-based controller is designed:

$$C(s) = 100 + \frac{2000}{s}. \tag{5.24}$$

The performance of the resulting closed loop system is shown in Figure 5.19.1. Clearly, the output closely tracks the reference and, thus, satisfies the specs.

Let us now apply controller (5.24) to the same plant in the framework of the initial stage of AW design, i.e., ignoring the saturation and removing the pre-compensator. The resulting performance is shown in Figure 5.19.2. Clearly, the overshoot spec is violated. Thus, controller (5.24) could not have been selected at the initial stage of AW design. This implies that QLC-based design brings into consideration controllers that do not emerge in the AW approach.

#### 5.1.5.3 The AW approach may not lead to a successful design in situations where QLC does

We now design a controller, using the anti-windup technique, for the same plant (5.22), $\alpha = 1.5$, and specs (5.23). In the initial stage of the design, select the PID controller

$$C(s) = 7 + \frac{100}{s} + 0.4s,$$

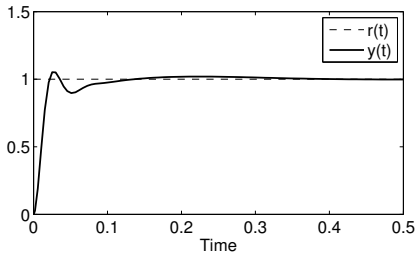


5.20.1: Tracking performance for linear actuator.

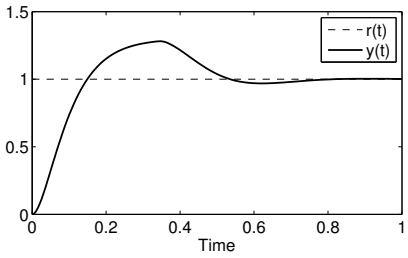


5.20.2: Tracking performance for nonlinear actuator.

Figure 5.20: Trajectories of the tracking systems in Subsection 5.1.5.3.

which satisfies the specs (Figure 5.20.1). The same controller implemented on the system with saturating actuator violates the overshoot specs (Figure 5.20.2). To alleviate this problem, introduce the anti-windup mechanism with back-calculation shown in Figure 5.21, where $K_{AW}$ is the anti-windup gain. In [66], the authors suggest to select $K_{AW}$ as the geometric mean of the derivative and integral actions, i.e., $K_{AW} = 6.3$. The resulting system performance is illustrated in Figure 5.22. The overshoot is 16%, which, despite being smaller than that of the system without anti-windup, still violates the specs. Since $K_{AW} = 6.3$ may not be an optimal solution, we numerically evaluate the overshoot of the system using different anti-windup gains between 1 and 50 (with the step of 0.1). As it turns out, the minimum overshoot is 10%, which is achieved with $K_{AW} = 15$. Thus, the design (5.24) with the above anti-windup mechanism cannot satisfy the specs.

This example illustrates that for a controller selected in the initial stage of design, the AW approach does not offer a constructive way of analyzing the performance after being augmented by an anti-windup mechanism. In contrast, in the QLC-based design, the performance of the selected controller can be directly ascertained using the S-root locus technique.

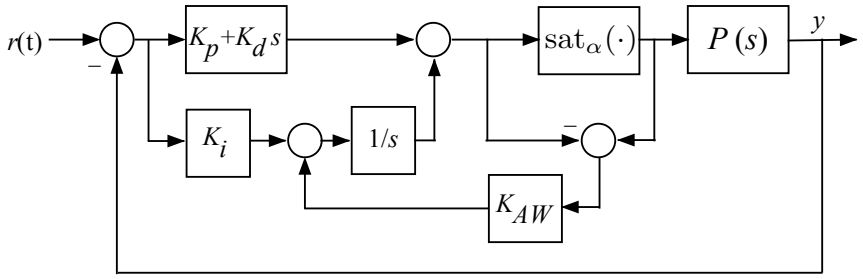


Figure 5.21: The anti-windup mechanism.

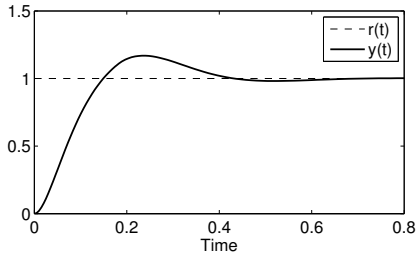


Figure 5.22: Tracking performance for the system with saturating actuator and anti-windup.

### 5.1.6 Step-tracking design for the asymmetric case

A method for designing step tracking controllers has been developed above for the symmetric case. In this subsection, we extend the method to the asymmetric case and demonstrate the technique with an example.

To design step-tracking controllers for the asymmetric case, assume that the specifications call for a controller to track a step change from $r_1$ to $r_2$. In other words, the goal is to track a step size of $r_2 - r_1$ starting from $r_1$. Note that this spec is a generalization of the specs presented for the symmetric case. Assume that the dynamic part of the specs is as before.

To achieve the specs, we select the pre-compensator $F_d(s)$, as before, based on the dynamic part of the specs. Accordingly, the adjoint bandwidth is the same as before. However, we modify the mean and standard deviation of the random reference to $r_1$ and $r_2 - r_1$, respectively. The goal now is to design a controller, using the performance loci method, to track a reference with bandwidth given by the adjoint

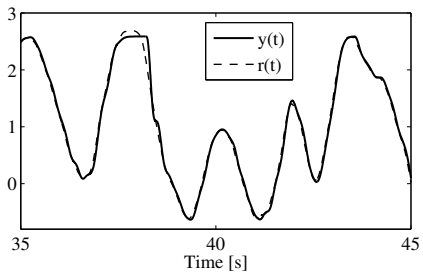


5.23.1: Random tracking.

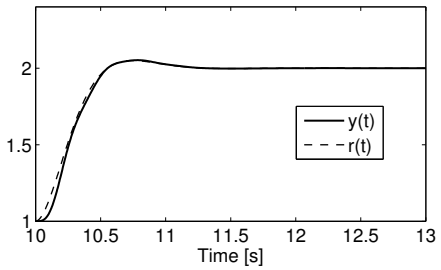


5.23.2: Step tracking.

Figure 5.23: Trajectories of the system in Subsection 5.1.6.

bandwidth and mean and standard deviation given by $r_1$ and $r_2 - r_1$, respectively. The same controller implemented on the system with precompensator $F_d(s)$ satisfies the step-tracking specifications.

**Example V.1.** Consider the second example in Subsection 5.1.4.3 with plant given by (5.17). Assume that $\alpha = -1$, $\beta = 3$, and that the step tracking specs are given by

$$\begin{aligned} &r_1 = 1,\ r_2 = 2; \\ &\text{Steady state error} = 0; \\ &\text{Overshoot} \leq 5\%; \\ &\text{Settling time} \leq 1\,\text{sec}. \end{aligned} \tag{5.25}$$

Similar to Subsection 5.1.4.3, $F_d(s)$ is given by (5.12) and the adjoint bandwidth is $\Omega_a = 3.8$. We select, as before, the PI controller $C(s) = K\left(3 + \frac{75}{s}\right)$. The resulting AS-root locus, constructed by assuming $\mu_r = 1$ and $\sigma_r = 1$, is the same as that shown in Figure 5.12. Selecting $K = 1$ places the AS-poles within the admissible domain. Note that, since the controller has an integrator, the TE locus is identically zero and the steady state tracking specs are satisfied. Figures 5.23.1 and 5.23.2 illustrate the tracking of random and step references. Clearly, the quality of tracking is good in both cases and the step-tracking specs are met.

## 5.2 Analysis and Design of Systems With Integrator Anti-windup Using Stochastic Linearization

### 5.2.1 Motivation

In practice, PID controllers are one of the most widely used controllers. However, in the presence of actuator saturation, their performance may be limited due to integrator windup. Moreover, because of this windup, the specs may not be satisfied even using the QLC-based approach described in Section 5.1. Since almost all real systems are subject to actuator saturation, design of anti-windup schemes is of great importance.

One of the most common integrator anti-windup designs is the so-called back calculation method shown in Figure 5.24.1. The inner loop feeds the difference between the input and output of the saturation to the integrator through the anti-windup gain $K_a$. When the actuator does not saturate, no signal is fed back and system behaves as if no anti-windup is present. When the actuator saturates, the anti-windup loop helps drive the input of the integrator towards zero and prevent windup.

To illustrate performance improvements with anti-windup, consider the system of Figure 5.24.1 with $K_{AW} = 0$ (i.e., no anti-windup) and $\alpha = -\infty$, $\beta = \infty$ (i.e., linear actuator). Assume that

$$P(s) = \frac{1}{s}, K_i = K_d = K_p = 1,$$

and that $r(t)$ is the unit step function. The output $y(t)$ for this system is shown in Figure 5.25.1. Now, assume that $\beta = -\alpha = 0.2$. The output $y(t)$ for this case is shown in Figure 5.25.2. Clearly, both overshoot and settling time have dramatically degraded. To see why this happens, Figure 5.25.3 plots the output of the integrator, as well as the output of the saturation. As can be seen, when the actuator saturates,

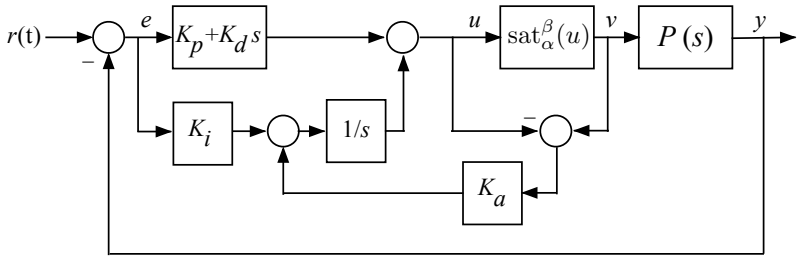


5.24.1: Anti-windup system with back calculation.

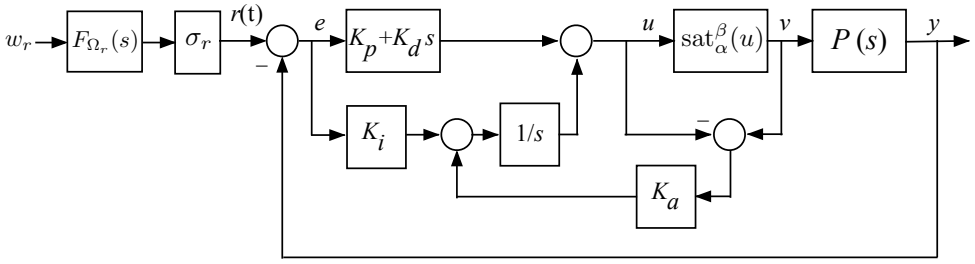


5.24.2: Anti-windup system with random input.

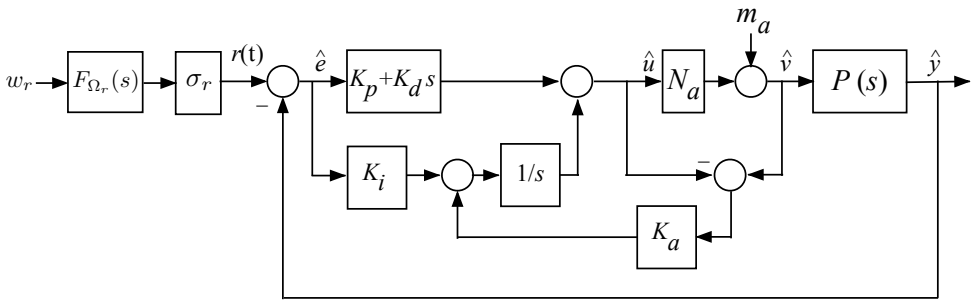


5.24.3: The quasilinear system.

Figure 5.24: Systems considered for controller design of systems with anti-windup.

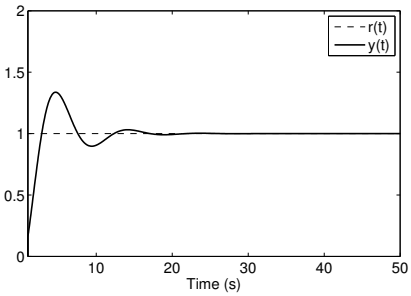


5.25.1: Step tracking with linear actuator and $K_a = 0$.

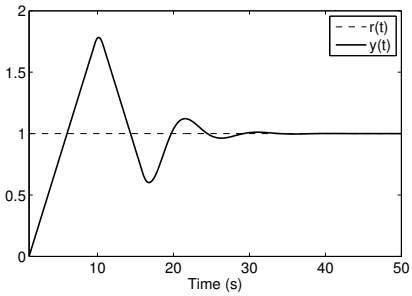


5.25.2: Step tracking with $\beta = -\alpha = 0.2$ and $K_a = 0$.

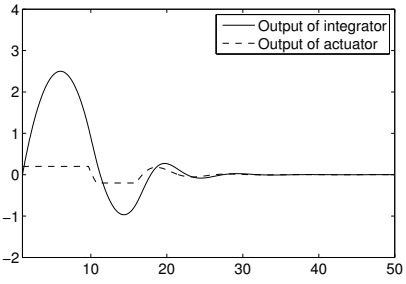


5.25.3: Integrator output and actuator output with $\beta = -\alpha = 0.2$ and $K_a = 0$.

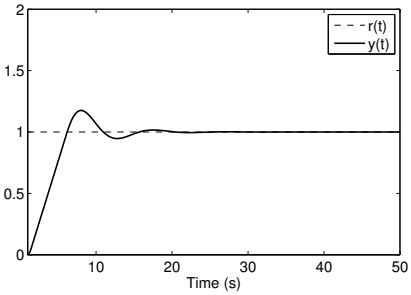


5.25.4: Step tracking with $\beta = -\alpha = 0.2$ and $K_a = 1$.

Figure 5.25: Motivating example.

the integrator winds up significantly. To alleviate this situation, we select $K_a = 1$. Figure 5.25.4 plots the output of this system. Clearly, performance has improved dramatically as compared to Figure 5.25.2.

But how can the anti-windup gain $K_a$ be chosen? In [66], the authors suggest to select $K_a$ large when there is no derivative action, and select $K_a$ as

$$K_a = \sqrt{K_i K_d},$$

when there is derivative action. For the above example, this implies that $K_a = 1$. However, this is a just a rule obtained from experience. In this section, we provide an optimal method for choosing $K_a$ using the method of stochastic linearization.

### 5.2.2 Design strategy

Consider the system shown in Figure 5.24.1. Assume $K_p$, $K_i$, and $K_d$ are already selected so that the underlying linear system without the saturating actuator behaves as desired. The goal is to choose the anti-windup gain $K_a$ in an optimal way to minimize performance degradation when the same controller is used on the A-LPNI system. We propose the following design method:

1. First, convert the step reference tracking specifications to random-reference tracking specifications using the notion of adjoint bandwidth developed in Subsection 5.1.3. This results in the system of Figure 5.24.2.

2. Second, apply stochastic linearization to the system of Figure 5.24.2 to obtain the quasilinear system of Figure 5.24.3.

3. Third, minimize $E[\hat{e}^2]$ over all anti-windup gains, i.e., find the minimizer

$$\min_{K_a} E[\hat{e}^2].$$

The first step is an essential part of the design method presented in Section 5.1 for step-tracking controller design. Therefore, for the sake of brevity, we refer the reader to Section 5.1 for details. Here, we focus on the last two steps. In particular, we derive the equations for stochastic linearization and formulate the optimization problem.

Assume that the plant and coloring filter in Figure 5.24.2 have the state space representations

$$\begin{aligned} \dot{x}_P &= A_P x_P + B_P \mathrm{sat}(u), \\ \dot{x}_F &= A_F x_F + B_F w_r, \\ y &= C_P x_P, \\ r &= C_F x_F, \end{aligned} \tag{5.26}$$

where $x_F$ and $x_P$ are, respectively, the states of the coloring filter and the plant. To model the derivative action, we approximate the derivative by a first order dynamical system with time constant $\tau$, i.e., by

$$\frac{K_d s}{\tau s + 1}. \tag{5.27}$$

Let $z_1$ be the state corresponding to the above dynamical equation. To model the integral action, let us denote the output of the integrator by $z_2$. Then, the input to the saturation can be expressed as

$$u = K_p e + \frac{K_d}{\tau} e + z_1 + z_2 = (K_p + \frac{K_d}{\tau})(C_F x_F - C_P x_P) + z_1 + z_2,$$

and the states $z_1$ and $z_2$ can be described by

$$\begin{aligned} \dot{z}_1 &= -\frac{1}{\tau} z_1 - \frac{K_d}{\tau^2}(C_F x_F - C_P x_P), \\ \dot{z}_2 &= K_i(C_F x_F - C_P x_P) + K_a(\text{sat}(u) - u). \end{aligned} \tag{5.28}$$

After application of stochastic linearization, it can be shown that the quasilinear system may be represented by the following state space system:

$$\dot{\hat{x}} = A\hat{x} + Bw_r + \tilde{B}m_a,$$

where $\hat{x} = [\hat{X}_F^T \;\; \hat{X}_P^T \;\; \hat{z}_1 \;\; \hat{z}_2]^T$, $\hat{X}_F, \hat{X}_P, \hat{z}_1$, and $\hat{z}_2$ are the states of the plant, coloring filter, integrator, and differentiator of the quasilinear system, $m_a = (\frac{K_a}{K_a - K_i P_0} - N)\mu_{\hat{u}}$,

$$A = \begin{bmatrix} A_F & 0 & 0 & 0 \\ B_P N[K_p + \frac{K_d}{\tau}] & A_P - B_P N[K_p + \frac{K_d}{\tau}]C_P & B_P N & B_P N \\ -\frac{K_d}{\tau^2} C_F & \frac{K_d}{\tau^2} C_P & -\frac{1}{\tau} & 0 \\ \left[K_i + K_a(N-1)(K_p + \frac{K_d}{\tau})\right] C_F & -\left[K_i + K_a(N-1)(K_p + \frac{K_d}{\tau})\right] C_P & K_a(N-1) & K_a(N-1) \end{bmatrix},$$

$$B = \begin{bmatrix} B_F \\ 0 \\ 0 \\ 0 \end{bmatrix},$$

and $\tilde{B}$ is an appropriate vector. As it is shown below, the actual form of $\tilde{B}$ is not required for this derivation.

Similar to the development in Chapter II, to derive the equations of stochastic linearization, the standard deviation $\sigma_{\hat{u}}$ must be developed, and the expected value of the output of the saturation must be expressed in terms of $\mu_{\hat{u}}$. To this end, the state covariance matrix of the closed loop quasilinear system is required. The state covariance matrix is given by the solution $P > 0$ of the Lyapunov equation

$$AP + PA^T + BB^T = 0.$$

Using the state covariance matrix, the variances of $\hat{e}$ and $\hat{u}$ are given by

$$\sigma_{\hat{e}}^2 = C_1 P C_1^T,$$

$$\sigma_{\hat{u}}^2 = C_2 P C_2^T,$$

where $C_1 = [C_F \ \ -C_P \ \ 0 \ \ 0]$ and $C_2 = [(K_p + \frac{K_d}{\tau})C_F \ \ -(K_p + \frac{K_d}{\tau})C_P \ \ 1 \ \ 1]$. Now, the expected value of the output of saturation can be shown to be given by:

$$M_a = \frac{K_a}{K_a - K_i P_0} \mu_{\hat{u}}.$$

Therefore, $N_a$ and $\mu_{\hat{u}}$ are the solutions of the transcendental equations

$$N_a - \mathcal{F}_N(\sqrt{C_2 P C_2^T}, \mu_{\hat{u}}) = 0, \tag{5.29}$$

$$\frac{K_a}{K_a - K_i P_0} \mu_{\hat{u}} - \mathcal{F}_M(\sqrt{C_2 P C_2^T}, \mu_{\hat{u}}) = 0, \tag{5.30}$$

where $\mathcal{F}_N$ and $\mathcal{F}_M$ are as in (2.8), (2.9).

We now formulate the optimization problem. First, note that the expected value of the signal $\hat{e}$ is given by

$$\mu_{\hat{e}} = \frac{K_a P_0}{K_i P_0 - K_a} \mu_{\hat{u}}.$$

Therefore, the second moment $E[\hat{e}^2]$ can be equivalently written as

$$E[\hat{e}^2] = \mu_{\hat{e}}^2 + \sigma_{\hat{e}}^2 = (\frac{K_a P_0}{K_i P_0 - K_a} \mu_{\hat{u}})^2 + C_1 P C_1^T.$$

Therefore, the optimization problem is as follows:

$$\min_{K_a>0, 0<N<1, \mu_{\hat{u}} \in \mathbb{R}} (\frac{K_a P_0}{K_i P_0 - K_a} \mu_{\hat{u}})^2 + C_1 P C_1^T,$$

$$\text{subject to} \tag{5.31}$$

$$\begin{aligned} AP + PA^T + BB^T &= 0, \\ N_a - \mathcal{F}_N(\sqrt{C_2 P C_2^T}, \mu_{\hat{u}}) &= 0, \\ \tfrac{K_a}{K_a - K_i P_0} \mu_{\hat{u}} - \mathcal{F}_M(\sqrt{C_2 P C_2^T}, \mu_{\hat{u}}) &= 0. \end{aligned}$$

This optimization problem can be solved using Matlab's "fmincon" function.

We now apply the above to the motivating example presented at the beginning of this Section. Based on the rise time and overshoot of the output shown in Figure 5.25.1, the adjoint bandwidth can be selected as

$$\Omega_a = 0.5.$$

We now consider three cases: $\beta = 0.1, \alpha = -0.1$ (symmetric), $\beta = 0.2, \alpha = -0.2$ (also symmetric), and $\beta = 0.3$, $\alpha = -0.1$ (asymmetric). In the first case, the total actuator authority is 0.2, while in the latter two cases the total actuator authority is

0.4. We use the above development to compute the optimal $K_a$ to be 6.2, 3.92, and 3.67 for the first, second, and third cases, respectively. Note that $K_a$ obtained using this method is not far from $K_a = 1$, which is what is suggested by the authors in [66]. Also note that the optimal gain depends on the actuator authority and asymmetry. Specifically, for this example, with a bigger actuator, the optimal anti-windup gain is smaller, i.e., less anti-windup action is required.

A remark on the pros and cons of the proposed method is in order. On the one hand, the proposed method is straight forward and systematic, while the method in [66] is heuristic. On the other hand, the proposed method is based on a conservative estimate of the adjoint bandwidth, which might lead to conservative design. In addition, the assumption is that stochastic linearization provides a faithful estimate of the first and second moments of the signals in the loop. Therefore, the proposed method works best when the plant is low pass filtering.

In conclusion, this section employs the method of stochastic linearization to find the optimal anti-windup gain in systems with back-calculation anti-windup. Note that the method developed here can be applied to other nonlinearities in the actuator as well.

# CHAPTER VI

# Linear Performance Recovery in A-LPNI Systems

This chapter is concerned with the problem of complete performance recovery in A-LPNI systems. The approach is, as before, based on the method of stochastic linearization. It is shown that linear disturbance rejection performance can be partially recovered in the A-LPNI system by introducing a boosting gain in the sensor and a boosting gain and bias in the controller.

## 6.1 Scenario

Consider the A-LPNI system of Figure 6.1, where $P(s)$ and $C(s)$ are the plant and controller, respectively, $f(\cdot)$ and $g(\cdot)$ are static nonlinearities describing the actuator and sensor, respectively, $y$ is the plant output, and $d$ is a disturbance generated by passing standard Gaussian white noise $w_d$ through the low pass filter $F_{\Omega_d}(s)$ with $\|F_{\Omega_d}(s)\|_2 = 1$. For simplicity, we assume that $d(t)$ has mean zero and standard deviation one. The general case can be treated in a similar manner.

To design a controller $C(s)$ that achieves satisfactory disturbance rejection, a designer typically ignores the nonlinearities in the actuator and sensor and designs a controller for the resulting linear system. This system is shown in Figure 6.2, where $y_l$ is the plant output and $C_l(s)$ is a controller that achieves satisfactory disturbance rejection for this system. Typically, the same controller implemented on the nonlinear

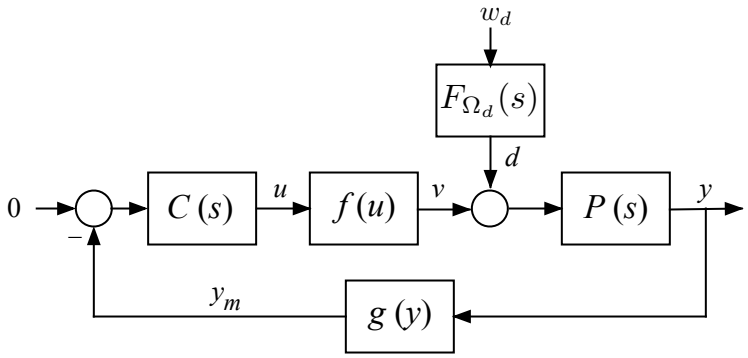


Figure 6.1: A-LPNI system considered for performance recovery.

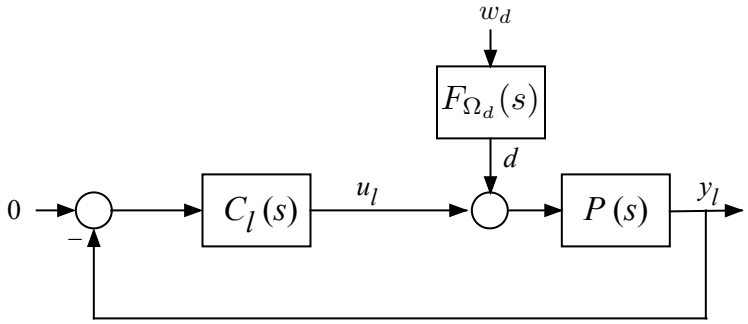


Figure 6.2: Linear system considered for controller design.

system exhibits a degradation in performance as compared with the linear system, i.e.,

$$\sigma_y > \sigma_{y_l}.$$

Furthermore, the asymmetry in the nonlinearities may induce a bias in the output of the system, i.e.,

$$|\mu_y| > 0.$$

This output bias, which is not present in the linear system, is undesirable.

Accordingly, this chapter explores the possibility of modifying $C_l(s)$ to recover linear disturbance rejection performance, i.e., $\sigma_y = \sigma_{y_l}$ and $\mu_y = 0$. In [1] a strategy is presented for symmetric LPNI systems: "boosting" the gain of the controller and the sensor. Here, we not only boost the gain of the controller and sensor, but we also introduce a bias at the controller output. To be consistent with the symmetric case,

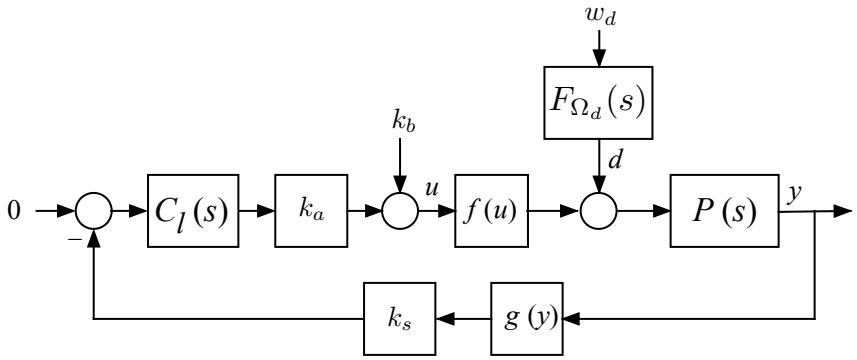


Figure 6.3: Boosted A-LPNI system.

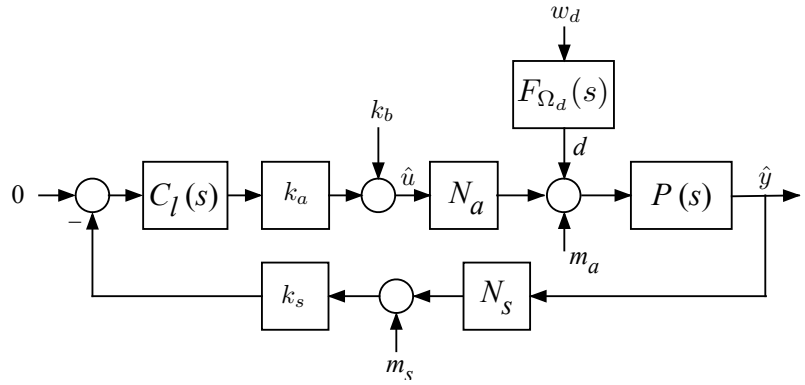


Figure 6.4: Stochastic linearization of the boosted A-LPNI system.

we refer to this strategy as simply boosting. The boosted A-LPNI system is shown in Figure 6.3. Here, $k_a$, $k_s$, and $k_b$ must be chosen so that

$$\sigma_y = \sigma_{y_l},$$
$$\mu_y = 0,$$

if possible. The approach for computing the gains $k_a$, $k_s$, and bias $k_b$ is, as before, based on the method of stochastic linearization. In the next section, we stochastically linearize the A-LPNI system of Figure 6.3 to compute the boosting gains.

## 6.2 Computing the Boosting Gains

Figure 6.4 shows the stochastic linearization of the system of Figure 6.3. Here, $N_a$, $N_s$, $m_a$, and $m_s$ can be found by solving the following system of transcendental equations in the unknowns $N_a$, $N_s$, $\mu_{\hat{u}}$, and $\mu_{\hat{y}}$:

$$N_a - \mathcal{F}_N(\left\| \frac{k_a F_{\Omega_d}(s)P(s)C_l(s)N_s k_s}{1+P(s)N_a k_a N_s k_s C_l(s)} \right\|_2, \mu_{\hat{u}}) = 0, \tag{6.1}$$

$$N_s - \mathcal{G}_N(\left\| \frac{F_{\Omega_d}(s)P(s)}{1+P(s)N_a k_a N_s k_s C_l(s)} \right\|_2, \mu_{\hat{y}}) = 0, \tag{6.2}$$

$$\frac{\mu_{\hat{y}}}{P_0} - \mathcal{F}_M(\left\| \frac{k_a F_{\Omega_d}(s)P(s)C_l(s)N_s k_s}{1+P(s)N_a k_a N_s k_s C_l(s)} \right\|_2, \mu_{\hat{u}}) = 0, \tag{6.3}$$

$$\frac{1}{k_a k_s C_{l_0}}(k_b - \mu_{\hat{u}}) - \mathcal{G}_M(\left\| \frac{F_{\Omega_d}(s)P(s)}{1+P(s)N_a k_s N_s k_s C_l(s)} \right\|_2, \mu_{\hat{y}}) = 0, \tag{6.4}$$

where $C_{l_0}$ is the dc-gain of $C_l$, $\mathcal{F}_N$ and $\mathcal{F}_M$ are as in (2.4) and (2.5), respectively, and $\mathcal{G}_N$ and $\mathcal{G}_M$ are the same as $\mathcal{F}_N$ and $\mathcal{F}_M$ in (2.4) and (2.5), except that $f(\cdot)$ is replaced by $g(\cdot)$. The constants $m_a$ and $m_s$ can be found from:

$$m_a = \frac{\mu_{\hat{y}}}{P_0} - \mu_{\hat{u}} N_a,$$
$$m_s = \frac{1}{k_a k_s C_{l_0}}(k_b - \mu_{\hat{u}}) - \mu_{\hat{y}} N_s.$$

To recover linear disturbance rejection performance, we choose $k_a$ and $k_s$ to offset $N_a$ and $N_s$, i.e.,

$$N_a k_a = N_s k_s = 1,$$

and choose $k_b$ such that $\mu_{\hat{y}} = 0$. If such $k_a$, $k_s$, and $k_b$ exist, linear performance is recovered in the quasilinear system.

To compute these boosting gains, we multiply both sides of (6.1) by $k_a$, both sides of (6.2) by $k_s$, and use the fact that $N_a k_a = N_s k_s = 1$ and $\mu_{\hat{y}} = 0$. Equations (6.1)-(6.4) then become:

$$1 - k_a \mathcal{F}_N(k_a \left\| \frac{F_{\Omega_d}(s)P(s)C_l(s)}{1+P(s)C_l(s)} \right\|_2, \mu_{\hat{u}}) = 0, \tag{6.5}$$

$$1 - k_s \mathcal{G}_N(\left\| \frac{F_{\Omega_d}(s)P(s)}{1+P(s)C_l(s)} \right\|_2, 0) = 0, \tag{6.6}$$

$$\mathcal{F}_M(k_a \left\| \frac{F_{\Omega_d}(s)P(s)C_l(s)}{1+P(s)C_l(s)} \right\|_2, \mu_{\hat{u}}) = 0, \tag{6.7}$$

$$\frac{1}{k_a k_s C_{l_0}}(k_b - \mu_{\hat{u}}) - \mathcal{G}_M(\left\| \frac{F_{\Omega_d}(s)P(s)}{1+P(s)C_l(s)} \right\|_2, 0) = 0, \tag{6.8}$$

The standing assumption is that the solution of the above equations is unique. Note that the above equations can be decoupled. First, (6.6) can be solved for $k_s$:

$$k_s = \frac{1}{\mathcal{G}_N(\left\| \frac{F_{\Omega_d}(s)P(s)}{1+P(s)C_l(s)} \right\|_2, 0)} = \frac{1}{\mathcal{G}_N(\sigma_{y_l}, 0)}.$$

Therefore, $k_s$ always exists. In other words, the sensor nonlinearity can always be boosted.

Second, (6.5) and (6.7) can be solved together for $\mu_{\hat{u}}$ and $k_a$. So, boosting of the actuator nonlinearity is only possible when (6.5), (6.7) have a solution.

Finally, (6.8) can be solved for $k_b$. Here, two cases can arise:

- $C_{l_0} = \infty$: In this case, boosting is only possible when $\mathcal{G}_M(\left\| \frac{F_{\Omega_d}(s)P(s)}{1+P(s)C_l(s)} \right\|_2, 0) = 0$. This equation is satisfied, for example, if the sensor nonlinearity is an odd function. Note that bias $k_b$ is not required in this case. We, thus, set $k_b = 0$.

- $C_{l_0} \neq \infty$: Here, $k_b$ can computed as follows:

$$k_b = \mu_{\hat{u}} + k_a k_s C_{l_0} \mathcal{G}_M(\left\| \frac{F_{\Omega_d}(s)P(s)}{1+P(s)C_l(s)} \right\|_2, 0).$$

  Note that if the sensor nonlinearity is an odd function, then $\mathcal{G}_M(\left\| \frac{F_{\Omega_d}(s)P(s)}{1+P(s)C_l(s)} \right\|_2, 0) = 0$. Therefore, $k_b = \mu_{\hat{u}}$.

**Remark VI.1.** The boosted controller, as designed above, may or may not perform as desired on the A-LPNI system. This depends on the accuracy of stochastic linearization: if stochastic linearization is accurate, then the boosted A-LPNI system performs well. As an example, consider a system with linear actuator and a sensor with deadzone. The above analysis implies that boosting is always possible for this system. However, as it can be shown using simulations, if the deadzone band is large enough compared to the output signal, then the accuracy of stochastic linearization is low, and the boosted controller does not perform as desired.

## 6.3 Example

Consider system of Figure 6.1 with a saturating actuator and a linear sensor. Assume that

$$P(s) = \frac{2}{20s+1}, \alpha = -0.5, \beta = 2,$$

and $F_{\Omega_d}(s)$ the usual third order Butterworth filter with bandwidth $\Omega_d = 1$. Let $C(s) = C_l(s) = 5$ be a controller that satisfies the disturbance rejection specifications for the underlying linear system without the saturating actuator. The resulting mean and standard deviation of the output of the linear system is:

$$\sigma_{y_l} = 0.136, \;\; \mu_{y_l} = 0.$$

The same controller implemented on the A-LPNI system results in:

$$\sigma_y = 0.209, \;\; \mu_y = 0.056.$$

Based on the standard deviation, the system performance has degraded by 53%. We now boost the controller using the method described in the previous section. The

resulting boosting gain and bias are:

$$k_a = 4.15,\ k_b = -1.695.$$

Note that $k_s = 1$ since the sensor is linear. The boosted controller implemented on the A-LPNI system results in:

$$\sigma_y = 0.186,\ \ \mu_y = 0.017,$$

an 11% and a 69% improvement as compared with the unboosted controller. The performance of the boosted controller on the A-LPNI system as compared with that of $C_l(s)$ on the linear system shows a 36% degradation as opposed to 53% shown previously. Clearly, the boosted system has superior performance as compared with the unboosted controller.

# CHAPTER VII

# LQR-based Design of A-LPNI Systems

This section introduces the A-SLQR problem, where $A$ stands for "asymmetric" and $S$ stands for "saturating". Similar to the usual linear LQR, the A-SLQR problem is concerned with designing a state feedback controller to reject disturbances in an optimal manner. However, unlike the LQR approach, the A-SLQR method takes into account the actuator saturation at the design stage. Therefore, as it is shown, the A-SLQR method performs better than the LQR approach.

## 7.1 Preliminaries

Consider the SISO LPNI system shown in Figure 7.1, where $P(s)$, $F_{\Omega_d}(s)$, and $\text{sat}_\alpha^\beta(u)$ are, as before, the plant, coloring filter with $H_2$ norm equal to 1, and the saturation function shown in Figure 1.3, $w$ is a Gaussian white noise process, and $\mu_d$ and $\sigma_d$ are constants. Assume that minimal realizations of $P(s)$ and $F_{\Omega_d}(s)$ are given

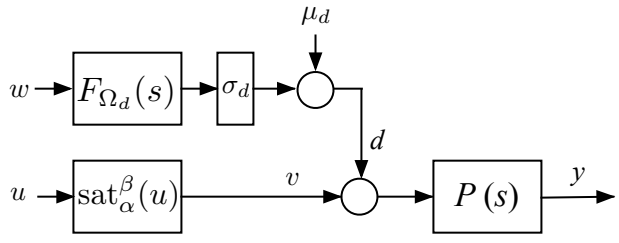


Figure 7.1: LPNI system used for analysis of state space feedback.

by $(A_P, B_P, C_P)$ and $(A_F, B_F, C_F)$, respectively. Then, the overall system is governed by

$$\begin{aligned} \dot{x} &= Ax + B_1 w + B_2 \text{sat}_\alpha^\beta(u) + B_2 \mu_d, \\ y &= Cx, \end{aligned} \tag{7.1}$$

where $x = [x_P^T \;\; x_F^T]^T$, $x_P$ and $x_F$ are the states of the plant and coloring filter, respectively, and

$$A = \begin{bmatrix} A_P & \sigma_d B_P C_F \\ 0 & A_F \end{bmatrix}, B_1 = \begin{bmatrix} 0 \\ B_F \end{bmatrix}, B_2 = \begin{bmatrix} B_P \\ 0 \end{bmatrix}, C = [C_P \quad 0].$$

With a state feedback controller $u = Kx$, the closed loop system is governed by

$$\begin{aligned} \dot{x} &= Ax + B_1 w + B_2 \text{sat}_\alpha^\beta(Kx) + B_2 \mu_d, \\ y &= Cx. \end{aligned} \tag{7.2}$$

Application of stochastic linearization to this system yields

$$\begin{aligned} \dot{\hat{x}} &= (A + B_2 NK)\hat{x} + B_1 w + B_2(m + \mu_d), \\ \hat{y} &= C\hat{x}, \end{aligned} \tag{7.3}$$

where $N$ and $m$ are the quasilinear gain and bias, respectively. Assuming that $K$ is chosen such that $A + B_2 NK$ is Hurwitz, it can be shown that

$$m = -\frac{\mu_{\hat{u}}}{K(A + B_2 NK)^{-1} B_2} - \mu_d$$

and $N$ and $\mu_{\hat{u}}$ can be obtained from the following two equations in unknowns $N$ and $\mu_{\hat{u}}$:

$$\begin{aligned} & N - \mathcal{F}_N(\sigma_{\hat{u}}, \mu_{\hat{u}}) = 0, \\ & \left(\frac{-1}{K(A + B_2 NK)^{-1} B_2} + N\right)\mu_{\hat{u}} - \mu_d - \mathcal{F}_M(\sigma_{\hat{u}}, \mu_{\hat{u}}) = 0, \end{aligned} \tag{7.4}$$

where $\sigma_{\hat{u}} = \sqrt{KRK^T}$, and $R$ is the positive definite solution of the Lyapunov equation

$$(A + B_2NK)R + R(A + B_2NK)^T + B_1B_1^T = 0.$$

Clearly, the average value of the signals in the loop depends not only on $\mu_d$, but also on the quasilinear bias $m$, which acts as an additional disturbance.

## 7.2 The A-SLQR Problem

In contrast to the symmetric case with $\mu_d = 0$, the plant output and control input are characterized not only by their variance, but also by their mean. Hence, the goal of the A-SLQR problem is design $K$ to minimize the cost function

$$J = \lim_{t\to\infty} E[\hat{y}(t)^2 + \rho\hat{u}(t)^2] = \sigma_{\hat{y}}^2 + \mu_{\hat{y}}^2 + \rho(\sigma_{\hat{u}}^2 + \mu_{\hat{u}}^2),$$

where $\rho$ is the control penalty. In terms of the system parameters, the A-SLQR problem can be recast into the following optimization problem: minimize

$$J = CRC^T + \left[\frac{C(A + B_2NK)^{-1}B_2}{K(A + B_2NK)^{-1}B_2}\right]^2 \mu_{\hat{u}}^2 + \rho(KRK^T + \mu_{\hat{u}}^2),$$

subject to

$$\begin{aligned}
&(A + B_2NK)R + R(A + B_2NK)^T + B_1B_1^T = 0,\\
&N - \mathcal{F}_N(\sigma_{\hat{u}}, \mu_{\hat{u}}) = 0,\\
&(\frac{-1}{K(A + B_2NK)^{-1}B_2} + N)\mu_{\hat{u}} - \mu_d - \mathcal{F}_M(\sigma_{\hat{u}}, \mu_{\hat{u}}) = 0,\\
&\sigma_{\hat{u}} = \sqrt{KRK^T}.
\end{aligned} \tag{7.5}$$

The solution of the A-SLQR problem is provided in the following theorem.

**Theorem VII.1.** *Assume that $(A, B_2)$ is stabilizable and $(C, A)$ is detectable. Then the solution, $K$, of the A-SLQR problem is given by the root of the following equations*

*in unknowns* $K, N, \mu_{\hat{u}}, R, Q$.

$$(A + B_2NK)R + R(A + B_2NK)^T + B_1B_1^T = 0, \tag{7.6}$$

$$N - \mathcal{F}_N(\sigma_{\hat{u}}, \mu_{\hat{u}}) = 0, \tag{7.7}$$

$$(\frac{-1}{K(A + B_2NK)^{-1}B_2} + N)\mu_{\hat{u}} - \mu_d - \mathcal{F}_M(\sigma_{\hat{u}}, \mu_{\hat{u}}) = 0, \tag{7.8}$$

$$(A + B_2NK)^TQ + Q(A + B_2NK) + CC^T + \rho K^TK - \frac{\lambda_3}{2\sigma_u^3}K^TK = 0, \tag{7.9}$$

$$\begin{aligned}\frac{\lambda_1}{\sqrt{2\pi}\sigma_u}\left[\exp(-(\frac{\beta-\mu_u}{\sqrt{2}\sigma_u})^2) - \exp(-(\frac{\alpha-\mu_u}{\sqrt{2}\sigma_u})^2)\right] + \lambda_2(N + \frac{1}{KA^{-1}B_2}) + \\ 2\mu_{\hat{u}}\Big[(\frac{C(A + B_2NK)^{-1}B_2}{K(A + B_2NK)^{-1}B_2})^2 + \rho\Big] = 0,\end{aligned} \tag{7.10}$$

*where*

$$\sigma_{\hat{u}} = \sqrt{KRK^T}, \tag{7.11}$$

$$\lambda_1 = -KRQB_2, \tag{7.12}$$

$$\lambda_2 = -\frac{\frac{\lambda_1}{\sigma_u}\left[\exp(-(\frac{\beta-\mu_u}{\sqrt{2}\sigma_u})^2)(\frac{\beta-\mu_u}{\sqrt{2}\sigma_u}) - \exp(-(\frac{\alpha-\mu_u}{\sqrt{2}\sigma_u})^2)(\frac{\alpha-\mu_u}{\sqrt{2}\sigma_u})\right]}{\left[\exp(-(\frac{\beta-\mu_u}{\sqrt{2}\sigma_u})^2) - \exp(-(\frac{\alpha-\mu_u}{\sqrt{2}\sigma_u})^2)\right]}, \tag{7.13}$$

$$\lambda_3 = 2\sigma_u\left(-N\lambda_1 + \frac{1}{KA^{-1}B_2}(\lambda_2\mu_{\hat{u}} - 2\frac{(CA^{-1}B_2)^2}{KA^{-1}B_2})\right). \tag{7.14}$$

*Proof.* See Section A.5. □

The root of the above equations can be found using Matlab's "fsolve" function.

**Proposition VII.1.** *Assume that* $C(sI - A)^{-1}B_1 \neq 0$. *Then,*

$$\inf_K E[\hat{y}^2] = \gamma_0 > 0. \tag{7.15}$$

*Proof.* See Section A.5. □

The above proposition implies that, unlike linear systems, the output of the quasi-linear system cannot be made arbitrarily small using cheap control. The value of $\gamma_0$

in (7.15) can be approximated using the A-SLQR algorithm with sufficiently small $\rho$. Note that, since $E[\hat{y}^2]$ approximates well $E[y^2]$, $\gamma_0$ also quantifies the limits of best achievable performance for the original LPNI system.

## 7.3 Example

Consider the LPNI system

$$P(s) = \frac{1}{s+1}, F(s) = \frac{2\sqrt{5}}{s+10}, \sigma_d = 3, \mu_d = 0,$$

and actuator given by $\text{sat}_{\alpha}^{\beta}(\cdot)$. A state space representation of this system is

$$A = \begin{bmatrix} -1 & 1 \\ 0 & -10 \end{bmatrix}, B_1 = \begin{bmatrix} 0 \\ 2\sqrt{5} \end{bmatrix}, B_2 = \begin{bmatrix} 1 \\ 0 \end{bmatrix}, C = [1 \quad 0].$$

We assume that the control penalty is given by $\rho = 10^{-5}$ and consider two cases: one in which the total width of saturation is 2, i.e., $\beta - \alpha = 2$, and one in which $\beta - \alpha = 1$. For each of these cases, we compute the solution of the A-SLQR problem for various values of $\frac{\beta+\alpha}{2}$. Note that when $\frac{\beta+\alpha}{2} = 0$, the system is symmetric; otherwise it is asymmetric. To analyze the performance of the A-SLQR controller on the original LPNI system, we simulate the LPNI system using the A-SLQR gains and calculate the minimum cost numerically. Figures 7.2.1 and 7.2.2 show the values of the minimum cost computed analytically and via simulations for both $\beta - \alpha = 2$ and $\beta - \alpha = 1$. Clearly, since the analytically computed minimum cost and numerically evaluated costs are close in both cases, the accuracy of stochastic linearization is very good.

Next, to compare the performance of the A-SLQR controller with the usual LQR approach, we apply the standard LQR technique to this system by ignoring the saturation. We then simulate the LPNI system using the obtained LQR gains to numerically compute the minimum cost. Figures 7.2.1 and 7.2.2 also show the minimum cost ob-

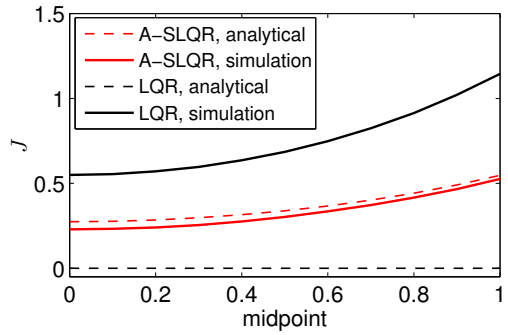


7.2.1: $\beta - \alpha = 2$.

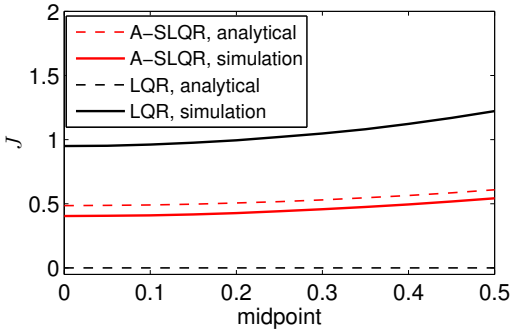


7.2.2: $\beta - \alpha = 1$.

Figure 7.2: Minimum cost as a function of asymmetry for the example of Section 7.3.

tained analytically and numerically using the LQR technique. Clearly, as compared with the LQR controllers, the A-SLQR controllers perform significantly better in all cases.

Finally, to approximate the value of $\gamma_0$ in Proposition 1, we let $\rho = 10^{-12}$ and compute $E[\hat{y}^2]$ using the A-SLQR approach. Figure 7.3 shows the minimum $E[\hat{y}^2]$ for both $\beta - \alpha = 2$ and $\beta - \alpha = 1$, as well as the open loop value of $E[\hat{y}^2]$. Clearly, as the authority of saturation becomes smaller, the best achievable performance degrades as expected.

**Remark VII.1.** Throughout this chapter, we assumed that all states are available for feedback. In practice, however, this is usually not the case. In this situation,

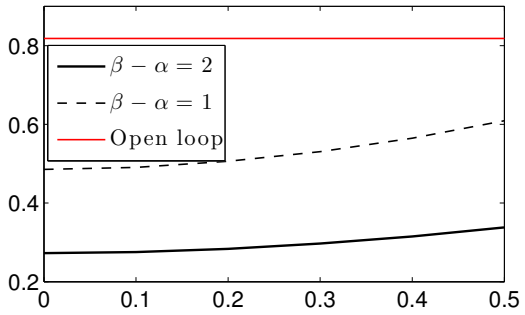


Figure 7.3: Best achievable performance using the A-SLQR technique as a function of $\frac{\alpha+\beta}{2}$ for the example of Section 7.3.

similar to the case of linear systems, a state estimator can be constructed as follows:

$$\begin{aligned} \dot{\hat{x}} &= A\hat{x} + B_2 \mathrm{sat}_\alpha^\beta(u) + B_2\mu_d - L(y - \hat{y}), \\ \hat{y} &= C\hat{x}, \end{aligned} \tag{7.16}$$

where it is assumed that $\mu_d$ is known. If not, a bias estimator can be designed to estimate $\mu_d$.

With the control law $u = K\hat{x}$, the LPNI system becomes

$$\begin{aligned} \dot{x} &= Ax + B_1 w + B_2 \mathrm{sat}_\alpha^\beta(K\hat{x}) + B_2\mu_d, \\ y &= Cx. \end{aligned} \tag{7.17}$$

Moreover, the dynamics of the error $e = x - \hat{x}$ are given by

$$\dot{e} = (A + LC)e + B_1 w.$$

Clearly, assuming $(A, C)$ is observable and the system is minimum phase, the observer gain $L$ can be chosen such that $e$ is arbitrarily small. The A-SLQR method can then be applied as if the states were known.

Of course, the above argument assumes that the sensor is not noisy. In the presence of sensor noise, the optimization problem in the A-SLQR problem can be reformulated

to take into account the observer error dynamics. This is a simple extension and will, therefore, not be pursued here.

# CHAPTER VIII

# Application: QLC-based Design of a Wind Farm Controller

In this section, QLC is used for controller design of a wind farm with multiple wind turbines. It is shown that each of these turbines can be modeled by a linear plant preceded by an asymmetric saturation nonlinearity, which accounts for limited availability of wind. Numerical simulations illustrate that the controllers obtained via QLC perform significantly better in a broad range of regimes as compared to those designed previously that ignore saturation.

## 8.1 Background

A wind farm is a collection of wind turbines used to generate electricity. Since a limiting factor for wide-spread use of wind power has been the intermittent and uncontrollable nature of wind, it is important to design wind farms that smoothly track reference signals provided by a grid operator, despite fluctuations in wind.

To accomplish this goal, it is necessary to design a control system, which can generally be represented in a block diagram form as shown in Figure 8.1. In this figure, the Wind Turbine Control Systems (WTCSs) represent the wind turbines together with their turbine-level controllers. The higher level Wind Farm Controller uses the

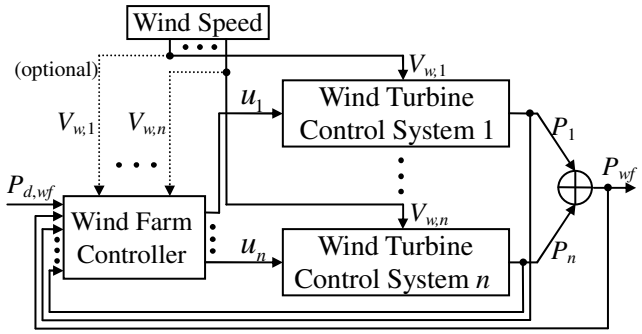


Figure 8.1: Block diagram of a wind farm control system.

desired power reference from a grid operator, $P_{d,wf}$, and various measurements to calculate the control signals $u_i$'s, so that the actual wind farm power output $P_{wf} \triangleq \sum_{i=1}^{n} P_i$ closely tracks $P_{d,wf}$.

This wind farm power control problem is receiving growing attention from researchers [67–76]. For example, to reduce variation in $P_{wf}$, [69] presents a fuzzy neural network WFC that adjusts the desired active power references (i.e., in this case the $u_i$'s are the power references). Through the use of either an external energy storage device, or a power reserve achieved through part-loading of some turbines, [71] suggests a supervisory scheme for making $P_{wf}$ smooth. In [67, 68], a hierarchical, supervisory WFC that determines the active and reactive power setpoints of every turbine so that $P_{wf}$ is regulated around $P_{d,wf}$, is proposed. In [70, 73], an optimization-based approach for designing WFCs is introduced, in which the wind turbines are assumed to be static. Reference [74] proposes a scheme for adjusting the blade pitch angles in unison, so that $P_{wf}$ is close to $P_{d,wf}$, and that damping power may be provided to the power grid as ancillary service. Furthermore, [72] utilizes a proportional-integral regulator-based method to manage the wind farm reactive powers for secondary voltage control. More recently, [75] develops a distributed learning WFC for maximizing wind farm energy production without explicitly modeling the aerodynamic interactions among the turbines, while [76] presents a tutorial on wind turbine active power control in the context of supporting power grid frequency.

In [77], a simple model of WTCS that is valid under normal wind farm operating conditions is presented and, for completeness, summarized in Section VIII-B. In this model, each turbine is modeled by a linear plant preceded by an asymmetric saturation nonlinearity, which accounts for limited availability of wind. Based on this model, [78] developed a wind farm controller consisting of two feedback loops: a model predictive controller on the outer loop, and an adaptive controller on the inner loop. Collectively, they enable the power output $P_{wf}$ to accurately and smoothly track a desired reference $P_{d,wf}$.

The model predictive controller uses forecast of the wind, forecast of $P_{d,wf}$, and measurement of the power output of each WTCS, $P_i$, to optimize the deterministic tracking accuracy of $P_{wf}(t)$ on a receding horizon. The output of the model predictive controller is a set of reference signals for the adaptive controller, which, in turn, uses these references and an estimate of the covariance of wind to adaptively tune the gains of a set of decentralized proportional controllers.

Although the controller developed in [78] possesses some positive features, it has a notable drawback: in order to simplify the design process, the saturation blocks in the otherwise linear WTCS model are neglected in the design of the adaptive controller. While this assumption greatly simplifies the controller design and the corresponding analysis, the results obtained may be overly optimistic and may not accurately reflect the performance when saturation is present. To alleviate this drawback, we leverage QLC theory. As we show, since the wind turbines are sufficiently slow as compared with the fluctuations in wind, QLC theory can be successfully applied.

## 8.2 Model

In [77], a WTCS model is developed based on standard system identification approaches and typical WTCS characteristics. Composed of a first order LTI system preceded by an asymmetric saturation nonlinearity, this structurally simple model was

shown via extensive validation in [77] to be accurate and versatile. In this section, we utilize this model and augment it with a simple wind speed model in essentially the same way as was done (and justified) in [79, 78]. Specifically, we assume that the wind speed $V_{w,i}(t)$ entering each WTCS $i$, $i \in \{1, 2, \ldots, n\}$, of Figure 8.1 may be expressed as

$$V_{w,i}(t) = \overline{V}_{w,i} + \widetilde{V}_{w,i}(t), \tag{8.1}$$

where $\overline{V}_{w,i} > 0$ represents the slow, average component of $V_{w,i}(t)$, and $\widetilde{V}_{w,i}(t) \in \mathbb{R}$ represents the fast, deviation-from-average component of $V_{w,i}(t)$. Each slow component $\overline{V}_{w,i}$ is assumed to be deterministic and specified by empirical data. In contrast, each fast component $\widetilde{V}_{w,i}(t)$ is assumed to be a stationary, zero-mean colored Gaussian random process specified by

$$\dot{\widetilde{V}}_{w,i}(t) = -\frac{1}{\tau_{w,i}}\widetilde{V}_{w,i}(t) + \frac{1}{\tau_{w,i}}w_i(t), \tag{8.2}$$

where $\tau_{w,i} > 0$ is a time constant for the wind speed model, $w(t) = (w_1(t), \ldots, w_n(t)) \in \mathbb{R}^n$ is a stationary, zero-mean white Gaussian noise with autocovariance function $E\{w(t)w(\tau)^T\} = W\delta(t-\tau)$, $W = W^T > 0$ is the covariance matrix, and $\delta$ is the Dirac delta function. In addition, similar to [79, 78] we let the dynamics of each WTCS $i$ be given by

$$\dot{P}_i(t) = -\frac{1}{\tau_i}P_i(t) + \frac{1}{\tau_i}\,\mathrm{sat}_0^{a_i V_{w,i}^3(t)}(P_{d,i}(t)) + \gamma_i \widetilde{V}_{w,i}(t), \tag{8.3}$$

where $\tau_i > 0$ is a time constant for the WTCS model, $a_i > 0$ is a unit conversion factor, $\gamma_i \geq 0$ is a scalar gain, and $\mathrm{sat}_\alpha^\beta(u)$ is the saturation function.

**Remark VIII.1.** Notice that since $\widetilde{V}_{w,i}(t)$ is Gaussian, despite $\overline{V}_{w,i}(t)$ being positive, the wind speed $V_{w,i}(t)$ in (8.1) may be negative with a small probability. For

simplicity, however, we will allow that in this section.

## 8.3 Problem formulation and controller design

In the subsequent discussion, we assume that the model predictive controller is already designed for the outer control loop. The outputs of the model predictive controller are reference signals, denoted by $P_i^*$, $i = 1, \ldots, n$, for the the inner control loop. For the details and rationale behind this design, we refer the reader to [78, 79].

For the inner loop, the control law for each WTCS $i$, $i \in \{1, 2, \ldots, n\}$, is given by

$$P_{d,i}(t) = K_i\Big(\frac{1+K_i}{K_i}P_i^*(t) - P_i(t)\Big), \tag{8.4}$$

where $\frac{1+K_i}{K_i}$ is a feedforward gain intended to yield an appropriate equilibrium point, and $K_i$ is to be optimized adaptively to yield smoothness of the wind farm power output (see below). Substituting control law (8.4) into WTCS model (8.3) and assuming that the intermediate power references $P_i^*(t)$'s are so slow that they may be treated as constants $P_i^*$'s, we obtain for each $i = 1, 2, \ldots, n$,

$$\dot{P}_i(t) = -\frac{1}{\tau_i}P_i(t) + \frac{1}{\tau_i}\,\mathrm{sat}_0^{a_i V_{w,i}^3(t)}\Big(K_i\big(\frac{1+K_i}{K_i}P_i^* - P_i(t)\big)\Big) + \gamma_i \widetilde{V}_{w,i}(t). \tag{8.5}$$

By introducing the variables

$$\Delta P_i(t) = P_i(t) - P_i^*, \tag{8.6}$$

$$\Delta P_{d,i}(t) = P_{d,i}(t) - P_i^*, \tag{8.7}$$

system (8.5) can be written as

$$\Delta\dot{P}_i(t) = -\frac{1}{\tau_i}\Delta P_i(t) + \frac{1}{\tau_i}\,\mathrm{sat}_{-P_i^*}^{a_i V_{w,i}^3(t) - P_i^*}(\Delta P_{d,i}(t)) + \gamma_i \widetilde{V}_{w,i}(t). \tag{8.8}$$

The goal is to design $K_i$ to minimize the cost function

$$J = \lim_{t\to\infty} E\Big\{ \Big(\sum_{i=1}^{n} \Delta P_i(t)\Big)^2 + \sum_{i=1}^{n} \epsilon_i \Delta P_{d,i}^2(t) \Big\}, \tag{8.9}$$

where $\epsilon_i > 0$ are control penalties. Note that the first term in $J$ is the steady-state variance of the regulation error reflecting the smoothness of the wind farm power output, and the second term is a weighted sum of the steady-state variances of the control magnitudes reflecting the control effort. We address this problem below using QLC.

Observe that system (8.8) is subject to $n$ decoupled asymmetric saturation functions, whose limits change over time. To facilitate the design of the wind farm controller using QLC, we assume that the upper saturation limits are constant; specifically, we assume that they depend only on the average component of the wind, i.e., $a_i\overline{V}_{w,i}^3(t) - P_i^*$. To further simplify the presentation, introduce the following notations:

$$\begin{aligned} &u_i \triangleq \Delta P_{d,i}, \quad y_i \triangleq \Delta P_i, \\ &\beta_i \triangleq a_i\overline{V}_{w,i}^3 - P_i^*, \quad \alpha_i \triangleq -P_i^*. \end{aligned} \tag{8.10}$$

With these notations, the WTCS model (8.8) becomes:

$$\dot{y}_i = -\frac{1}{\tau_i} y_i + \frac{1}{\tau_i} \mathrm{sat}_{\alpha_i}^{\beta_i}(u_i) + \gamma_i \widetilde{V}_{w,i}, \quad i = 1, \ldots, n. \tag{8.11}$$

With $u_i$ given by (8.4) and $\widetilde{V}_{w,i}$ given by (8.2), the block diagram of this system is shown in Figure 8.2.1. Application of stochastic linearization to this system yields the quasilinear system shown in Figure 8.2.2. Note that since the WTCS's are decoupled, stochastic linearization of each WTCS is independent of the others. To compute $N_i$ and $m_i$, $i = 1, \ldots, n$, the following two transcendental equations in the unknowns $N_i$ and $M_i$ must be solved:

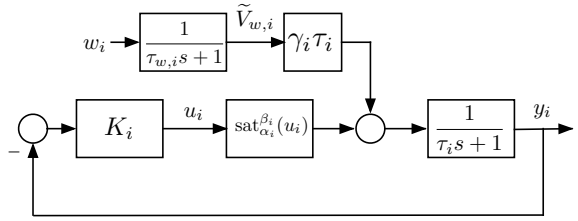


8.2.1: LPNI model of WTCS.

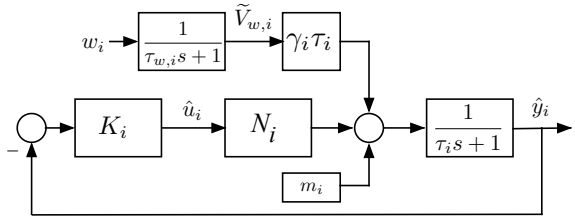


8.2.2: Quasilinear version of the LPNI model.

Figure 8.2: Control system for the $i$th turbine, $i = 1, \ldots, n$.

$$N_i = \frac{1}{2}\left[\mathrm{erf}\left(\frac{\beta_i - \mu_{\hat{u}_i}}{\sqrt{2}\sigma_{\hat{u}_i}}\right) - \mathrm{erf}\left(\frac{\alpha_i - \mu_{\hat{u}_i}}{\sqrt{2}\sigma_{\hat{u}_i}}\right)\right], \tag{8.12}$$

$$\begin{aligned} M_i = {} & \frac{\alpha_i + \beta_i}{2} + \frac{\mu_{\hat{u}_i} - \beta_i}{2}\mathrm{erf}\left(\frac{\beta_i - \mu_{\hat{u}_i}}{\sqrt{2}\sigma_{\hat{u}_i}}\right) - \frac{\mu_{\hat{u}_i} - \alpha_i}{2}\mathrm{erf}\left(\frac{\alpha_i - \mu_{\hat{u}_i}}{\sqrt{2}\sigma_{\hat{u}_i}}\right) \\ & - \frac{\sigma_{\hat{u}_i}}{\sqrt{2\pi}}\left[\exp\left(-(\frac{\beta_i - \mu_{\hat{u}_i}}{\sqrt{2}\sigma_{\hat{u}_i}})^2\right) - \exp\left(-(\frac{\alpha_i - \mu_{\hat{u}_i}}{\sqrt{2}\sigma_{\hat{u}_i}})^2\right)\right], \end{aligned} \tag{8.13}$$

where $\mu_{\hat{u}_i}$ and $\sigma_{\hat{u}_i}$ are given by

$$\begin{aligned} \mu_{\hat{u}_i} &= -K_i M_i, \\ \sigma_{\hat{u}_i} &= K_i\gamma_i\tau_i\sqrt{\frac{W_{ii}}{2(1 + K_i N_i)(\tau_i + \tau_{w,i}(1 + K_i N_i))}}. \end{aligned} \tag{8.14}$$

The quantities $\mu_{\hat{u}_i}$ and $\sigma_{\hat{u}_i}$ are, respectively, the expected value and standard deviation of the signal $\hat{u}_i$ in Figure 8.2.2. Once the solution of (8.12), (8.13) is found, $m_i$ can be calculated as $m_i = M_i(1 + N_i K_i)$. It can be shown that the average value of the output $\hat{y}_i$ in Figure 8.2.2 is given by:

$$\mu_{\hat{y}_i} = M_i.$$

Using these notations, the dynamics of the quasilinear systems and the wind can be shown to be governed by:

$$\begin{bmatrix} \dot{\widetilde{V}}_w(t) \\ \dot{\hat{y}} \end{bmatrix} = \underbrace{\begin{bmatrix} A_{11} & 0 \\ A_{21} & A_{22} \end{bmatrix}}_{A} \begin{bmatrix} \widetilde{V}_w(t) \\ \hat{y} \end{bmatrix} + \underbrace{\begin{bmatrix} -A_{11} \\ 0 \end{bmatrix}}_{B} w(t) + \begin{bmatrix} 0 \\ A_m \end{bmatrix} m, \qquad (8.15)$$

where $\widetilde{V}_w(t) = (\widetilde{V}_{w,1}(t), \ldots, \widetilde{V}_{w,n}(t)) \in \mathbb{R}^n$ and $\hat{y} = (\hat{y}_1, \ldots, \hat{y}_n) \in \mathbb{R}^n$ are the $2n$ states, $w(t) = (w_1(t), \ldots, w_n(t)) \in \mathbb{R}^n$ is the white noise with covariance matrix $W$, $A_{11} = \text{diag}(-\frac{1}{\tau_{w,1}}, \ldots, -\frac{1}{\tau_{w,n}})$, $A_{21} = \text{diag}(\gamma_1, \ldots, \gamma_n)$, $A_{22} = \text{diag}(-\frac{1+N_1K_1}{\tau_1}, \ldots, -\frac{1+N_nK_n}{\tau_n})$, $m = [m_1, \ldots, m_n]$, and $A$ is asymptotically stable since $\tau_{w,i} > 0$ and $\tau_i > 0$.

To re-formulate the optimization problem posed above in terms of the parameters in the quasilinear system, let us denote the zero mean part of $\hat{y}_i$ by $y_{0,i}$. Then, $\hat{y}_i = y_{0,i} + M_i$. Therefore, letting $M = [M_1 \ \ldots \ M_N]^T$, the cost function $J$ given in (8.9), becomes:

$$\begin{aligned} J &= \lim_{t\to\infty} E\left\{ \left( \sum_{i=1}^{n} (y_{0,i}(t) + M_i) \right)^2 + \sum_{i=1}^{n} \epsilon_i K_i^2 (y_{0,i}(t) + M_i)^2 \right\} \\ &= \lim_{t\to\infty} E\left\{ \left( \sum_{i=1}^{n} y_{0,i}(t) \right)^2 + \sum_{i=1}^{n} \epsilon_i K_i^2 y_{0,i}^2(t) \right\} + \left( \sum_{i=1}^{n} M_i \right)^2 + \sum_{i=1}^{n} \epsilon_i K_i^2 M_i^2 \\ &= \lim_{t\to\infty} E\Big\{ \begin{bmatrix} \widetilde{V}_w(t)^T & \hat{y}_{0,i}^T \end{bmatrix} \underbrace{\begin{bmatrix} 0 & 0 \\ 0 & Q_{22} \end{bmatrix}}_{Q} \begin{bmatrix} \widetilde{V}_w(t) \\ \hat{y}_{0,i} \end{bmatrix} \Big\} + \left( \sum_{i=1}^{n} M_i \right)^2 + \sum_{i=1}^{n} \epsilon_i K_i^2 M_i^2 \\ &= \text{trace}(SQ) + M^T Q_{22} M, \end{aligned} \qquad (8.16)$$

where $Q_{22} = \mathbf{1} \cdot \mathbf{1}^T + \text{diag}(\epsilon_1 K_1^2, \ldots, \epsilon_n K_n^2)$, $\mathbf{1} \in \mathbb{R}^n$ is an all-one column vector, and $S = S^T > 0$ is the unique solution of the Lyapunov equation

$$AS + SA^T + BWB^T = 0. \qquad (8.17)$$

Thus, the optimal QLC-based controller is the solution of the following optimization problem:

$$\min_{K_i, N_i, M_i, 1 \le i \le n} J, \tag{8.18}$$

subject to equality constraints given by (8.12) and (8.13) with $\mu_{\hat{u}_i}$ and $\sigma_{\hat{u}_i}$ given by (8.14), $i = 1, \ldots, n$. In the next section, we numerically solve this optimization problem to evaluate the performance of the QLC-based controller.

## 8.4 Performance evaluation

To carry out the evaluation, the system parameters are divided into two groups. The first group contains parameters to be held constant throughout the evaluation process. These parameters and their fixed values are: $n = 10$ and, for each $i = 1, 2, \ldots, n$, $\tau_{w,i} = 1$, $\tau_i = 60$, $a_i = 0.657$, and $\gamma_i = 0.02$. The second group contains parameters to be varied. These parameters represent operating regimes of the WFCS and, hence, varying their values allows us to examine the WFCS performance in different regimes. For simplicity, we let their values be governed by four scalar parameters $(\mathsf{v}, \mathsf{p}, \mathsf{r}, \mathsf{e})$ in the following manner:

- *Wind speed* $\mathsf{v}$: For all $i$, let the slow wind speed component $\overline{V}_{w,i}(t) = \mathsf{v}$, where $\mathsf{v} \in \{0.4, 1\}$, so that $\mathsf{v} = 0.4$ and $\mathsf{v} = 1$ represent low and high wind speed regimes, respectively. With this $\mathsf{v}$, the saturation in (8.8) becomes $\mathrm{sat}_{-P_i^*}^{0.657\mathsf{v}^3 - P_i^*}$. Thus, its linear region is narrow if $\mathsf{v} = 0.4$ and wide if $\mathsf{v} = 1$.

- *Power generation* $\mathsf{p}$: For all $i$, let the intermediate power reference $P_i^*(t) = \mathsf{p} a_i \overline{V}_{w,i}^3(t) = 0.657\mathsf{p}\mathsf{v}^3$, where $\mathsf{p} \in \{0.7, 1\}$. Since $a_i \overline{V}_{w,i}^3(t)$ is the maximum power turbine $i$ can generate, the quantity $\mathsf{p}$ is the fraction of the maximum power. Hence, $\mathsf{p} = 0.7$ and $\mathsf{p} = 1$ correspond to medium (70%) and high (100%) power generation regimes, respectively. With both $\mathsf{v}$ and $\mathsf{p}$, the saturation

in (8.8) further becomes $\mathrm{sat}_{-0.657\mathsf{p}\mathsf{v}^3}^{0.657(1-\mathsf{p})\mathsf{v}^3}$. Therefore, its linear region is nearly symmetric about the origin if $\mathsf{p} = 0.7$ and one-sided if $\mathsf{p} = 1$.

- *Wind correlation* $\mathsf{r}$: Let the covariance matrix $W = [W_{ij}]$ with $W_{ij} = \mathsf{v}^2/9\ \mathsf{r}^{|i-j|}$, where $\mathsf{r} \in \{0, 0.999\}$, so that $\mathsf{r} = 0$ and $\mathsf{r} = 0.999$ represent, respectively, weak and strong wind correlation regimes. The scaling $\mathsf{v}^2/9$ is intended to make the standard deviation of $\widetilde{V}_i$ one third of the average value $\overline{V}_i$ so that the wind is negative with negligible probability.

- *Control penalty* $\mathsf{e}$: For all $i$, let the control penalty $\epsilon_i = \mathsf{e}$, where $\mathsf{e} \in \{0.05, 0.1, 0.2, 0.5, 1, 2, 5, 10, 20, 100\}$, so that $\mathsf{e} = 0.05$ may be regarded as a cheap control regime and $\mathsf{e} = 100$ an expensive one.

Observe that $\mathsf{v}$, $\mathsf{p}$, and $\mathsf{r}$ each has two possible values, while $\mathsf{e}$ has ten. Thus, a total of $2^3 \cdot 10 = 80$ distinct scenarios are considered, covering a wide range of operating conditions.

For each scenario defined by $(\mathsf{v}, \mathsf{p}, \mathsf{r}, \mathsf{e})$, we use Matlab to evaluate analytically and via simulation both the performance of the QLC method and the linear method (i.e., by ignoring the saturations, as performed in [77]). We denote the minimum cost computed analytically and via simulation with the linear method by $J_{\mathrm{lin}}^{\mathrm{a}}(\mathsf{v}, \mathsf{p}, \mathsf{r}, \mathsf{e})$ and $J_{\mathrm{lin}}^{\mathrm{s}}(\mathsf{v}, \mathsf{p}, \mathsf{r}, \mathsf{e})$, respectively. Similarly, we denote the minimum cost computed analytically and via simulation with the QLC method by $J_{\mathrm{QLC}}^{\mathrm{a}}(\mathsf{v}, \mathsf{p}, \mathsf{r}, \mathsf{e})$ and $J_{\mathrm{QLC}}^{\mathrm{s}}(\mathsf{v}, \mathsf{p}, \mathsf{r}, \mathsf{e})$. Note that the difference between $J_{\mathrm{lin}}^{\mathrm{a}}(\cdot)$ and $J_{\mathrm{lin}}^{\mathrm{s}}(\cdot)$, and that between $J_{\mathrm{QLC}}^{\mathrm{a}}(\cdot)$ and $J_{\mathrm{QLC}}^{\mathrm{s}}(\cdot)$, quantify the accuracy of the linear and QLC methods, respectively. Moreover, the extent to which $J_{\mathrm{QLC}}^{\mathrm{s}}(\cdot)$ is less than $J_{\mathrm{lin}}^{\mathrm{s}}(\cdot)$ represents the improvement offered by the QLC method. For convenience, the percentage of such improvement is denoted as $\delta(\mathsf{v}, \mathsf{p}, \mathsf{r}, \mathsf{e})$ and defined as

$$\delta(\mathsf{v}, \mathsf{p}, \mathsf{r}, \mathsf{e}) = 100 \times \frac{J_{\mathrm{lin}}^{\mathrm{s}}(\mathsf{v}, \mathsf{p}, \mathsf{r}, \mathsf{e}) - J_{\mathrm{QLC}}^{\mathrm{s}}(\mathsf{v}, \mathsf{p}, \mathsf{r}, \mathsf{e})}{J_{\mathrm{lin}}^{\mathrm{s}}(\mathsf{v}, \mathsf{p}, \mathsf{r}, \mathsf{e})}. \tag{8.19}$$

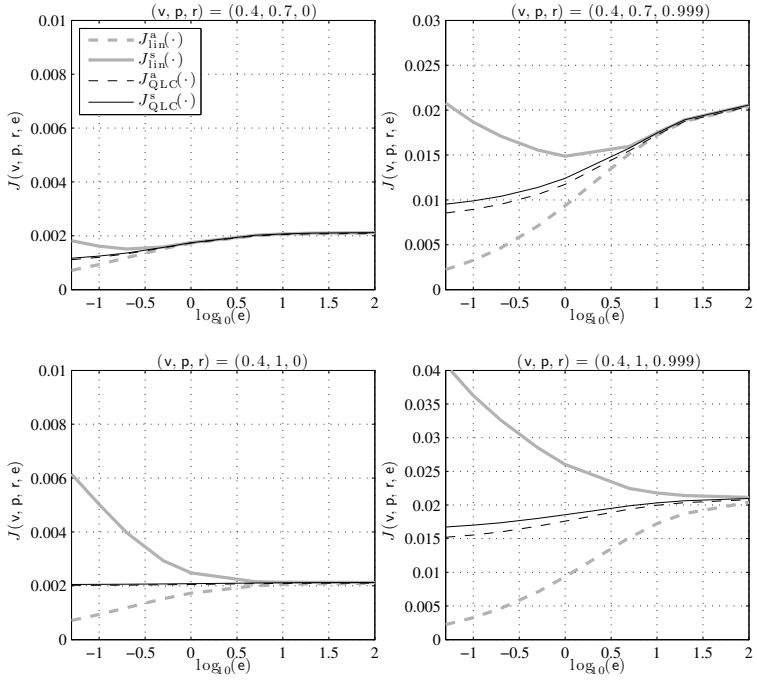


Figure 8.3: Values of cost functions $J^{\mathrm{a}}_{\mathrm{lin}}(\cdot)$, $J^{\mathrm{s}}_{\mathrm{lin}}(\cdot)$, $J^{\mathrm{a}}_{\mathrm{QLC}}(\cdot)$, and $J^{\mathrm{s}}_{\mathrm{QLC}}(\cdot)$ in the *low* wind speed regime ($\mathsf{v} = 0.4$).

Figures 8.3–8.5 show the evaluation results. Analyzing these figures, the following observations about the accuracy and effectiveness of the linear and QLC methods can be made:

- *Accuracy of linear method*: Regardless of $(\mathsf{v}, \mathsf{p}, \mathsf{r})$, when control is expensive (i.e., when $\mathsf{e}$ is large), $J^{\mathrm{a}}_{\mathrm{lin}}(\mathsf{v}, \mathsf{p}, \mathsf{r}, \mathsf{e})$ and $J^{\mathrm{s}}_{\mathrm{lin}}(\mathsf{v}, \mathsf{p}, \mathsf{r}, \mathsf{e})$ are indistinguishable. This agrees with expectation because when $\mathsf{e}$ is large, the optimal $K_i$'s are small, causing the WFCS to operate mostly in the linear regime, so that $J^{\mathrm{a}}_{\mathrm{lin}}(\cdot) \approx J^{\mathrm{s}}_{\mathrm{lin}}(\cdot)$. As control becomes cheap (i.e., as $\mathsf{e}$ goes to zero), $J^{\mathrm{a}}_{\mathrm{lin}}(\mathsf{v}, \mathsf{p}, \mathsf{r}, \mathsf{e})$ approaches zero. This is also expected as it is well known that for minimum-phase linear systems, cheap control can yield arbitrarily good disturbance rejection [80]. However, as

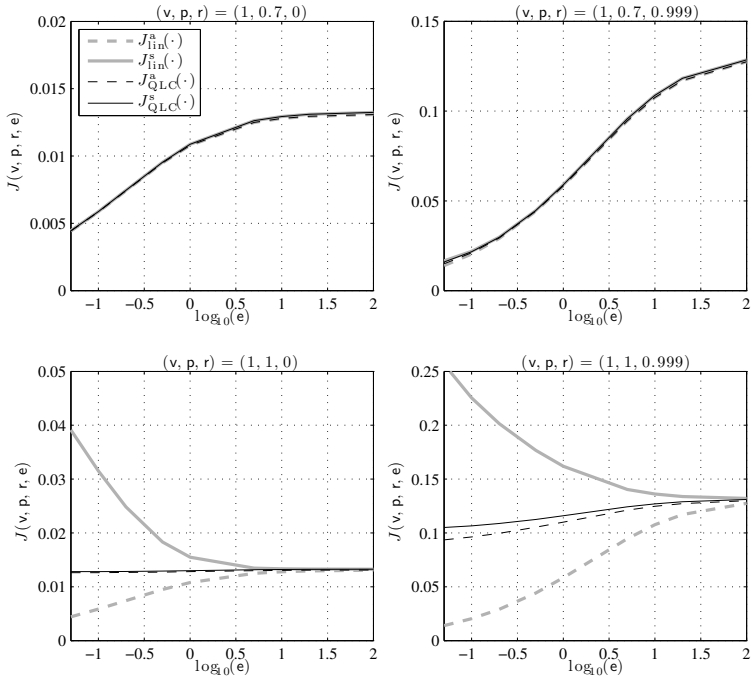


Figure 8.4: Values of cost functions $J^{\mathrm{a}}_{\mathrm{lin}}(\cdot)$, $J^{\mathrm{s}}_{\mathrm{lin}}(\cdot)$, $J^{\mathrm{a}}_{\mathrm{QLC}}(\cdot)$, and $J^{\mathrm{s}}_{\mathrm{QLC}}(\cdot)$ in the high wind speed regime.

$\mathsf{e}$ goes to zero, not only is $J^{\mathrm{s}}_{\mathrm{lin}}(\mathsf{v},\mathsf{p},\mathsf{r},\mathsf{e})$ bounded away from zero, it actually increases substantially in most cases. This suggests that the linear method has poor accuracy when $\mathsf{e}$ is small. The result also implies that ignoring saturation and attempting a cheap control design of the WFCS may not be advisable.

- *Accuracy of QLC method*: Similar to $J^{\mathrm{a}}_{\mathrm{lin}}(\cdot)$ and $J^{\mathrm{s}}_{\mathrm{lin}}(\cdot)$ above, regardless of $(\mathsf{v},\mathsf{p},\mathsf{r})$, when $\mathsf{e}$ is large, $J^{\mathrm{a}}_{\mathrm{QLC}}(\cdot)$ and $J^{\mathrm{s}}_{\mathrm{QLC}}(\cdot)$ are indistinguishable, which again agrees with expectation. However, unlike $J^{\mathrm{a}}_{\mathrm{lin}}(\cdot)$ and $J^{\mathrm{s}}_{\mathrm{lin}}(\cdot)$ above, as $\mathsf{e}$ goes to zero, $J^{\mathrm{a}}_{\mathrm{QLC}}(\cdot)$ and $J^{\mathrm{s}}_{\mathrm{QLC}}(\cdot)$ remain close to each other, with the former being slightly below the latter. This implies that the QLC method is accurate, providing an analytical means for estimating the true performance that is only

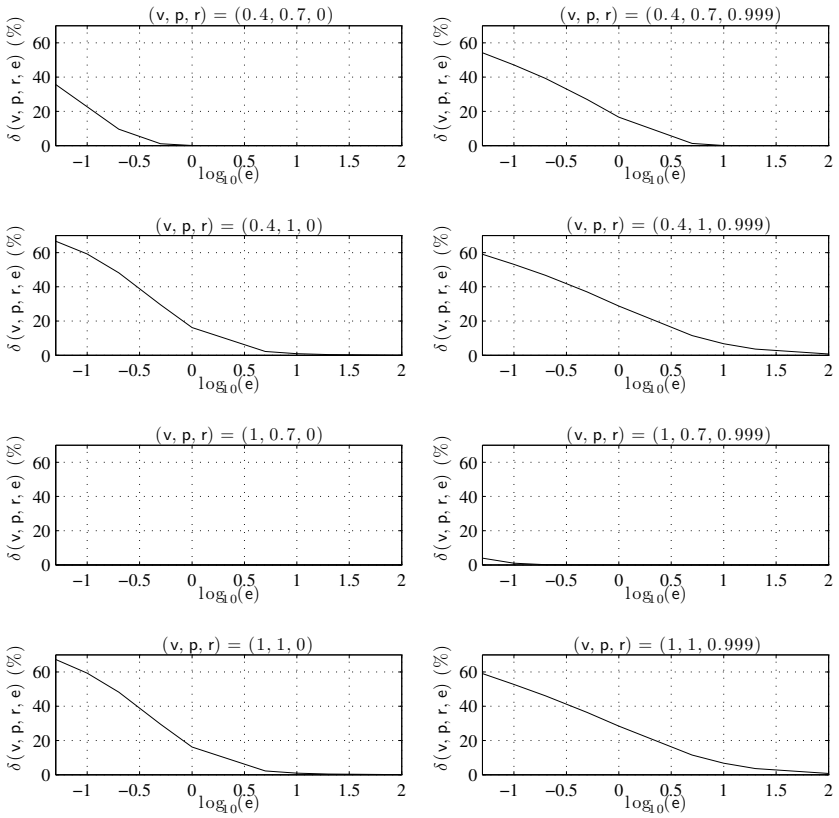


Figure 8.5: Percentage of improvement $\delta(\mathsf{v}, \mathsf{p}, \mathsf{r}, \mathsf{e})$ across various regimes.

slightly more optimistic than reality. The result also implies that stochastic linearization performs well for the WFCS, which has good low-pass filtering characteristics.

- *Linear method versus QLC method*: To compare the effectiveness of the two methods, consider the improvement curve $\delta(\cdot)$ in Figure 8.5. Note that as $\mathsf{e}$ decreases, the percentage of improvement $\delta(\cdot)$ monotonically increases, reaching 40%–60% in all regimes but two. This result shows that the QLC method is significantly better than the linear method if control is not expensive, and as good as the linear method otherwise.

# CHAPTER IX

# Conclusions and Future Work

## 9.1 Conclusions

In this dissertation, the theory of Quasilinear Control (QLC) for Asymmetric Linear Plant/Nonlinear Instrumentation (A-LPNI) systems has been developed. The approach, similar to the symmetric case, is based on the method of stochastic linearization, which reduces nonlinear systems to quasilinear ones. It is shown that stochastic linearization in the asymmetric case results in not only a quasilinear gain, but also a quasilinear bias. This bias leads to steady state errors incompatible with the usual error coefficients, which makes the QLC theory for asymmetric systems a non-trivial extension of the symmetric case.

In this work, the problems addressed and the main results are as follows.

- The notion of symmetric LPNI (S-LPNI) and asymmetric LPNI (A-LPNI) systems is formally introduced. It is shown that symmetry depends not only on the nonlinear elements in the loop, but also on all functional blocks and exogenous signals of the system. In addition, a measure of asymmetry is introduced and analyzed.

- Stochastic linearization for the closed loop environment has been developed. It is shown that stochastic linearization results in a system of two transcenden-

tal equations in two unknowns. Using these equations, the so-called quasilinear gain and bias can be computed. Necessary and sufficient conditions for existence of solutions of these equations are provided. Moreover, accuracy of stochastic linearization in the closed loop environment is investigated. It has been shown that, even though accuracy in the asymmetric case is lower than the symmetric case, stochastic linearization still provides good accuracy as far as first and second moments of the output are concerned. Furthermore, accuracy is higher for sufficiently slow plants. This is because a low pass filtering plant Gaussianizes its input, leading to a higher accuracy of stochastic linearization.

- The issue of performance analysis in A-LPNI systems is addressed. It is shown that stochastic linearization provides faithful prediction for quality of tracking and disturbance rejection. Moreover, the phenomenon of noise-induced tracking error in systems with anti-windup and sensor noise has been successfully quantified. As far as tracking is concerned, the notions of trackable domain, system types, saturating random sensitivity function, and quality indicators have been extended from the symmetric case to the asymmetric one. Some results here are proper extensions of the symmetric case, while others are pertinent only to the asymmetric case.

- The notion of performance loci is introduced and analyzed. Specifically, it is shown that in the asymmetric case, the performance of closed loop system is characterized by a modified root locus (AS-root locus) and, in addition, by a tracking error locus (TE locus), which does not emerge in the symmetric case.

- A method for random-reference tracking controller design based on the performance loci is introduced. In this method, the AS-root and TE loci must both be placed within their respective admissible domains for good tracking.

- The problem of step tracking controller design is addressed. The proposed

method consists of three steps: on the first step, a second order pre-compensator is introduced, whose step response satisfies the step-tracking specifications. Then, the output of this precompensator is "mapped" into a random reference signal with a bandwidth determined by the dynamic part of the step tracking specifications. At the third step, the performance loci approach is used to design a controller that tracks this random reference. The same controller is used to track the output of the precompensator.

- The problem of selecting an optimal anti-windup gain in an anti-windup system with back-calculation is formulated and solved.

- The problem of complete performance recovery for A-LPNI systems is addressed. This problem is concerned with recovering linear disturbance rejection performance in the presence of nonlinearities in the actuators and sensors. The design consists of two boosting gains at the controller and sensor to cancel the effects of the quasilinear gains, and a bias at the controller to account for the quasilinear bias. It is shown that, if the accuracy of stochastic linearization is good, this design leads to improved performance of the nonlinear system.

- The A-SLQR method is developed for disturbance rejection controller design. This method is carried out by minimizing a weighted combination of the second moment of the plant output and controller output of the quasilinear system. The optimization problem has equality constraints to account for the usual Lyapunov equation and the quasilinear gain and bias equations. Using examples, it is shown that the A-SLQR controllers perform better than those based on linear LQR.

- The methods developed in this work are applied for controller design of a wind farm with multiple wind turbines. Each of these turbines is modeled by a first order plant preceded by an asymmetric saturation function, which accounts for

limited availability of wind. It is shown that in a broad range of regimes, the QLC-based controllers perform better than controllers designed by ignoring the nonlinearities.

It is fair to say that the QLC theory for asymmetric LPNI systems is a proper extension of the symmetric case. However, as it is demonstrated in this dissertation, this extension is not a trivial one because of the quasilinear bias. Moreover, many new phenomena arise in the asymmetric case that are not present in the symmetric case: new quality indicators for tracking, the TE locus, the modified cost functions in the optimization problems, etc. Finally, it is worth mentioning that symmetric LPNI systems are only a small subset of LPNI systems. Therefore, the results obtained here are more powerful and are applicable to a larger class of systems.

The theory developed in this dissertation is expected to have impact on both academia and industry. In academia, in opens a new area of research. In the next section, some possible future research directions are listed. In industry, it provides new methods for design of controllers, which are "slight" extension of the usual linear techniques.

As a final comment, a personal reflection on this dissertation follows. In developing the theory presented herein, I faced many interesting challenges, of which the most prominent ones were:

- The quasilinear bias: One of the earliest challenges I faced in this work was formalizing a stochastic linearization in A-LPNI systems that accounts for both dynamic and steady state behaviors. After much thinking, I introduced the quasilinear bias, which accounted for steady state behavior of the system.

- The degree of asymmetry: Throughout this work, I introduced different measures to quantify asymmetry in for A-LPNI systems, none of which was satisfactory. Towards the end of my doctoral studies, I devised the measure $A$

introduced in Chapter II, which captured the essence of asymmetry.

- The TE locus: It was not at first clear how both dynamics and steady state behaviors can be characterized for tracking controller design of A-LPNI systems. The TE locus was the outcome of a long study to address this problem.

- Step-tracking controller design: Since all our methods have been based on stochastic linearization, it was not clear how the results could be extended to tracking deterministic signals, e.g., steps. The introduction of the pre-compensator and the adjoint bandwidth enabled converting the step-tracking problem into a random-tracking problem, followed by subsequent application of stochastic linearization.

Even though these and other challenges brought frustration at times, they led me to learn a great deal about quasilinear control and control theory in general. Undoubtedly, this work has enabled me to expand my horizons as a researcher.

## 9.2 Future Work

Future work in this area is abundant:

- The phenomenon of Gaussianization must be analytically proven, and the accuracy of stochastic linearization for Gaussianizing systems thoroughly studied. While such a study has been done for a small class of systems in [64], the general case has not been treated. The method of cumulants [81] may be applicable for the study of Gaussianization.

- QLC theory can be extended to other nonlinearities in the sensors and actuators. For example, the performance loci and A-SLQR approaches can be extended to systems with saturating sensor, sensor with deadzone or quantization, actuator with deadzone or relay, etc.

- It has been observed that if the solution of quasilinear gain and bias equations is not unique, the jumping phenomenon occurs. As a future direction, this phenomenon can be thoroughly studied and analytically proven.

- The results can be extended to the MIMO case. Multi-loop and state feedback control of systems with decoupled saturating actuators is a natural extension of this work.

- The relationship between existence of solution to the quasilinear gain and bias equations and existence of an invariant measure in the original LPNI system can be explored.

- Other linear control methods such as $H_\infty$ and LMI approaches can be extended to the quasilinear control of S- and A-LPNI systems.

- QLC can be applied to standard nonlinear control techniques (e.g., feedback linearization of systems with saturating actuators) for performance analysis and controller design.

- The robustness of the quasilinear gain and bias must be analyzed with respect to the system parameters. Moreover, robustness of the resulting QLC controllers must be quantified in terms of stability and performance.

- Lastly, a comprehensive experimental validation of the theory in an industrial setting is important.

The solutions of these problems will provide a relatively complete theory of Quasilinear Control.

# APPENDICES

# APPENDIX A

# Proofs

## A.1 Proofs for Chapter II

**Proof of Proposition II.1:** We prove each part of this proposition below:

1. Let $\sigma_u > 0$ be fixed. Differentiating the quasilinear gain equation (2.8) with respect to $\mu_u$ and setting the result equal to zero, we obtain

$$\exp(-(\frac{\beta-\mu_u}{\sqrt{2}\sigma_u})^2) = \exp(-(\frac{\alpha-\mu_u}{\sqrt{2}\sigma_u})^2).$$

The above equality holds when and only when $\beta = \alpha$ or $\mu_u = \frac{\alpha+\beta}{2}$. The first case gives the minimum while the second case gives the maximum.

2. Substituting $\mu_u = \frac{\alpha+\beta}{2}$ into (2.8) and noting that $\text{erf}(x) < \frac{2}{\sqrt{\pi}}x$, we obtain that

$$N = \frac{1}{2}[\text{erf}\left(\frac{\beta-\mu_u}{\sqrt{2}\sigma_u}\right) - \text{erf}\left(\frac{\alpha-\mu_u}{\sqrt{2}\sigma_u}\right)] \leq \frac{1}{2}[\text{erf}\left(\frac{\beta-\frac{\alpha+\beta}{2}}{\sqrt{2}\sigma_u}\right) - \text{erf}\left(\frac{\alpha-\frac{\alpha+\beta}{2}}{\sqrt{2}\sigma_u}\right)]$$

$$= \text{erf}(\frac{\beta-\alpha}{2}\frac{1}{\sqrt{2}\sigma_u}) < \frac{\beta-\alpha}{\sqrt{2\pi}\sigma_u}.$$

This proves the result.

3. By part (2),

$$\sigma_{\hat{v}} = N\sigma_u < \sigma_u \text{erf}(\frac{\beta-\alpha}{2}\frac{1}{\sqrt{2}\sigma_u}) < \frac{\beta-\alpha}{\sqrt{2\pi}} < \frac{\beta-\alpha}{2},$$

which proves this part.

4. Since $m = M - N\mu_u$ and $\alpha < M < \beta$, it suffices to show that $N\mu_u$ is always bounded. Since $0 < N < 1$, it follows that for small $\mu_u$, $m$ is indeed bounded. It remains to show that $\mu_u N$ is bounded for large $\mu_u$. According to the expression for $N$, as $\mu_u$ tends to $\infty$, $N$ tends to zero. Therefore, to study $\lim_{\mu_u\to\infty} \mu_u N$, we use L'Hospital's rule:

$$\lim_{\mu_u\to\infty} \mu_u N = \lim_{\mu_u\to\infty} \frac{N}{\frac{1}{\mu_u}} = \lim_{\mu_u\to\infty} -\mu_u^2 N' = -\frac{\mu_u^2}{\sqrt{2\pi}\sigma_u}\left(e^{-(\frac{\beta-\mu_u}{\sqrt{2}\sigma_u})^2} - e^{-(\frac{\alpha-\mu_u}{\sqrt{2}\sigma_u})^2}\right).$$

Since the exponentials dominate the polynomial $\mu_u^2$, it follows that $\lim_{\mu_u\to\infty} \mu_u N = 0$. Therefore, $\mu_u N$ is equal to 0 both when $\mu_u = 0$ and when $\mu_u = \infty$. Thus, continuity of $\mu_u N$ implies that $\mu_u N$ is bounded. Same argument holds when $\mu_u \to -\infty$.

5. ($\Rightarrow$): Assume that $\mu_u = \frac{\alpha+\beta}{2}$. Then, equation (2.9) simplifies to

$$M = \frac{\alpha+\beta}{2}.$$

Since equation (2.9) implies that $M = \mu_{\hat{v}} = \mu_v$, the result follows.

($\Leftarrow$): Now assume that $\mu_v = \frac{\alpha+\beta}{2}$. Then, the quasilinear bias equation equation (2.9) can be written as:

$$0 = \frac{\mu_u-\beta}{2}\text{erf}\left(\frac{\beta-\mu_u}{\sqrt{2}\sigma_u}\right) - \frac{\mu_u-\alpha}{2}\text{erf}\left(\frac{\alpha-\mu_u}{\sqrt{2}\sigma_u}\right) - \frac{\sigma_u}{\sqrt{2\pi}}\left[\exp\left(-(\frac{\beta-\mu_u}{\sqrt{2}\sigma_u})^2\right) - \exp\left(-(\frac{\alpha-\mu_u}{\sqrt{2}\sigma_u})^2\right)\right].$$

To simplify this expression, define the function $f(x) = x\text{erf}(x) + \frac{1}{\sqrt{\pi}}e^{-x^2}$. Then,

the above can be written as

$$0 = f\left(\frac{\beta - \mu_u}{\sqrt{2}\sigma_u}\right) - f\left(\frac{\alpha - \mu_u}{\sqrt{2}\sigma_u}\right).$$

It can be shown, using the graph of $f(x)$, that $f(x) = f(y)$ when and only when $x = y$ or $x = -y$. The former implies that $\alpha = \beta$, which is not the case. The latter implies that $\left(\frac{\beta-\mu_u}{\sqrt{2}\sigma_u}\right) = -\left(\frac{\alpha-\mu_u}{\sqrt{2}\sigma_u}\right)$, which simplifies to $\mu_u = \frac{\alpha+\beta}{2}$. This proves this part of the proposition.

6. This part can be proved by direct manipulation of the equation for quasilinear gain (2.8).

7. This part can be proved by direct manipulation of the equation for quasilinear bias (2.9).

□

**Proof of Theorem II.2**: If either $C_0 = \infty$ or $P_0 = \infty$, (2.22) can be written as

$$\frac{\mu_r}{P_0} = \mathcal{F}_M(\sigma_{\hat{u}}, \mu_{\hat{u}}).$$

Since the range of $\mathcal{F}_M$ is $\mathscr{M}_a$, a necessary condition for the above equation to have a solution is $\frac{\mu_r}{P_0} \in \mathscr{M}_a$. This proves the theorem. □

**Proof of Theorem II.3**: We consider two cases. First assume that $C_0 \neq \infty$ and $P_0 \neq \infty$. Therefore, using (2.19), we rewrite (2.21), (2.22) as

$$N_a = \mathcal{F}_N\left(\sigma_{\hat{u}}, C_0(\mu_r - P_0 M_a)\right), \tag{A.1}$$

$$M_a = \mathcal{F}_M\left(\sigma_{\hat{u}}, C_0(\mu_r - P_0 M_a)\right), \tag{A.2}$$

where $\sigma_{\hat{u}}$ is given in (2.18). The first assumption of this theorem implies that for any value of $N_a \in \mathscr{N}_a$, the standard deviation $\sigma_{\hat{u}}$ exists and is a continuous function of $N_a$. Therefore, the right hand sides of (A.1), (A.2) form continuous functions of $N_a$ and $M_a$. Now, if the sets $\mathscr{N}_a$ and $\mathscr{M}_a$ are closed, then by the second assumption, they are also compact. Therefore, by Brouwer's fixed point theorem [82], system (A.1), (A.2) has a solution and the result follows. If, however, the sets $\mathscr{N}_a$ and $\mathscr{M}_a$ are not closed, we proceed formally and consider their closures. Application of Brouwer's fixed point theorem proves existence of at least one solution in the closures of $\mathscr{N}_a$ and $\mathscr{M}_a$. This proves the first case.

For the second case, assume that either $C_0 = \infty$ or $P_0 = \infty$ or both. Then, (2.22) becomes:

$$\frac{\mu_r}{P_0} - \mathcal{F}_M(\sigma_{\hat{u}}, \mu_{\hat{u}}) = 0.$$

Note that $\frac{\mu_r}{P_0}$ is a constant. By the third assumption in the theorem, for each $\sigma_{\hat{u}}$, the above equation has a solution $\mu_{\hat{u}}$. Since $\mathcal{F}_M$ is an analytic function of the variable $\mu_{\hat{u}}$, its zero forms a continuous function of the parameter $\sigma_{\hat{u}}$, i.e.,

$$\mu_{\hat{u}} = g(\sigma_{\hat{u}}),$$

where $g$ is continuous. Substituting the above instead of $\mu_{\hat{u}}$ in equation (2.21), yields one equation in the unknown $N$. Now, the resulting right hand side is a continuous function of $N$. Therefore, by Brouwer's fixed point theorem, the result follows. □

**Proof of Theorem II.5**: Since $u$ is a Gaussian process, we have that

$$P[u \leq \alpha] = \int_{-\infty}^{\alpha} \frac{1}{\sqrt{2\pi}\sigma_u} e^{\left(-(\frac{x-\mu_u}{\sqrt{2}\sigma_u})^2\right)} dx = \frac{1}{2}(1 + \mathrm{erf}(\frac{\alpha - \mu_u}{\sqrt{2}\sigma_u})),$$

$$P[u \geq \beta] = \int_{\beta}^{\infty} \frac{1}{\sqrt{2\pi}\sigma_u} e^{\left(-(\frac{x-\mu_u}{\sqrt{2}\sigma_u})^2\right)} dx = 1 - \frac{1}{2}(1 + \text{erf}(\frac{\beta - \mu_u}{\sqrt{2}\sigma_u})) = \frac{1}{2}(1 - \text{erf}(\frac{\beta - \mu_u}{\sqrt{2}\sigma_u})).$$

Subtracting the above two expressions results in (2.29). □

**Proof of Corollary II.2**: For convenience, let $A = \frac{\alpha - \mu_u}{\sqrt{2}\sigma_u}$ and $B = \frac{\beta - \mu_u}{\sqrt{2}\sigma_u}$. Then, we can express $N$ in terms of $A$ as follows:

$$N = 0.5\,(\text{erf}(B) - \text{erf}(A)) = 0.5\,(\text{erf}(B) + \text{erf}(A) - 2\text{erf}(A)) = -A - \text{erf}(A).$$

Now, since $\text{erf}(A) > -1$, we have that

$$N < -A + 1.$$

Similarly, we can write

$$N = 0.5\,(\text{erf}(B) - \text{erf}(A)) = 0.5\,(-\text{erf}(B) - \text{erf}(A) + 2\text{erf}(B)) = A + \text{erf}(B) < A + 1.$$

Together, these expressions imply that $N < 1 - |A|$. This proves one of the inequalities. The second inequality follows from the fact that $N$ is the probability that saturation does not take place; hence, $N > 0$. □

**Proof of Theorem II.6**: We first make the following claim: In the open loop environment, assuming that $\sigma_u$ is finite and non-zero and $\mu_u$ is finite, $A = 0$ iff $\mu_u = \frac{\alpha + \beta}{2}$. To show this, note that (2.29) implies that $A = 0$ iff $\text{erf}(\frac{\beta - \mu_u}{\sqrt{2}\sigma_u}) = -\text{erf}(\frac{\alpha - \mu_u}{\sqrt{2}\sigma_u})$. Since the error function is odd, this implies that $\frac{\beta - \mu_u}{\sqrt{2}\sigma_u} = -\frac{\alpha - \mu_u}{\sqrt{2}\sigma_u}$, which simplifies to $\mu_u = \frac{\alpha + \beta}{2}$. This proves the above claim. We now prove the theorem. Note that, according to Section 1.2, if condition (1.4) is satisfied, the system in the canonical form has a symmetric saturation nonlinearity. Stationarity of closed loop signals implies that

the average value of signal at the input of this nonlinearity must be 0. This, in turn, implies that the average value of the signal at the input of the saturation in the original LPNI system is $\frac{\alpha+\beta}{2}$. Thus, according to the above claim, $A = 0$. This proves one direction. To prove the other direction, assume that $A = 0$. Then, $\mu_u = \frac{\alpha+\beta}{2}$. By part 5 of Proposition II.1, $\mu_v = \frac{\alpha+\beta}{2}$. Now, using the fact that $\mu_u = \mu_v = \frac{\alpha+\beta}{2}$, we have that $\frac{\alpha+\beta}{2} = \mu_u = C_0(\mu_r - P_0\frac{\alpha+\beta}{2})$. Solving for $\frac{\alpha+\beta}{2}$ leads to condition (1.4). This proves the theorem. □

## A.2 Proofs for Chapter III

**Proof of Theorem III.1**: For convenience, introduce the following notations: $v_{ss} = \lim_{t\to\infty} v(t)$ and $u_{ss} = \lim_{t\to\infty} u(t)$. We consider two cases: (a) $|P_0| < \infty$ and (b) $|P_0| = \infty$.

Case (a): $|P_0| < \infty$. Under the assumption of unique $e_{ss}$ only one of these cases may happen: $v_{ss} = \alpha, v_{ss} = \beta, \alpha < v_{ss} < \beta$. First consider $\alpha < v_{ss} < \beta$. In this case, the saturation is inactive and steady state error is the same as that for the underlying linear system: $e_{ss} = \frac{r_0}{1+P_0C_0}$. Now, since the saturation is inactive, we have that $\alpha < u_{ss} < \beta$, which implies that

$$\alpha < u_{ss} = \frac{r_0 C_0}{1 + P_0 C_0} < \beta.$$

The above can be written in terms of $r_0$ as follows: if $\frac{1}{C_0} + P_0 > 0$, then $(\frac{1}{C_0} + P_0)\alpha < r_0 < (\frac{1}{C_0} + P_0)\beta$, and if $\frac{1}{C_0} + P_0 < 0$, then $(\frac{1}{C_0} + P_0)\alpha > r_0 > (\frac{1}{C_0} + P_0)\beta$. Combining the two, we can write

$$r_0 \operatorname{sign}(\frac{1}{C_0} + P_0) \in \left[ |\frac{1}{C_0} + P_0|\alpha, |\frac{1}{C_0} + P_0|\beta \right].$$

This proves part (1) of the theorem for case (a).

To prove parts (2) and (3) of the theorem for case (a), we consider two sub-cases: $(i)\frac{1}{C_0} + P_0 > 0$ and $(ii)\frac{1}{C_0} + P_0 < 0$.

Case (i) $\frac{1}{C_0} + P_0 > 0$: Since the saturation must be activated, we either have that $v_{ss} = \alpha$ or $v_{ss} = \beta$. We divide the range of possible $r_0$'s that can lead to this situation into two parts: $r_0 > (\frac{1}{C_0} + P_0)\beta$ and $r_0 < (\frac{1}{C_0} + P_0)\alpha$. First assume $r_0 > (\frac{1}{C_0} + P_0)\beta$. In what follows, we show that $e_{ss} = r_0 - P_0\beta$ if $C_0 > 0$ and $e_{ss} = r_0 - P_0\alpha$ if $C_0 < 0$.

When $r_0 > (\frac{1}{C_0} + P_0)\beta$, one of the following takes place: $v_{ss} = \alpha$ or $v_{ss} = \beta$. If $v_{ss} = \alpha$, then $e_{ss} = r_0 - P_0\alpha$ and $u_{ss} = C_0(r_0 - P_0\alpha) < \alpha$. This implies that $r_0 < (\frac{1}{C_0} + P_0)\alpha$ if $C_0 > 0$ and $r_0 > (\frac{1}{C_0} + P_0)\alpha$ if $C_0 < 0$. But $r_0 < (\frac{1}{C_0} + P_0)\alpha$ contradicts the assumption that $r_0 > (\frac{1}{C_0} + P_0)\beta$. Therefore, this case only happens when $C_0 < 0$. Now, if $v_{ss} = \beta$, then $e_{ss} = r_0 - P_0\beta$ and $u_{ss} = C_0(r_0 - P_0\beta) > \beta$. This implies that $r_0 > (\frac{1}{C_0} + P_0)\beta$ if $C_0 > 0$ and $r_0 < (\frac{1}{C_0} + P_0)\beta$ if $C_0 < 0$. But $r_0 < (\frac{1}{C_0} + P_0)\beta$ contradicts the assumption that $r_0 > (\frac{1}{C_0} + P_0)\beta$. Therefore, this case only happens when $C_0 > 0$. Combining the two cases, we have proved that $e_{ss} = r_0 - P_0\beta$ if $C_0 > 0$ and $e_{ss} = r_0 - P_0\alpha$ if $C_0 < 0$. Using a similar argument, we can show that when $r_0 < (\frac{1}{C_0} + P_0)\alpha$, $e_{ss} = r_0 - P_0\beta$ if $C_0 < 0$ and $e_{ss} = r_0 - P_0\alpha$ if $C_0 > 0$.

In sum, when $\frac{1}{C_0} + P_0 > 0$, $e_{ss} = r_0 - P_0\alpha$ when $C_0 < 0$ and $r_0 > (\frac{1}{C_0} + P_0)\beta$, or when $C_0 > 0$ and $r_0 < (\frac{1}{C_0} + P_0)\alpha$. Moreover, $e_{ss} = r_0 - P_0\beta$ when $C_0 > 0$ and $r_0 > (\frac{1}{C_0} + P_0)\beta$, or when $C_0 < 0$ and $r_0 < (\frac{1}{C_0} + P_0)\alpha$.

Case (ii) $\frac{1}{C_0} + P_0 < 0$: In this case, similar to case $(i)$, it can be shown that $e_{ss} = r_0 - P_0\alpha$ when $C_0 < 0$ and $r_0 < (\frac{1}{C_0} + P_0)\alpha$, or when $C_0 > 0$ and $r_0 < -(\frac{1}{C_0} + P_0)\beta$. Moreover, $e_{ss} = r_0 - P_0\beta$ when $C_0 < 0$ and $r_0 > (\frac{1}{C_0} + P_0)\beta$, or when $C_0 > 0$ and $r_0 > -(\frac{1}{C_0} + P_0)\alpha$.

Combining cases $(i)$ and $(ii)$, we obtain that $e_{ss} = r_0 - P_0\alpha$ if

$$1 + P_0C_0 > 0, r_0 < |\tfrac{1}{C_0} + P_0|\alpha,$$
$$OR$$
$$1 + P_0C_0 < 0, r_0 < |\tfrac{1}{C_0} + P_0|(-\beta),$$

and $e_{ss} = r_0 - P_0\beta$ if

$$1 + P_0C_0 > 0, r_0 > |\tfrac{1}{C_0} + P_0|\beta,$$
$$OR$$
$$1 + P_0C_0 < 0, r_0 > |\tfrac{1}{C_0} + P_0|(-\alpha),$$

which proves parts (2) and (3) of the theorem are proven for case $(a)$.

case $(b)$: If $|P_0| = \infty$, then $v_{ss} = 0$ for unique steady state to exist. Now, this implies that zero must necessarily be in the range $(\alpha, \beta)$, in which case system runs in the linear region. This implies that only case 1 of the theorem occurs and $e_{ss} = 0$. This proves the theorem for case $(b)$. □

**Proof of Theorem III.2**: The proof is similar to the proof of Theorem 3.3 in [1]. Note that with the ramp input $r(t) = r_1 t\mathbf{1}(t)$, Figure A.1.1 can be equivalently represented by Figure A.1.2, in which the input is now a step of size $r_1$. Define $\hat{P}(s) = sP(s)$ and $\hat{C}(s) = \frac{1}{s}C(s)$ and note that $\hat{P}_0 = P_1$ and $\hat{C}_0 = \infty$. Applying Theorem III.1 yields the result. □

**Proof of Theorem III.3**:

1. We know that as $\sigma_r \to 0$,

$$\sigma_{\hat{u}} = \|\frac{F_{\Omega_r(s)}C(s)}{1 + N_aP(s)C(s)}\|_2\sigma_r \to 0.$$

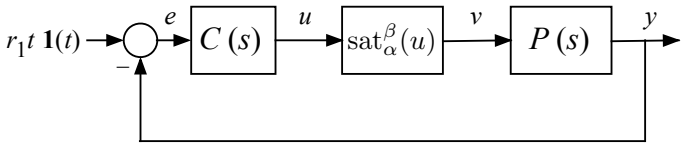


A.1.1: System with ramp input.

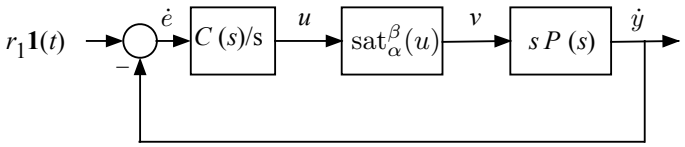


A.1.2: Equivalent system.

Figure A.1: System with ramp input and its equivalent system.

Now, conisder three cases: (i) $\alpha < \mu_{\hat{u}} < \beta$, (ii) $\mu_{\hat{u}} \geq \beta$, (iii) $\mu_{\hat{u}} \leq \alpha$.

Case (i): when $\alpha < \mu_{\hat{u}} < \beta$, we have that $\frac{\beta - \mu_{\hat{u}}}{\sqrt{2}\sigma_{\hat{u}}} \to \infty$, and $\frac{\alpha - \mu_{\hat{u}}}{\sqrt{2}\sigma_{\hat{u}}} \to -\infty$. Therefore, the quasilinear gain equation implies that $N \to 1$ as $\sigma_r \to 0$, and

$$SRS \to \| \frac{F_{\Omega_r(s)}}{1 + P(s)C(s)} \|_2.$$

The second equation of stochastic linearization implies that $\mu_{\hat{u}} = \frac{C_0}{1+C_0P_0}\mu_r$. This, together with the fact that $\alpha < \mu_{\hat{u}} < \beta$, implies that $\mu_r \in TD$.

Case (ii) when $\mu_{\hat{u}} \geq \beta$, we have that $\frac{\beta - \mu_{\hat{u}}}{\sqrt{2}\sigma_{\hat{u}}} \to -\infty$, and $\frac{\alpha - \mu_{\hat{u}}}{\sqrt{2}\sigma_{\hat{u}}} \to -\infty$. Therefore, the first equation of stochastic linearization implies that $N \to 0$ as $\sigma_r \to 0$, and

$$SRS \to 1.$$

The second equation of stochastic linearization implies that $M = \beta$. This implies that $\mu_r \notin TD$.

Case (iii): the proof here is similar to case (ii). The result is that $SRS \to 1$ and $\mu_r \notin TD$. This completes the proof of (1).

2. We show that as $\Omega_r \to \infty$,

$$\|\frac{F_{\Omega_r(s)}}{1+N_aP(s)C(s)}\|_2^2 \to 1.$$

To prove the above use the fact that $\|F_{\Omega_r(s)}\|_2 = 1$, assume $w_0 > 0$, and write

$$\Big|1 - \|\frac{F_{\Omega_r(s)}}{1+N_aP(s)C(s)}\|_2^2\Big| = \Big|1 - \frac{1}{\pi}\int_0^\infty |F_{\Omega_r}(jw)\frac{1}{1+N_aP(jw)C(jw)}|^2 dw\Big|$$

$$= \Big|\frac{1}{\pi}\int_0^\infty |F_{\Omega_r}(jw)|^2(1-|\frac{1}{1+N_aP(jw)C(jw)}|^2)dw\Big|$$

$$\leq \frac{1}{\pi}\int_0^\infty |F_{\Omega_r}(jw)|^2\Big|1-\frac{1}{|1+N_aP(jw)C(jw)|}\Big|^2 dw\Big|$$

$$= \frac{1}{\pi}\int_0^{w_0} |F_{\Omega_r}(jw)|^2\Big|1-\frac{1}{|1+N_aP(jw)C(jw)|}\Big|^2 dw + \frac{1}{\pi}\int_{w_0}^\infty |F_{\Omega_r}(jw)|^2\Big|1-\frac{1}{|1+N_aP(jw)C(jw)|}\Big|^2 dw$$

Let $\epsilon > 0$. We now bound each of the above integrals by $\epsilon/2$ so that the above expression is less than $\epsilon$. To bound the first integral, note that since $F_{\Omega_r}(s)$ is the third order Butterworth filter, $|F_{\Omega_r}(jw)|^2 < \frac{3}{\Omega_r}$. Therefore,

$$\frac{1}{\pi}\int_0^{w_0} |F_{\Omega_r}(jw)|^2\Big|1-\frac{1}{|1+N_aP(jw)C(jw)|}\Big|^2 dw \leq \frac{3}{\pi\Omega_r}\int_0^{w_0}\Big|1-\frac{1}{|1+N_aP(jw)C(jw)|}\Big|^2 dw$$

Since the above integral is bounded, for large enough $\Omega_r$, the first integral can be made less than $\epsilon/2$. To bound the second integral, note that regardless of $N_a$, the magnitude of the sensitivity function $\frac{1}{1+N_aP(jw)C(jw)}$ converges to 1 as $w \to \infty$; therefore, for the given $\epsilon$, $w_0$ can be chosen such that $w > w_0$ implies $|1 - \frac{1}{|1+N_aP(jw)C(jw)|}|^2 < \epsilon/2$. Therefore, the second integral can be made less than $\epsilon/2$.

3. Let $\epsilon > 0$. We show that for small enough $\Omega_r$,

$$\Big| |\frac{1}{1+N_0P_0C_0}|^2 - \|\frac{F_{\Omega_r}}{1+N_aPC}\|_2^2 \Big| < \epsilon,$$

where $N_0$ is the solution of

$$\begin{aligned} N_0 - \mathcal{F}_N(\Big\|\frac{F_{\Omega_{r0}}C_0}{1+N_0P_0C_0}\Big\|_2\sigma_r, \mu_{\hat{u}}) = 0, \\ \frac{\mu_r}{P_0} - \frac{\mu_{\hat{u}}}{P_0C_0} - \mathcal{F}_M(\Big\|\frac{F_{\Omega_{r0}}C_0}{1+N_0P_0C_0}\Big\|_2\sigma_r, \mu_{\hat{u}}) = 0, \end{aligned}$$

and $N_a$ is the solution of

$$\begin{aligned} N_a - \mathcal{F}_N(\Big\|\frac{F_{\Omega_r}C}{1+N_aPC}\Big\|_2\sigma_r, \mu_{\hat{u}}) = 0, \\ \frac{\mu_r}{P_0} - \frac{\mu_{\hat{u}}}{P_0C_0} - \mathcal{F}_M(\Big\|\frac{F_{\Omega_r}C}{1+N_aPC}\Big\|_2\sigma_r, \mu_{\hat{u}}) = 0. \end{aligned}$$

Similar to part (2) of the theorem, we write

$$\Big| |\frac{1}{1+N_0P_0C_0}|^2 - \|\frac{F_{\Omega_r}}{1+N_aPC}\|_2^2 \Big|$$

$$\leq \frac{1}{\pi}\int_0^{w_0} |F_{\Omega_r}|^2 \Big| |\frac{1}{1+N_0C_0P_0}|^2 - |\frac{1}{1+N_aCP}|^2 \Big| dw + \frac{1}{\pi}\int_{w_0}^{\infty} |F_{\Omega_r}|^2 \Big| |\frac{1}{1+N_0C_0P_0}|^2 - |\frac{1}{1+N_aCP}|^2 \Big| dw.$$

We now show that both integrals can be made smaller than $\epsilon/2$. To bound the first integral, note that since the equations of quasilinear gain and bias are analytic, $N_a$ can be made arbitrarily close to $N_0$ for small enough $w$. Furthermore, the magnitude of the sensitivity function can be made arbitrarily close to the dc gain of the sensitivity function for small enough $w$. Therefore, $w_0$ can be chosen such that $\forall w < w_0$, $||\frac{1}{1+N_0C_0P_0}|^2 - |\frac{1}{1+N_aCP}|^2| < \epsilon/2$. Therefore, the first integral can be made smaller than $\epsilon/2$.

To bound the second integral, note that $|F_{\Omega_r}(jw)|^2 < \frac{3}{\Omega_r}$. So, for large enough

$\Omega_r$, the second integral can be made less than $\epsilon/2$. This proves this part of the theorem.

4. We conisder the three cases in the theorem separately:

   - For the case $|C_0| = \infty$ and $|P_0| \neq \infty$, we prove that SRS is undefined. Since $|C_0| = \infty$, the expected value of the error signal must be zero, which implies that $M_a = \frac{\mu_r}{P_0}$, where $M_a$ is the expected value of the output of saturation. Now, $M_a$ must be bounded above and below by $\alpha < M_a < \beta$. Therefore, $\alpha < \frac{\mu_r}{P_0} < \beta$, which implies that $\mu_r$ must be bounded. Therefore, if $\mu_r \to \pm\infty$, system cannot be stochastically linearized. Therefore, SRS cannot be defined for this case.

   - For the case $P_0 \neq \infty$ and $C_0 \neq \infty$, we first note that $M_a = \frac{\mu_r}{P_0} - \frac{\mu_{\hat{u}}}{C_0 P_0}$ must be bounded between $\alpha$ and $\beta$. Therefore, $\mu_{\hat{u}} \to \pm\infty$ as $\mu_r \to \pm\infty$. Also, note that $\sigma_{\hat{u}}$ is always finite; therefore,

   $$N = \frac{1}{2}\left[\text{erf}\left(\frac{\beta - \mu_{\hat{u}}}{\sqrt{2}\sigma_{\hat{u}}}\right) - \text{erf}\left(\frac{\alpha - \mu_{\hat{u}}}{\sqrt{2}\sigma_{\hat{u}}}\right)\right] \to 0,$$

   which implies that $SRS \to 1$.

   - If $P_0 = \infty$, as shown in Section 1.2, $\mu_r$ does not affect the error dynamics. Therefore, $SRS$ remains the same as the SRS of system with $P_0 = \infty$, i.e.,

   $$SRS = \left\| \frac{F_{\Omega_r}(s)}{1 + N_a P(s)C(s)} \right\|_2,$$

   where $N_a$ is the solution of

   $$\begin{aligned} N_a - \mathcal{F}_N(\left\| \frac{F_{\Omega_r}(s)C(s)}{1 + N_a P(s)C(s)} \right\|_2 \sigma_r, \mu_{\hat{u}}) = 0, \\ \mathcal{F}_M(\left\| \frac{F_{\Omega_r}(s)C(s)}{1 + N_a P(s)C(s)} \right\|_2 \sigma_r, \mu_{\hat{u}}) = 0. \end{aligned}$$

This completes the proof. □

**Proof of Proposition III.1:** When $P_0 < \infty$, $\mu_{\hat{e}}$ satisfies

$$\mu_{\hat{e}} = \mu_r - P_0 M_a.$$

The result follows from the fact that $\alpha < M_a < \beta$ and $I_{1,mean} = \frac{|\mu_{\hat{e}}|}{\sigma_r}$. □

## A.3 Proofs for Chapter IV

**Proof of Lemma IV.1**: By Theorem II.3, the quasilinear equations (4.3) and (4.4) are guaranteed to have a solution for all $K > 0$, and this solution is unique by the assumption. Furthermore, these equations are both analytic functions. Therefore, $K_e(K)$ and $\mu_{\hat{u}}(K)$ are roots of analytic functions that depend on the parameter $K$. We know that roots of analytic functions form continuous functions of the parameters. Hence, $K_e(K)$ and $\mu_{\hat{u}}(K)$ are continuous. □

**Proof of Lemma IV.2**:

Part (1) of the lemma follows from (4.7) since $\phi^*$ is equal to an $H_2$ norm. To prove part (2), we set $\phi^* = 0$ in equation (4.8) and solve for $\eta^*$: $\eta^* = \sqrt{2}\text{erf}^{-1}(\frac{\frac{\mu_r}{P_0} - \frac{\alpha+\beta}{2}}{\frac{\beta-\alpha}{2}})$. Part (3) can be shown by substituting the given point in (4.7) and (4.8). □

**Proof of Theorem IV.1**:

Denote by $K_e^*$ and $\mu_{\hat{u}}^*$ the limiting $K_e$ and $\mu_{\hat{u}}$, i.e.,

$$K_e^* = \lim_{K\to\infty} K_e(K), \mu_{\hat{u}}^* = \lim_{K\to\infty} \mu_{\hat{u}}(K).$$

Define

$$\phi(K) = \left\| \frac{F_\Omega(s)C(s)}{1 + K_e(K)P(s)C(s)} \right\|_2 \sigma_r,$$

and let $\phi^* = \lim_{K\to\infty} \phi(K)$.

Then, applying Taylor series expansions, we obtain

$$K_e(K) = \frac{K}{2}\left[\operatorname{erf}\left(\frac{\beta - \mu_{\hat{u}}(K)}{\sqrt{2}K\phi(K)}\right) - \operatorname{erf}\left(\frac{\alpha - \mu_{\hat{u}}(K)}{\sqrt{2}K\phi(K)}\right)\right]$$

$$= \frac{1}{\sqrt{\pi}}\left[\left(\frac{\beta - \mu_{\hat{u}}(K)}{\sqrt{2}\phi(K)}\right) - \frac{K}{3}\left(\frac{\beta - \mu_{\hat{u}}(K)}{\sqrt{2}K\phi(K)}\right)^3 + \cdots - \left(\left(\frac{\alpha - \mu_{\hat{u}}(K)}{\sqrt{2}\phi(K)}\right) - \frac{K}{3}\left(\frac{\alpha - \mu_{\hat{u}}(K)}{\sqrt{2}K\phi(K)}\right)^3 + \cdots\right)\right]. \tag{A.3}$$

We now consider four cases: (i) $K_e^* < \infty$, $\mu_{\hat{u}} < \infty$, (ii) $K_e^* = \infty$, $\mu_{\hat{u}} < \infty$, (iii) $K_e^* < \infty$, $\mu_{\hat{u}} = \infty$, (iv) $K_e^* = \infty$, $\mu_{\hat{u}} = \infty$.

Case (i) $K_e^* < \infty$, $\mu_{\hat{u}} < \infty$: We take limit of both sides of (A.3) and obtain:

$$K_e^* = \frac{1}{\sqrt{\pi}}\left(\frac{\beta - \alpha}{\sqrt{2}\phi^*}\right),$$

and

$$\phi^* = \left\| \frac{F_\Omega(s)C(s)}{1 + \frac{1}{\sqrt{\pi}}\left(\frac{\beta-\alpha}{\sqrt{2}\phi^*}\right)P(s)C(s)} \right\|_2 \sigma_r.$$

Now, the second equation of quasilinear bias implies that $\frac{\mu_r}{P_0} = \frac{\alpha+\beta}{2}$. So, case (i) arises only when the system is symmetric at $K = \infty$.

Case (ii) $K_e^* = \infty$, $\mu_{\hat{u}} < \infty$: This case can be solved similar to case (i). In this case, $\phi^* = 0$.

Case (iii) $K_e^* < \infty$, $\mu_{\hat{u}} = \infty$:

$$K_e^* = \lim_{K\to\infty} \frac{1}{\sqrt{\pi}} \frac{\beta - \alpha}{\sqrt{2}\phi^*}\left(1 - \frac{1}{3}\frac{3\mu_{\hat{u}}^2}{(\sqrt{2}K\phi^*)^2} + \frac{1}{10}\frac{5\mu_{\hat{u}}^4}{(\sqrt{2}K\phi^*)^4} - \cdots\right).$$

Define $\eta^* = \lim_{K\to\infty} \frac{\mu_{\hat{u}}(K)}{K\phi(K)}$. Then,

$$K_e^* = \frac{1}{\sqrt{\pi}} \frac{\beta-\alpha}{\sqrt{2}\phi^*} \sum_{n=0}^{\infty} \frac{1}{n!} (-(\frac{\eta^*}{\sqrt{2}})^2)^n = \frac{\beta-\alpha}{\sqrt{2\pi}\phi^*} e^{-\eta^{*2}/2}.$$

We now expand the quasilinear bias equation in Taylor series term by term:

- $\frac{\mu_{\hat{u}}(K)}{2}(\text{erf}(\frac{\beta-\mu_{\hat{u}}}{\sqrt{2}K\phi}) - \text{erf}(\frac{\alpha-\mu_{\hat{u}}}{\sqrt{2}K\phi})) \to \frac{\beta-\alpha}{\sqrt{2\pi}}\eta^* e^{-\eta^{*2}/2}$.
- $-\frac{\beta}{2}\text{erf}(\frac{\beta-\mu_{\hat{u}}}{\sqrt{2}K\phi}) + \frac{\alpha}{2}\text{erf}(\frac{\alpha-\mu_{\hat{u}}}{\sqrt{2}K\phi}) \to \frac{\beta-\alpha}{2}\text{erf}(\eta^*/\sqrt{2})$.
- $\frac{K\phi}{\sqrt{2\pi}}[e^{-(\frac{\beta-\mu_{\hat{u}}}{\sqrt{2}K\phi})^2} - e^{-(\frac{\alpha-\mu_{\hat{u}}}{\sqrt{2}K\phi})^2}] \to \frac{\beta-\alpha}{\sqrt{2\pi}}\eta^* e^{-\eta^{*2}/2}$.

Therefore, in the limit, the second equation becomes

$$\frac{\mu_r}{P_0} - \frac{\phi^*\eta^*}{C_0 P_0} = \frac{\alpha+\beta}{2} + \frac{\beta-\alpha}{2}\text{erf}(\eta^*/2),$$

by noting that $\lim_{K\to\infty} \mu_{\hat{u}}(K)/K = \eta^*\phi^*$. Therefore, the two equations in two unknowns that lead to this case are (4.7) and (4.8). Moreover, $K_e^*$ for this case is the same as before:

$$K_e^* = \frac{\beta-\alpha}{\sqrt{2\pi}\phi^*} e^{-(\frac{\eta^{*2}}{2})}.$$

Note that cases (i) and (ii) can be covered by these equations as well.

Case (iv) $K_e^* = \infty$, $\mu_{\hat{u}} = \infty$: Since $K_e^* = \infty$, the equation for $K_e^*$ implies that $\phi^* = 0$ and the limiting quasilinear bias equation implies that $\eta^*$ is a finite number: $\eta^* = \sqrt{2}\text{erf}^{-1}(\frac{\frac{\mu_r}{P_0} - \frac{\alpha+\beta}{2}}{\frac{\beta-\alpha}{2}})$. Therefore, equations (4.7), (4.8) cover this case also. □

**Proof of Theorem IV.2** (by contradiction): suppose there exists a $K$ such that $K_e(K) = \Gamma$. Then,

$$\Gamma = \frac{K}{2}(\text{erf}(\frac{\beta-\mu_{\hat{u}}}{\sqrt{2}K\phi}) - \text{erf}(\frac{\alpha-\mu_{\hat{u}}}{\sqrt{2}K\phi})).$$

Since the closed loop transfer function becomes unstable at $K_e = \Gamma$, we have that

$\phi(K) = \infty$. Therefore,

$$\Gamma = 0,$$

which is a contradiction. □

**Proof of Theorem IV.3**

Denote by $K_e^*$ and $\mu_{\hat{u}}^*$ the limiting $K_e$ and $\mu_{\hat{u}}$, i.e.,

$$K_e^* = \lim_{K\to\infty} K_e(K), \mu_{\hat{u}}^* = \lim_{K\to\infty} \mu_{\hat{u}}(K).$$

We prove each case below:

(Part a:) First note that if $C_0 = \infty$, then $\mu_{\hat{e}} = 0$ for all $K$. Therefore, $\mu_{\hat{e}}(0) = 0$. This proves parts (a) for this case. Therefore, assume that $C_0 \neq \infty$. Then, as $K \to 0$, $\sigma_{\hat{u}} \to 0$ and $\mu_{\hat{u}} \to 0$. Hence, $N \to 1$ and $m \to 0$. Moreover, using (4.3), (4.4), it can be shown, similar to the proof of Theorem IV.1, that as $K \to 0$, $\frac{m}{K} \to 0$. Now, consider two cases: $P_0 \neq \infty$ and $P_0 = \infty$. If $P_0 \neq \infty$, since $N \to 1$ and $m \to 0$, $\mu_{\hat{e}}$ satisfies:

$$\mu_{\hat{e}} = \frac{\mu_r + P_0 m}{1 + KNP_0C_0} \to \mu_r.$$

If $P_0 = \infty$,

$$\mu_{\hat{e}} \to \frac{m}{KNC_0} \to 0.$$

This proves part (a).

(Part b:) This part follows from the definition of $\eta^*$ in Theorem IV.1.

(Part c:) This part follows from the definition of symmetry, i.e., (1.4). □

**Proof of Theorem IV.4**:

(part a:) This part follows from definition of TE locus.

(part b:)

($\Leftarrow$): First note that, according to the (a), $C_0 = \infty$ implies that $\mu^*_{\hat{e}} = 0$. Now, assume that $K^*_e = \infty$. Then, by definition of $K^*_e$, we have that

$$\infty = \frac{\beta - \alpha}{\sqrt{2\pi}\phi^*} e^{-(\frac{\eta^{*2}}{2})}.$$

Note that the exponential is always bounded above by 1, so $\phi^*$ must tend to 0. Then, since $\eta^*$ is bounded,

$$\lim_{K\to\infty} \mu_{\hat{e}}(K) = \lim_{K\to\infty} \frac{1}{KC_0}\mu_{\hat{u}}(K) = \frac{\phi^*\eta^*}{C_0} = 0.$$

Now, assume that system is symmetric at $K = \infty$, i.e., $\mu_r = P_0\frac{\alpha+\beta}{2}$. When the system becomes symmetric, the average value of the signals must be equal to those of the underlying linear system, i.e., $\mu^*_{\hat{e}} = 0$. Now, when $\mu_r = P_0\frac{\alpha+\beta}{2}$, (4.8) implies that $\eta^* = 0$, from which (4.7) implies that $\phi^*$ is the same as that for the symmetric LPNI system. Uniqueness implies that this is the only possible solution.

($\Rightarrow$): Assume that $\mu^*_{\hat{e}} = 0$. Note that we may write

$$\mu^*_{\hat{e}} = \lim_{K\to\infty} \frac{\mu_{\hat{u}}(K)}{KC_0}.$$

Therefore, $\mu^*_{\hat{e}} = 0$ implies that either $C_0 = \infty$ or $\lim_{K\to\infty} \frac{\mu_{\hat{u}}(K)}{K} = 0$.

Now, using the definition of $\phi^*$ and $\eta^*$, we can write $\lim_{K\to\infty} \frac{\mu_{\hat{u}}(K)}{K} = \phi^*\eta^*$. Therefore, $\lim_{K\to\infty} \frac{\mu_{\hat{u}}(K)}{K} = 0$ implies that either $\phi^* = 0$ or $\eta^* = 0$ (note that both cannot be zero). If $\phi^* = 0$, then $K^*_e = \infty$. If $\eta^* = 0$, then by (4.7), $\frac{\mu_r}{P_0} = \frac{\alpha+\beta}{2}$ meaning system is symmetric. This proves (b). $\square$.

(part c:) This follows from the fact that $\alpha < M < \beta$, and that $\mu_{\hat{e}} = \mu_r - P_0 M$.

(part d, e:) These follow directly from definitions of $\mu_{\hat{e}}(0)$ and $\mu_{\hat{e}}(\infty)$. $\square$.

**Proof of Proposition IV.5**:

(part a): If $C_0 \neq \infty$, then $\mu_{\hat{u}} = KC_0\mu_{\hat{e}}$, which tends to zero as $K$ tends to zero. This proves part a for the case of $C_0 \neq \infty$. Now assume $C_0 = \infty$. In this case, stationarity of the signals implies that $\mu_{\hat{v}} = \frac{\mu_r}{P_0}$. If $\frac{\mu_r}{P_0} \in [\alpha, \beta]$, then $\mu_{\hat{u}} = \frac{\mu_r}{P_0}$, which belongs to the linear range of saturation. Hence, saturation is not activated and the signal at the input of the saturation has standard deviation tending to zero. This implies that $A$ tends to 0. If $\frac{\mu_r}{P_0} \notin [\alpha, \beta]$, however, saturation is completely activated on one side; hence, $A$ tends to 1.

(part b): If $\frac{\mu_r}{P_0} = \frac{\alpha+\beta}{2}$, system becomes symmetric as $K$ tends to infinity, which implies that $\mu_{\hat{u}}$ is finite. By Theorem II.6, $A$ must tend to 0. If, however, system does not becomes symmetric, note that $\mu_{\hat{u}}$ and $\sigma_{\hat{u}}$ both tend to infinity as $K$ tends to infinity. Hence, $\frac{\beta-\mu_{\hat{u}}}{\sqrt{2}\sigma_{\hat{u}}} \to \frac{-\mu_{\hat{u}}}{\sqrt{2}\sigma_{\hat{u}}}$. Similarly, $\frac{\alpha-\mu_{\hat{u}}}{\sqrt{2}\sigma_{\hat{u}}} \to \frac{-\mu_{\hat{u}}}{\sqrt{2}\sigma_{\hat{u}}}$. Therefore, $A \to \lim_{K\to\infty} \operatorname{erf}(\frac{\mu_{\hat{u}}}{\sqrt{2}\sigma_{\hat{u}}})$. The result follows from definition of $\eta^*$.

## A.4 Proofs for Chapter V

**Proof of Proposition V.1:**

The derivation of (5.7) is based on the notion of step trackable domain ($TD^{step}$) introduced in Chapter III. Using the expressions for the trackable domain and steady state error, specs (5.6) can be represented in terms of $P_0$ and $C_0$ as follows:

$$r_0^* \leq (\frac{1}{C_0} + P_0)\beta, \tag{A.4}$$

$$e_{ss}^* \geq \frac{1}{1 + C_0P_0}. \tag{A.5}$$

For convenience, we re-writte (A.5) as

$$\frac{1}{C_0} \leq \frac{P_0}{\frac{1}{e_{ss}^*} - 1}. \tag{A.6}$$

We now prove the proposition.

*Necessity:* Assume (5.7) is satisfied. Then, if the plant has a pole at the origin, (A.4) and (A.5) are satisfied. If $P_0$ is finite, we show, by construction, that there exists a controller that satisfies (A.4) and (A.5). Let $C(s)$ be such that $C_0 = \frac{1-e_{ss}^*}{P_0 e_{ss}^*}$. With this $C_0$

$$\frac{1}{1+C_0P_0} = e_{ss}^*,$$

implying that (A.5) is satisfied. Using this $C_0$, it also follows that

$$(\frac{1}{C_0} + P_0)\beta = \frac{P_0\beta}{1-e_{ss}^*},$$

which, together with (5.7), implies that (A.4) holds.

*Sufficiency:* Assume that there exists a controller that satisfies (A.4) and (A.5). Then, substituting (A.6) into (A.4), we obtain (5.7). □

## A.5 Proofs for Chapter VII

**Proof of Theorem VII.1**: We use the method of Lagrange multipliers to solve the problem. Form the Lagrangian:

$$\begin{aligned}
\Phi(\mu_{\hat{u}}, \sigma_{\hat{u}}, K, &R, N, Q, \lambda_1, \lambda_2, \lambda_3) = \\
&CRC^T + \left[\frac{C(A+B_2NK)^{-1}B_2}{K(A+B_2NK)^{-1}B_2}\right]^2 \mu_{\hat{u}}^2 + \rho(KRK^T + \mu_{\hat{u}}^2) \\
&+ \mathrm{tr}\{[(A+B_2NK)R + R(A+B_2NK)^T + B_1B_1^T]Q\} \\
&+ \lambda_1(N - \mathcal{F}_N(\sigma_{\hat{u}}, \mu_{\hat{u}})) \\
&+ \lambda_2((\frac{-1}{K(A+B_2NK)^{-1}B_2} + N)\mu_{\hat{u}} - \mu_d - \mathcal{F}_M(\sigma_{\hat{u}}, \mu_{\hat{u}})) \\
&+ \lambda_3(\sigma_{\hat{u}} - \sqrt{KRK^T}).
\end{aligned} \tag{A.7}$$

In the subsequent discussion we use the fact that $K(A+B_2NK)^{-1}B_2 = \frac{KNA^{-1}B_2}{1+NKA^{-1}B_2}$.

Differentiating $\Phi$ with respect to $\sigma_{\hat{u}}, \mu_{\hat{u}}, R, K, N$ and setting the results equal to zero yields:

$$\frac{\lambda_1}{\sigma_u}\left[\exp(-(\frac{\beta-\mu_u}{\sqrt{2}\sigma_u})^2)(\frac{\beta-\mu_u}{\sqrt{2}\sigma_u}) - \exp(-(\frac{\alpha-\mu_u}{\sqrt{2}\sigma_u})^2)(\frac{\alpha-\mu_u}{\sqrt{2}\sigma_u})\right] + \lambda_2\left[\exp(-(\frac{\beta-\mu_u}{\sqrt{2}\sigma_u})^2) - \exp(-(\frac{\alpha-\mu_u}{\sqrt{2}\sigma_u})^2)\right] = 0, \tag{A.8}$$

$$\frac{\lambda_1}{\sqrt{2\pi}\sigma_u}\left[\exp(-(\frac{\beta-\mu_u}{\sqrt{2}\sigma_u})^2) - \exp(-(\frac{\alpha-\mu_u}{\sqrt{2}\sigma_u})^2)\right] + \lambda_2(N + \frac{1}{KA^{-1}B_2}) + 2\mu_{\hat{u}}\Big[(\frac{C(A+B_2NK)^{-1}B_2}{K(A+B_2NK)^{-1}B_2})^2 + \rho\Big] = 0, \tag{A.9}$$

$$(A+B_2NK)^TQ + Q(A+B_2NK) + CC^T + \rho K^TK - \frac{\lambda_3}{2\sigma_u^3}K^TK = 0, \tag{A.10}$$

$$NB_2^TQR + \lambda_2(\frac{\mu_{\hat{u}}}{(KA^{-1}B_2)^2}B_2^TA^{-T}) - \frac{\lambda_3}{2\sigma_u^3}KR + (CA^{-1}B_2)^2\frac{-2}{(KA^{-1}B_2)^3}B_2^TA^{-T} = 0, \tag{A.11}$$

$$KRQB_2 + \lambda_1 = 0. \tag{A.12}$$

Note that (7.12) follows immediately from (A.12). Right-multiplying (A.11) by $K^T$ and rearranging terms yields (7.14). Moreover, rearranging (A.8) yields (7.13). The rest of the equations in the theorem are the same as above. □

**Proof of Proposition VII.1**: It is a well known fact, from linear system theory, that in order to achieve arbitrarily small output variance, the gain of the controller must be large, which implies that the signal at the plant input must be large. However, as suggested by part 3 of Proposition II.1, the input to the plant in the quasi-linear system is always bounded and, hence, arbitrary disturbance rejection cannot be achieved. □

# APPENDIX B

# QLC Toolbox

## B.1 Introduction

QLC Toolbox consists of MATLAB functions that implement the methods for analysis and design of feedback systems with nonlinear actuators and sensors. A copy of the QLC toolbox can be downloaded free of charge from

```
http://www.quasilinearcontrol.com/toolbox_download.php
```

In this appendix, we present the MATLAB functions currently included in the QLC toolbox. Specifically, we explain each function's usage followed by an examples. All terms and notations used here, as well as the methods themselves, can be found in this dissertation and in [1].

## B.2 QLC Functions

### B.2.1 stochlinearize

This function performs stochastic linearization of a closed loop S-LPNI system. The return values Na and Ns are the equivalent gains of the actuator and sensor nonlinearities, respectively.

**Syntax**

```
[Na, Ns] = stochlinearize(plant, controller, actuator, sensor,
    actuator_parameters, sensor_parameters, coloring_filter, sigma_w,
    control_problem, Tol, plot_or_no_plot)
```

**Inputs**

- plant: The plant model specified either as transfer function or state space or gain.
- controller: The controller model specified either as transfer function or state space or gain.
- actuator: The actuator nonlinearity. Takes one of following values: 'sat', 'dz', 'qz', 'satdz', 'linear'.
- actuator_parameters: A number corresponding to the actuator nonlinearity: (i) for 'sat', the saturation limit, (ii) for 'dz', the deadzone half-width, (iii) for 'qz', the quantization increment and (iv) for 'satdz', the saturation limit and and deadzone half-width (specified as a 2-element vector).
- sensor: The sensor nonlinearity. Takes one of following values: 'sat', 'dz', 'qz', 'satdz', 'linear'.
- sensor_parameters: A number corresponding to the sensor nonlinearity: (i) for 'sat', the saturation limit, (ii) for 'dz', the deadzone half-width, (iii) for 'qz', the quantization increment and (iv) for 'satdz', the saturation limit and and deadzone half-width (specified as a 2-element vector).
- coloring_filter: The coloring filter specified either as transfer function or state space or gain. The 2-norm of the filter must be equal to 1.

- sigma_w: The driving-noise intensity at the input of the coloring filter.
- control_problem: Takes one of two values: 'track' or 'distreject' for reference tracking or disturbance rejection, respectively.
- Tol: The error tolerance for the solver.
- plot_or_no_plot: If equal to 1, the function, besides finding the quasilinear gains, plots traces of the output of the LPNI system and that of the quasilinear system. If 0, no plotting takes place.

**Outputs**

- Na: The quasilinear gain for the actuator.
- Ns: The quasilinear gain for the sensor.

Note: if the quasilinear gain is not unique, the function returns an error message.

**Example**

In this example, we perform stochastic linearization of an S-LPNI system with a saturating actuator. The coloring filter is a third-order Butterworth filter with 3-dB bandwidth equal to 5.

```
s = tf('s');
omega = 5;
F = tf([sqrt(3/omega)*omega^3],[1 2*omega 2*omega^2 omega^3]);
[Na, Ns] = stochlinearize(1/(s+1), tf(10,1), 'sat', 'linear', 1, 1, F,
    1, 'track', 1e-6, 0);
```

### B.2.2 stochlinearizeMIMO

This function performs stochastic linearization of a closed loop MIMO S-LPNI system. The problem considered is that of disturbance rejection. The return values are the quasilinear gains of the system.

**Syntax**

```
[N, sigma]=stochlinearizeMIMO (At, B1t, B2t, C1t, C2t, actuator, sensor,
    actuator_param, sensor_param, sigma_w, Tol)
```

**Inputs**

- At, B1t, B2t, C1t, C2t: The matrices in the QLC disturbance rejection problem. 't' stands for tilde. These matrices must be in the format specified in Chapter 4 of [1].
- actuator, sensor: the actuator and sensor nonlinearities. They both must be in Matlab cell format. Each cell takes one of the values: 'sat', 'dz'.
- actuator_parameters, sensor_parameters: A vector whose elements correspond to actuator/sensor nonlinearities. The order must be the same as that specified in 'actuator' and 'sensor' fields.
- sigma_w: The driving-noise covariance matrix. Each row $i$ corresponds to noise $w_i$.
- Tol: The error tolerance for the solver.

**Outputs**

- N: A vector containing the stochastically linearized gains. The first part corresponds to actuators, and second part to sensors. The order is the same as that specified in 'actuator' and 'sensor' vectors.
- sigma: the standard deviation of the performance output.

**Example**

In this example, we perform stochastic linearization of a MIMO S-LPNI system with two saturating actuators and two saturating sensors. The system is that of Example 4.1 of [1].

```
At2 = [A zeros(4,4); zeros(4,4), M]; B1t2 = [B1;-L*D21];C1t2=[C1 zeros
    (2, 4)]; B2t2=[B2 zeros(4,2); zeros(4,2) -L];
C2t2=[zeros(2,4) K; C2 zeros(2,4)]
ac{1}='sat '; ac{2}='sat ';
sn{1}='sat '; sn{2}='sat ';
[N,s]=stochlinearizeMIMO(At2,B1t2,B2t2,C1t2,C2t2,ac,sn,[1 1],[1 1],eye
    (4), 1e-6)
```

### B.2.3 SRS

This function returns the saturating random sensitivity (SRS) function for an S-LPNI system with saturating actuator. The range of coloring filter cutoff frequencies must be provided by the user. A third order Butterworth filter structure is used for the coloring filter.

**Syntax**

```
[returnSRS, returnN] = SRS(plant, controller, actuator_parameter,
    sigma_w, coloring_filter_frequencies, Tol)
```

**Inputs**

- plant: The plant model specified either as transfer function or state space or gain.
- controller: The controller model specified either as transfer function or state space or gain.
- actuator_parameter: The saturation limit.

- sigma_w: The driving-noise intensity at the input of the coloring filter.
- coloring_filter_frequencies: The frequencies at which the random sensitivity function is evaluated and plotted.
- Tol: The error tolerance for the solver.

**Outputs**

- returnSRS: A vector containing the SRS.
- returnN: A vector containing the quasilinear gains N at each frequency.

**Example**

In this example, we plot the SRS for a logarithmically distributed range of frequencies.

```
s = tf('s');
w = logspace(-2,2,20);
[retSRS, retN] = SRS(1/(s+1), tf(10,1), 1, 1, w, 1e-6);
semilogx(w,retSRS);
```

### B.2.4 trackingind

This function computes the tracking quality indicators $I_0 - I_3$, as well as the peak of the saturating random sensitivity (SRS) function for the symmetric case.

**Syntax**

```
[I0, I1, I2, I3, peak] = trackingind(plant, controller, frequency,
    sigma_w, actuator_param, Tol)
```

**Inputs**

- plant: The plant model specified either as transfer function or state space or gain.
- controller: The controller model specified either as transfer function or state space or gain.
- frequency: The 3-dB bandwidth of the coloring filter. A third order Butterworth filter is used.
- sigma_w: The driving-noise intensity at the input of the coloring filter.
- actuator_param: the saturation limit.
- Tol: The error tolerance for the solver.

**Outputs**

- I0–I3: Indicators $I_0 - I_3$.
- peak: peak of the random sensitivity function.

**Example**

In this example, we calculate the tracking quality indicators for a system.

```
s = tf('s');
[I0, I1, I2, I3, peak] = trackingind(1/(s+1), 10, 5, 1, 1, 1e-6);
```

### B.2.5 admissibledomain

This function plots the admissible domain for specified values of the tracking quality indicators $I_2$ and $I_3$.

**Syntax**

```
admissibledomain(I2, I3, frequency)
```

**Inputs**

- I2: The value of the level curve for indicator $I_2$.
- I3: The value of the level curve for indicator $I_3$.
- frequency: The 3-dB bandwidth of the coloring filter. A third order Butterworth filter is used.

**Outputs**

None.

**Example**

In this example, we plot the admissible domain for selected values of $I_2$ and $I_3$.

```
admissibledomain(0.3, 0.3, 2);
```

### B.2.6 srlocus

This function plots the S-root locus for a given S-LPNI system with saturating actuator.

**Syntax**

```
[K_ter, K_tr] = srlocus(plant, controller, coloring_filter, sigma_w,
    actuator_param, Tol)
```

**Inputs**

- plant: The plant model specified either as transfer function or state space or gain.
- controller: The controller model specified either as transfer function or state space or gain.

- coloring_filter: The coloring filter model specified either as transfer function or state space or gain. The 2-norm of this filter must be equal to 1.
- sigma_w: The driving-noise intensity at the input of the coloring filter.
- actuator_param: The saturation limit.
- Tol: The error tolerance for the solver.

**Outputs**

- K_ter: the S-termination equivalent gain of the S-root locus.
- K_tr: the S-truncation gain of the S-root locus.

**Example**

In this example, we plot the S-root locus and calculate the termination and truncation gains. The coloring filter is a 3rd order Butterworth filter with 3-dB bandwidth equal to 5.

```
s = tf('s');
omega = 5;
F = tf([sqrt(3/omega)*omega^3],[1 2*omega 2*omega^2 omega^3]);
[K_ter, K_tr] = srlocus(1/(s+1), tf(10,1), F, 1, 1, 1e-6)
```

### B.2.7 boosting

This function calculates the boosting gains for a disturbance rejection S-LPNI system. The return values Ka and Ks are the a-boosting and s-boosting gains, respectively.

**Syntax**

```
[Ka, Ks] = boosting(plant, controller, actuator, sensor,
    actuator_parameters, sensor_parameters, coloring_filter, sigma_w,
    Tol)
```

**Inputs**

- plant: The plant model specified either as transfer function or state space or gain.
- controller: The controller model specified either as transfer function or state space or gain.
- actuator: The actuator nonlinearity. Takes one of following values: 'sat', 'dz', 'qz', 'satdz', 'linear'.
- actuator_parameters: A number corresponding to the actuator nonlinearity: (i) for 'sat', the saturation limit, (ii) for 'dz', the deadzone half-width, (iii) for 'qz', the quantization increment and (iv) for 'satdz', the saturation limit and and deadzone half-width (specified as a 2-element vector).
- sensor: The sensor nonlinearity. Takes one of following values: 'sat', 'dz', 'qz', 'satdz', 'linear'.
- sensor_parameters: A number corresponding to the sensor nonlinearity: (i) for 'sat', the saturation limit, (ii) for 'dz', the deadzone half-width, (iii) for 'qz', the quantization increment and (iv) for 'satdz', the saturation limit and and deadzone half-width (specified as a 2-element vector).
- coloring_filter: The coloring filter specified either as transfer function or state space or gain. The 2-norm of the filter must be equal to 1.
- sigma_w: The driving-noise intensity at the input of the coloring filter.

- Tol: The error tolerance for the solver.

**Outputs**

- Ka: The a-boosting gain for the actuator.
- Ks: The s-boosting gain for the sensor.

**Example**

In this example, we find the boosting gains for an S-LPNI system. The coloring filter is a third-order Butterworth filter with 3-dB bandwidth equal to 5.

```
s = tf('s');
omega = 5;
F = tf([sqrt(3/omega)*omega^3],[1 2*omega 2*omega^2 omega^3]);
[Ka, Ks] = boosting(1/(s+1), tf(10,1), 'sat', 'linear', 1, 1, F, 1, 1e
    -6);
```

### B.2.8 slqr

This function computes the gain vector $K$ that solves the SLQR problem.

**Syntax**

```
[K, sigz] = slqr(A, B1, B2, C1, nonlinearity_parameter, sigma_w, rho,
    Tol)
```

**Inputs**

- A, B1, B2, C1: The matrices in the SLQR Problem.
- Nonlinearity_parameter: Actuator saturation limit.
- sigma_w: The driving-noise covariance matrix at the input of the coloring filter.

- rho: The control penalty.
- Tol: The error tolerance for the solver.

**Outputs**

- K: The gain vector.
- sigz: Minimum standard deviation of the performance output achieved by K.

**Example**

In this example, we find the solution of the SLQR problem for the following system: $P(s) = \frac{1}{s+1}$, coloring filter the third-order butterworth filter with 3-dB bandwidth 1, and $\rho = 0.1$. The resulting matrices are assumed to be:

$$A = \begin{bmatrix} -1 & 0 & 0 & \sqrt{3} \\ 0 & -2 & -2 & -1 \\ 0 & 1 & 0 & 1 \\ 0 & 0 & 1 & 0 \end{bmatrix}, B_1 = \begin{bmatrix} 0 \\ 1 \\ 0 \\ 0 \end{bmatrix}, B_2 = \begin{bmatrix} 1 \\ 0 \\ 0 \\ 0 \end{bmatrix}, C_1 = \begin{bmatrix} 0.1 & 0 & 0 & 0 \\ 0 & 0 & 0 & 0 \end{bmatrix}.$$

```
[K,s]=slqr(A,B1,B2,C1,1,1,0.1,1e-6);
```

### B.2.9 slqg

This function computes the gain vectors $K$ and $L$ and the observer matrix $M$ that solve the SLQG problem.

**Syntax**

```
[K, L, M, sigz] = slqg(A, B1, B2, C1, C2, nonlinearity_parameter,
    sigma_w, rho, mu, Tol)
```

**Inputs**

- A, B1, B2, C1, C2: The matrices in the SLQG Problem.
- Nonlinearity_parameter: Actuator saturation limit.
- sigma_w: The driving-noise intensity at the input of the coloring filter.
- rho: The control penalty.
- mu: The number $\mu$ in the SLQG problem.
- Tol: The error tolerance for the solver.

**Outputs**

- K: The control gain vector.
- L: The observer gain vector.
- M: The observer system matrix.
- sigz: Minimum standard deviation of the performance output achieved by K, L, M.

**Example**

In this example, we find the solution of the SLQG problem for the following system:

$$A = \begin{bmatrix} -1 & -2 & -1 \\ 1 & 0 & 0 \\ 0 & 1 & 0 \end{bmatrix}, B_1 = \begin{bmatrix} 0 \\ 0 \\ 1 \end{bmatrix}, B_2 = \begin{bmatrix} 1 \\ 5 \\ 0 \end{bmatrix}, C_1 = \begin{bmatrix} 0 & 1 & 1 \end{bmatrix}, C_2 = \begin{bmatrix} 0 & 0 & 3 \end{bmatrix},$$

$$\rho = 0.0095, \mu = 1 \times 10^{-4}.$$

```
[K,L,M,sigz] = slqg(A,B1,B2,C1,C2,1,1,rho,mu,1e-6)
```

### B.2.10 ilqr

This function calculates the gain matrix $K$ and the saturation limit $\alpha$ that solve the ILQR problem.

**Syntax**

```
[K, alpha, sig] = ilqr(A, B1, B2, C1, sigma_w, Tol, rho, nu)
```

**Inputs**

- A, B1, B2, C1: The matrices in the ILQR Problem.
- sigma_w: The driving-noise intensity at the input of the coloring filter.
- rho: The control penalty.
- nu: The actuator penalty.
- Tol: The error tolerance for the solver.

**Outputs**

- K: The gain vector.
- alpha: The saturation limit.
- sigz: Minimum standard deviation of the performance output achieved by K and alpha.

**Example**

In this example, we find the solution of the ILQR problem for the following system:

$$A = \begin{bmatrix} 0 & 0 \\ 1 & 0 \end{bmatrix}, B_1 = B_2 = \begin{bmatrix} 1 \\ 0 \end{bmatrix}, C_1 = \begin{bmatrix} 0 & 1 \\ 0 & 0 \end{bmatrix}.$$

```
[K, alpha, sig] = ilqr(A, B1, B2, C1, 1, 1e-6, 0.1, 0.1)
```

### B.2.11 ilqg

This function computes the gain matrices $K$, $L$ and $M$ and actuator and sensor limits that solve the ILQG problem

**Syntax**

```
[K, L, M, alpha, beta, sig] = ilqg(A, B1, B2, C1 ,C2, mu, rho, nu1, nu2,
    Tol)
```

**Inputs**

- A, B1, B2, C1, C2: The matrices in the ILQG Problem.
- rho: The control penalty.
- mu: $\mu$ in the ILQG problem.
- nu1: The actuator penalty.
- nu2: The sensor penalty.
- Tol: The error tolerance for the solver.

**Outputs**

- K: The control gain vector.
- L: The observer gain vector.
- M: The observer system matrix.
- alpha: The saturation limit for the actuator.

- beta: The saturation limit for the sensor.
- sigz: Minimum standard deviation of the performance output achieved by the above.

**Example**

In this example, we find the solution of the ILQG problem for the following system:

$$A = \begin{bmatrix} -1 & -2 & -1 \\ 1 & 0 & 0 \\ 0 & 1 & 0 \end{bmatrix}, B_1 = \begin{bmatrix} 0 \\ 0 \\ 1 \end{bmatrix}, B_2 = \begin{bmatrix} 1 \\ 5 \\ 0 \end{bmatrix}, C_1 = \begin{bmatrix} 0 & 1 & 1 \end{bmatrix}, C_2 = \begin{bmatrix} 0 & 0 & 3 \end{bmatrix},$$

$$\rho = 0.0095, \mu = 1 \times 10^{-4}.$$

```
[K,L,M,alpha,beta,sig] = ilqg (A,B1,B2,C1,C2,mu,rho,1e-4,1e-6,1e-10)
```

### B.2.12 stepTracker

This function determines the pre-compensator and the adjoint bandwidth from given step-tracking specifications on settling time and overshoot, plots the S-root locus and the admissible domain for the a controller provided by the user, and plots the trajectories of the random tracking system and step tracking system for a controller gain provided by the user.

**Syntax**

```
[Kter, Ktr, Fd, adjointBW] = stepTracker (plant, controller, K, r_0,
    actuator_param, Tsettling, Overshoot)
```

**Inputs**

- plant: The plant model specified either as transfer function or state space or gain.

- controller: The controller model specified either as transfer function or state space or gain.
- K: The controller gain.
- r_0: The step size to be tracked.
- actuator_param: The saturation limit.
- Tsettling: The settling time specification.
- Overshoot: The overshoot specification in percents.

**Outputs**

- Kter: The termination equivalent gain of the S-root locus.
- Ktr: The truncation gain of the S-root locus.
- Fd: The pre-compensator filter.
- adjointBW: The adjoint bandwidth.

**Example**

In this example, we plot the S-root locus and trajectories for the following specifications: settling time $<$ 1s, overshoot $<$ 5%.

```
s = tf('s');
[Kter, Ktr, Fd, adjointbw] = stepTracker(10/(s^2+10*s), (s+20)/(s+100),
    200, 1, 4, 1, 5)
```

### B.2.13 graphicalStochLinearize

This function evaluates and plots the transcendental equation that arises during closed loop stochastic linearization of the tracking system with saturating actuator and linear sensor. The zero-crossings indicate the resulting quasilinear gains. Multiple crossings indicate non-unique solutions. This function is intended for the S-LPNI case.

**Syntax**

```
graphicalStochLinearize (plant, controller, coloring_filter,
    actuator_param, sigma_w, Tol, rangeN)
```

**Inputs**

- plant: The plant model specified either as transfer function or state space or gain.
- controller: The controller model specified either as transfer function or state space or gain.
- coloring_filter: The coloring filter specified either as transfer function or state space or gain.
- actuator_param: The saturation limit.
- sigma_w: The driving-noise intensity at the input of the coloring filter.
- Tol: The error tolerance for the solver.
- rangeN: the values for which the function is to be evaluated (i.e., the points on the abscissa).

**Outputs**

None.

**Example**

```
s = tf('s');
graphicalStochLinearize(1/(s+1), 20, 1/(s+10), 3, 1, 1e-6, [0:.01:1])
```

### B.2.14 stochlinearizeAsym

This function performs stochastic linearization of a closed loop A-LPNI system.

**Syntax**

```
[Na, Mu, Ns, My] = stochlinearize(plant, controller, actuator, sensor,
    actuator_parameters, sensor_parameters, coloring_filter, sigma_r,
    mu_r, control_problem, Tol)
```

**Inputs**

- plant: The plant model specified either as transfer function or state space or gain.
- controller: The controller model specified either as transfer function or state space or gain.
- actuator: The actuator nonlinearity. Currently, it can only take one of following values: 'sat', 'dz', 'linear'.
- actuator_parameters: Numbers corresponding to the actuator nonlinearity: (i) for 'sat', the lower saturation limit followed by the upper saturation limit, (ii) for 'dz', the lower deadzone limit followed by the upper deadzone limit.
- sensor: currently only linear sensor is implemented.
- sensor_parameters: N/A.

- coloring_filter: The coloring filter specified either as transfer function or state space or gain. The 2-norm of the filter must be equal to 1.
- sigma_r: The standard deviation of the reference.
- mu_r: The mean of the reference.
- control_problem: Takes one of two values: 'track' or 'distreject' for reference tracking or disturbance rejection, respectively.
- Tol: The error tolerance for the solver.

**Outputs**

- Na: The quasilinear gain for the actuator.
- Mu: The mean of the signal at the input of the actuator.
- Ns: The quasilinear gain for the sensor.
- My: The mean of the signal at the input of the sensor.

**Example**

In this example, we perform stochastic linearization of an A-LPNI system with a saturating actuator.

```
s=tf('s')
F = sqrt(3) / (s^3 + 2*s^2 + 2*s + 1);
[Na,Mu,Ns,My] = stochlinearizeAsym(1/(s+1), 5, 'sat', 'linear', [-1 2],
    1, F, 1, 0, 'track', 1e-6)
```

### B.2.15 srlocusAsym

This function plots the AS-root locus and TE locus for a given A-LPNI system with saturating actuator.

**Syntax**

```
[K_ter, M_e_ter, K_I0, M_e_I0, K_e, M_e] = srlocus(plant, controller,
    coloring_filter, sigma_r, mu_r,  alpha, beta, plottingGains, Tol)
```

**Inputs**

- plant: The plant model specified either as transfer function or state space or gain.
- controller: The controller model specified either as transfer function or state space or gain.
- coloring_filter: The coloring filter model specified either as transfer function or state space or gain. The 2-norm of this filter must be equal to 1.
- sigma_r: The standard deviation of the reference.
- mu_r: The mean of the reference.
- alpha: Lower saturation limit.
- beta: Upper saturation limit.
- PlottingGains: The gains at which TE locus is evaluated.
- Tol: The error tolerance for the solver.

**Outputs**

- K_ter: The AS-termination equivalent gain of the AS-root locus.

- M_e_ter: The termination point of the TE locus.
- K_I0: The truncation gain of the AS-root locus.
- M_e_I0: The TE locus evaluated at the truncation gain.
- K_e: The effective gain of the AS-root locus evaluated at the plottingGains.
- M_e: The TE locus evaluated at the plottingGains.

**Example**

In this example, we plot the AS-root locus and the TE locus of a simple system.

```
s = tf('s');
F = sqrt(3) / (s^3 + 2*s^2 + 2*s + 1);
admissibledomain(0.3,0.3,1);
[k1,m1,k2,m2,ke,me]=srlocusAsym(1/(s+5), 2/(s+10), F, 1, 0, -1, 4, [0.1
    0.5 1 5 10], 1e-6);
figure;
plot([0.1 0.5 1 5 10], me)
```

# BIBLIOGRAPHY

# BIBLIOGRAPHY


[1] S. Ching, Y. Eun, C. Gokcek, P. T. Kabamba, and S. M. Meerkov, *Quasilinear Control: Performance Analysis and Design of Feedback Systems with Nonlinear Sensors and Actuators*. Cambridge University Press, 2010.

[2] Y. Eun, "Noise-induced tracking in systems with measurement noise and anti-windup," in *Advances in Systems Theory: Control, Communication Networks, Production Systems and Rational Behavior* (J. Li and P. T. Kabamba, eds.), ch. 5, WingSpan Press, 2009. pp. 153-175.

[3] Y. Guo, *Control and optimization of variable-speed wind turbines and large-scale wind farms.* PhD Dissertation, University of Oklahoma, 2012.

[4] M. Schwager, A. Annaswamy, and E. Lavretsky, "Adaptation-based reconfiguration in the presence of actuator failures and saturation," *American Control Conference.*, 2005.

[5] Y. Fu, N. Kottenstette, Y. Chen, C. Lu, X. Koutsoukos, and H. Wang, "Feedback thermal control for real-time systems.," *16th IEEE Real-Time and Embedded Technology and Applications Symposium.*, 2010.

[6] J. B. Roberts and P. D. Spanos, *Random Vibration and Statistical Linearization*. Dover Publications, 2003.

[7] A. Lur'e, *Nonlinear problems in the theory of automatic control*. Gostechizdat, 1951. In Russian.

[8] V. M. Popov, "On the absolute stability of nonlinear control systems," *Automation and Remote Control*, vol. 22, pp. 961–979, 1961.

[9] R. Kalman, "Lyapunov functions for the problem of lur'e in automatic control," *Proceedings of the National Academy of Sciences*, vol. 49, pp. 201–205, 1963.

[10] V. Yakubovich, "Matrix inequalities method in stability theory for nonlinear control systems: I. absolute stability of forced vibrations," *Automation and Remote Control*, vol. 7, pp. 905–917, 1964.

[11] M. Aizermann and F. Gantmacher, *Absolute stability of regulator systems*. Holden-Day, 1964.

[12] S. Lefschetz, *Stability of nonlinear control systems*. New York: Academic, 1965.

[13] H. K. Khalil, *Nonlinear Systems*. Prentice Hall, third ed., 2002.

[14] C. Pittet, S. Tarbouriech, and C. Burgat, "Stability regions for linear systems with saturating controls via circle and Popov criteria," *Proceedings of the 36th IEEE Conference on Decision and Control*, pp. 4518–4523, 1997.

[15] A. Teel, "Semi-global stabilizability of linear null controllable systems with input nonlinearities," *Automatic Control, IEEE Transactions on*, vol. 40, pp. 96–100, 1995.

[16] A. Teel, "Semi-global stabilization of linear controllable systems with input nonlinearities," *IEEE Trans. Automat. Contr.*, vol. 40, pp. 96–100, 1995.

[17] A. Saberi, Z. Lin, and A. Teel, "Control of linear systems with saturating actuators," *IEEE Transactions on Automatic Control*, vol. 41, 1996.

[18] B. Yang and W. Lin, "On semi-global stabilizability of mimo nonlinear systems by output feedback," *Automatica*, vol. 42, pp. 1049–1054, 2006.

[19] D. Abramovitch and G. Franklin, "On the stability of adaptive pole-placement controllers with a saturating actuator," *Automatic Control, IEEE Transactions on*, vol. 35, pp. 303–306, 1990.

[20] H. Hindi and S. Boyd, "Analysis of linear systems with saturation using convex optimization," *Proceedings of the 37th IEEE Conference on Decision and Control*, pp. 903–908, 1998.

[21] V. Kapila, A. Sparks, and H. Pan, "Control of systems with actuator saturation nonlinearities: an lmi approach," *International Journal of Control*, vol. 74, pp. 586–599, 2001.

[22] A. Saberi, A. Stoorvogel, and P. Sannuti, *Internal and External Stabilization of Linear Systems with Constraints*. Birkhauser, 2012.

[23] D. Bernstein and A. Michel, "A chronological bibliography on saturating actuators.," *International Journal of robust and nonlinear control*, vol. 5, pp. 375–380, 1995.

[24] T. Hu, A. Pitsillides, and Z. Lin, "Null controllability and stabilization of linear systems subject to asymmetric actuator saturation.," *Proceedings of the IEEE Conference on Decision and Control.*, 2000.

[25] K. Hui and C. Chan, "Stabilization of systems with deadzone nonlinearity.," *Proceedings of the 1998 IEEE conference on Control Applications.*, vol. 2, pp. 1036–1040, 1998.

[26] D. Delchamps, "Stabilizing a linear system with quantized state feedback.," *IEEE Trans. on Automatic Control*, vol. 35, pp. 916–924, 1990.

[27] G. Kreisselmeier, "Stabilization of linear systems in the presence of output measurement saturation," *Systems and Control Letters*, vol. 29, pp. 27–30, 1996.

[28] Z. Lin and T. Hu, "Semi-global stabilization of linear systems subject to output saturation," *Systems and Controls Letters*, vol. 43, pp. 2011–217, 2001.

[29] Y. Cao, Z. Lin, and B. Chen, "An output feedback $h_\infty$ controller design for linear systems subject to sensor nonlinearities.," *IEEE Trans. on Circuits and Systems.*, vol. 50, pp. 914–921, 2003.

[30] D. Liberzon and D. Nesic, "Input-to-state stabilization of linear systems with quantized state measurements," *IEEE Transactions on Automatic Control*, vol. 52, pp. 767–781, 2007.

[31] V. Kapila and M. Haddad, "Actuator amplitude saturation control for systems with exogenous disturbances," in *American Control Conference, 1998. Proceedings of the 1998*, vol. 3, pp. 1468–1472 vol.3, 1998.

[32] G. Stein, "Respect the unstable," *Control Systems, IEEE*, vol. 23, pp. 12–25, 2003.

[33] A. Isidori, *Nonlinear control systems*. Springer, third ed., 1995.

[34] W. Dayawansa, D. Elliot, and W. Boothby, "Global linearization by feedback and state transformations," *Proc. 25th IEEE Conf. Decision Contr.*, pp. 11–13, 1985.

[35] J. Grizzle and P. V. Kokotovic, "Feedback linearization of sampled-data systems," *Automatic Control, IEEE Transactions on*, vol. 33, pp. 857–859, 1988.

[36] J. Doyle, R. S. Smith, and D. F. Enns, "Control of plants with input saturation nonlinearities," in *Proceedings of the American Control Conference*, pp. 1034–1039, 1987.

[37] M. V. Kothare, P. J. Campo, M. Morari, and C. N. Nett, "A unified framework for the study of anti-windup designs," *Automatica*, vol. 30, no. 12, pp. 1869–1883, 1994.

[38] A. Zheng, M. V. Kothare, and M. Morari, "Anti-windup design for internal model control," *Int. J. Contr.*, vol. 60, pp. 1015–1024, 1994.

[39] N. Kapoor, A. Teel, and P. Daoutidis, "An anti-windup design for linear systems with input saturation," *Automatica*, vol. 34, no. 5, pp. 559–574, 1998.

[40] V. Kapila and K. Grigoriadis, eds., *Actuator Saturation Control*. CRC Press, 2002.

[41] L. Zaccarian and A. Teel, *Modern Anti-windup Synthesis: Control Augmentation for Actuator Saturation*. Princeton University Press, 2011.

[42] E. G. Gilbert and I. Kolmanovsky, "Discrete-time reference governors and the nonlinear control of systems with state and control constraints," *International Journal of robust and nonlinear control*, vol. 5, 1995.

[43] A. Bemporad, "Reference governor for constrained nonlinear systems," *IEEE trans. on Automatic Control*, vol. 43, no. 3, 1998.

[44] A. Bemporad and M. Morari, "Control of systems integrating logic, dynamics, and constraints," *Automatica*, vol. 35, 1999.

[45] E. G. Gilbert and I. Kolmanovsky, "Fast reference governors for systems with state and control constraints and disturbance inputs," *International Journal of robust and nonlinear control*, vol. 9, pp. 1117–1141, 1999.

[46] J. De Doni, G. Goodwin, and M. Seron, "Anti-windup and model predictive control: Reflections and connections," *European Journal of Control*, vol. 6, no. 5, 2000.

[47] E. F. Camacho and C. B. Alba, *Model Predictive Control*. Prentice Hall, 2000.

[48] M. Morari, C. Garcia, D. Prett, and J. Lee, *Model Predictive Control*. Prentice Hall – PTR, 2004.

[49] M. Dahleh and J. Pearson, "$\mathcal{L}_1$-optimal compensators for continuous-time systems," *Automatic Control, IEEE Transactions on*, vol. 32, pp. 889–895, 1987.

[50] P. Kapasouris, M. Athans, and G. Stein, "Design of feedback control systems for stable plants with saturating actuators," in *Decision and Control, 1988., Proceedings of the 27th IEEE Conference on*, pp. 469–479 vol.1, 1988.

[51] A. Teel, "Linear systems with input nonlinearities: Global stabilization by scheduling a family of $h_\infty$ type controllers," *International Journal of Robust and Nonlinear Control*, vol. 5, pp. 399–411, 1995.

[52] H. Risken, *The Fokker-Planck Equation: Methods of Solution and Applications*. Springer – Verlag, 1989.

[53] D. Liberzon and R. W. Brockett, "Nonlinear feedback systems perturbed by noise: Steady-state probability distributions and optimal control," *IEEE Transactions on Automatic Control*, vol. 45, pp. 1116–1130, 2000.

[54] P. Grensted, "Frequency response methods applied to nonlinear systems," *Prog. Contr. Eng.*, vol. 33, pp. 105–139, 1962.

[55] A. Gelb and W. Vander Velde, *Multiple input describing function and nonlinear design.* New York: McGraw-Hill, 1968.

[56] A. Mees, "Describing functions, circle criteria and multiple-loop feedback systems," *Electrical Engineers, Proceedings of the Institution of*, vol. 120, pp. 126–130, 1973.

[57] I. Kazakov, "Approximate method for the statistical analysis of nonlinear systems," Technical Report VVIA 394, Trudy, 1954.

[58] R. Boonton, "Nonlinear control systems with random inputs," *IRE Trans. on Circuit Theory*, vol. 1, pp. 9–18, 1954.

[59] I. Kazakov and B. Dostupov, *Statistical Dynamics of Nonlinear Control Systems*. Fizmatgiz, 1962. In Russian.

[60] S. Crandall, "On using non-gaussian distributions to perform statistical linearization.," *International Journal of Non-linear Mechanics*, vol. 39, pp. 1395–1406, 2004.

[61] G. Q. Cai and Y. Suzuki, "On statistical quasi-linearization," *International Journal of Non-Linear Mechanics*, vol. 40, pp. 1139–1147, 2005.

[62] G. Ricciardi, "A non-gaussian stochastic linearization method," *Probabilistic Engineering Mechanics*, vol. 22, pp. 1–11, 2007.

[63] J. Skrzypczyk, "Accuracy analysis of statistical linearization methods applied to nonlinear dynamical systems," *Reports on mathematical physics.*, vol. 36, pp. 1–20, 1995.

[64] S. Ching, S. M. Meerkov, and T. Runolfsson, "Gaussianization of random inputs by filtering plants: The case of poisson white and telegraph processes," in *American Control Conference*, Submitted for publication.

[65] G. C. Goodwin, S. F. Graebe, and M. E. Salgado, *Control System Design*. Prentice Hall, 2000.

[66] K. Astrom and T. Hagglund, *PID Controllers: Theory, design and tuning*. ISA Press, 1995.

[67] J. L. Rodriguez-Amenedo, S. Arnalte, and J. C. Burgos, "Automatic generation control of a wind farm with variable speed wind turbines," *IEEE Transactions on Energy Conversion*, vol. 17, pp. 279–284, June 2002.

[68] A. D. Hansen, P. Sorensen, F. Iov, and F. Blaabjerg, "Centralized power control of wind farm with doubly fed induction generators," *Renewable Energy*, vol. 31, pp. 935–951, June 2006.

[69] T. Senjyu, R. Sakamoto, N. Urasaki, T. Funabashi, and H. Sekine, "Output power leveling of wind farm using pitch angle control with fuzzy neutral network," in *Power Engineering Society General Meeting*, (Montreal, Canada), pp. 1–8, 2006.

[70] R. G. de Almeida, E. D. Castronuovo, and J. A. Pecas Lopes, "Optimum generation control in wind parks when carrying out system operator requests," *IEEE Transactions on Power Systems*, vol. 21, pp. 718–725, May 2006.

[71] Z. Lubosny and J. W. Bialek, "Supervisory control of a wind farm," *IEEE Transactions on Power Systems*, vol. 22, pp. 985–994, August 2007.

[72] G. Tapia, A. Tapia, and J. X. Ostolaza, "Proportional-integral regulator-based approach to wind farm reactive power management for secondary voltage control," *IEEE Transactions on Energy Conversion*, vol. 22, pp. 488–498, June 2007.

[73] C. F. Moyano and J. A. Pecas Lopes, "An optimization approach for wind turbine commitment and dispatch in a wind park," *Electric Power Systems Research*, vol. 79, pp. 71–79, January 2009.

[74] P. Li, P. Keung, and B. Ooi, "Development and simulation of dynamic control strategies for wind farms," *IET Renewable Power Generation*, vol. 3, pp. 180–189, June 2009.

[75] J. R. Marden, S. D. Ruben, and L. Pao, "Surveying game theoretic approaches for wind farm optimization," in *AIAA Aerospace Sciences Meeting*, (Nashville, TN), pp. 1–10, 2012.

[76] J. Aho, A. Buckspan, J. Laks, P. Fleming, Y. Jeong, F. Dunne, M. Churchfield, L. Pao, and K. Johnson, "A tutorial of wind turbine control for supporting grid frequency through active power control," in *American Control Conference*, (Montreal, Canada), pp. 3120–3131, 2012.

[77] Y. Guo, S. H. Hosseini, C. Y. Tang, J. N. Jiang, and R. G. Ramakumar, "An approximate wind turbine control system model for wind farm power control," *IEEE Transactions on Sustainable Energy*, vol. 4, pp. 262–274, January 2013.

[78] Y. Guo, W. Wang, C. Y. Tang, J. N. Jiang, and R. G. Ramakumar, "Model predictive and adaptive wind farm power control," in *Proc. American Control Conference*, (Washington, DC), 2013. to appear.

[79] Y. Guo, *Control and Optimization of Variable-Speed Wind Turbines and Large-Scale Wind Farms*. Ph.D. Dissertation, University of Oklahoma, Norman, OK, 2012.

[80] H. Kwakernaak and R. Sivan, *Linear Optimal Control Systems*. New York, NY: Wiley-InterScience, 1972.

[81] L. D. Lutes, "Cumulants of stochastic response for linear systems," *Journal of Engineering Mechanics*, vol. 112, pp. 1062–1075, 1986.

[82] D. R. Smart, *Fixed Point Theorems*. Cambridge University Press, 1980.